

**ANALYTICAL STUDY OF CORRODED STEEL-FRP CONFINED
CONCRETE BOND UNDER FATIGUE CYCLIC LOADING**

by

Safeer Abbas

B.Sc. University of Engineering and Technology, Pakistan, 2007

A THESIS SUBMITTED IN PARTIAL FULFILLMENT
OF THE REQUIREMENTS FOR THE DEGREE OF

MASTER OF APPLIED SCIENCE

in

The College of Graduate Studies

(Civil Engineering)

THE UNIVERSITY OF BRITISH COLUMBIA
(Okanagan)

May 2010

© Safeer Abbas, 2010

Abstract

The steel-concrete bond and the cracking behaviour of concrete affect the performance of reinforced concrete structures. This is due to the fact that the transfer of forces between the steel and the concrete are accomplished through the bond. The bond between the steel and the concrete is affected by many factors such as corrosion of reinforcement, type of applied loading, and the confinement level. Reinforcement corrosion is one of the primary causes of the loss of steel-concrete bond. On the other hand, an accumulation of bond damage occurs due to the application of fatigue cyclic loading, as in the case of bridges and marine structures. It is known that fibre reinforced polymer (FRP) confinement improves the bond strength, even in the case of corroded reinforcing steel bars.

The objective of this thesis was to develop an analytical tool for structural engineers to evaluate the corroded steel-FRP confined concrete bond under fatigue cyclic loading. Two models have been developed; 1) slip-fatigue model; and 2) bond stress-slip model. These models considered the effect of corrosion of reinforcement, the external confinement provided by the FRP sheets, and the fatigue cyclic loading.

Slip after ' N ' number of cycles for unwrapped and FRP wrapped cases were developed as a function of the initial slip, the final slip, and the fatigue bond life. These models were capable of capturing the experimental behaviour reported in the literature. Slip-life models for unwrapped and FRP wrapped beam specimens were developed using non linear regression analysis.

Harajli et al. (2004) static bond stress-slip law was modified in order to model the bond stress-slip behaviour for the unwrapped and FRP wrapped beam specimen under monotonic and cyclic loading. The proposed cyclic bond stress-slip behaviour followed the monotonic bond stress-slip envelope and satisfactorily modeled the experimental behaviour.

From the principles of statics of bond and using the derived cyclic bond stress-slip envelope, an equation to calculate the required development length of steel reinforcement was derived. The proposed equation is dependent on the material and the geometrical properties of a structural member. The derived equation was able to satisfactorily predict the fatigue bond life.

Table of Contents

Abstract	ii
Table of Contents	iii
List of Tables	v
List of Figures	vi
Acknowledgements	ix
Dedication	x
Chapter 1 : Introduction	1
1.1 Problem Statement	1
1.2 Thesis Overview.....	3
Chapter 2 : Literature Review and Research Objectives	4
2.1 Corrosion.....	4
2.1.1 Corrosion Process.....	4
2.1.2 Concrete Environment.....	4
2.1.3 Corrosion Initiation Process	5
2.1.4 Carbonation Induced Corrosion	6
2.1.5 Chloride Induced Corrosion	6
2.1.6 Corrosion in Concrete.....	7
2.1.7 Corrosion Effects on Concrete Structures	8
2.2 Fibre Reinforced Polymers.....	9
2.2.1 Fibres	9
2.2.2 Resin.....	10
2.2.3 Properties of FRP	10
2.2.4 Construction Applications of FRP.....	11
2.3 Fatigue Failure in Reinforced Concrete Structures	11
2.4 Bond between Steel and Concrete.....	12
2.4.1 Bond Mechanism.....	13
2.4.2 Factors Affecting the Bond Behaviour.....	14
2.4.3 Bond Test Specimens	16
2.5 Confinement of FRP in Bond Anchorage Zone	17
2.6 Effect of Corrosion on Bond	18
2.7 Effect of FRP Confinement on the Bond Behaviour of Corroded Steel Bar.....	19
2.8 Bond Behaviour under Repeated Cyclic Loading	20

2.8.1 Oh and Kim Model.....	22
2.9 Bond Behaviour of Corroded Steel-FRP Confined Concrete under Fatigue Cyclic Loading.....	23
2.10 Research Motivation.....	28
2.11 Research Objectives	28
Chapter 3 : Numerical Modeling	29
3.1 General	29
3.2 Slip-Fatigue Model.....	29
3.2.1 For Unwrapped Beam Specimen.....	30
3.2.2 FRP Wrapped Beam Specimen	35
3.3 Bond Stress-Slip Model.....	40
3.3.1 Bond Stress-Slip under Static Load.....	40
3.3.2 Finite Element Analysis	45
3.3.3 Bond Stress-Slip under Cyclic Load	49
Chapter 4 : Analytical Modeling.....	58
4.1 General	58
4.2 Slip-Development Length Model.....	58
4.3 Final Slip-Fatigue Bond Life.....	66
4.4 Design Considerations.....	68
4.4.1 Implementation of Model	69
Chapter 5 : Conclusions and Future Recommendations	73
5.1 Summary and Conclusions	73
5.2 Limitations and Future Research Recommendations	74
Appendix A	76
Appendix B.....	78
Appendix C	83
Appendix D	86
Appendix E.....	90
Bibliography.....	94

List of Tables

Table 2.1 Thermosetting polymer resin properties (ACI 440, 2007)	10
Table 2.2 Details of experimental setup (Rteil, 2007).....	24
Table 3.1 Corrosion dependent variables for unwrapped beam specimen	32
Table 3.2 Corrosion dependent variable for FRP wrapped beam specimen.....	37
Table 3.3 Specimen parameters for bond stress slip relation	43
Table 3.4 Bond stress-slip relation parameters.....	43
Table 3.5 Proposed values for q_i and t_i for different corrosion level.....	51
Table 3.6 Proposed values for m_i and n_i for different corrosion level	55
Table A.1 Fatigue bond life for unwrapped beam specimens (Rteil, 2007).....	76
Table A.2 Fatigue bond life for FRP wrapped beam specimens (Rteil, 2007).....	77

List of Figures

Figure 2.1 Steel reinforcement corrosion in the concrete (Broomfield, 1997).....	5
Figure 2.2 Corrosion mechanism in concrete (Broomfield, 1997).....	7
Figure 2.3 Cross sectional view of corrosion induced cracks	8
Figure 2.4 Carbon and glass fibres	9
Figure 2.5 Stress-strain plots of FRP (ACI, 1996)	11
Figure 2.6 Bond force mechanism.....	13
Figure 2.7 Forces and stresses in concrete (ACI 408, 2003).....	14
Figure 2.8 Relative rib ratio (R_r) (ACI 408, 2003).....	15
Figure 2.9 Pull out and beam specimen (ACI 408, 2003)	17
Figure 2.10 Effect of FRP confinement (Harajli et al., 2004)	18
Figure 2.11 Schematic of the effect of corrosion on bond strength.....	19
Figure 2.12 Bond strength under FRP confinement and corrosion (Soudki and Sherwood, 2003)	20
Figure 2.13 Reinforcing steel slip behavior under cyclic loading (Balazs, 1991).....	21
Figure 2.14 Details of the test specimen (Rteil, 2007)	23
Figure 2.15 Unwrapped corroded beams (Rteil, 2007)	24
Figure 2.16 FRP wrapped corroded beams (Rteil, 2007)	25
Figure 2.17 Slip behavior for unwrapped beam specimen (Rteil, 2007).....	26
Figure 2.18 Slip behavior for FRP wrapped beam specimen (Rteil, 2007).....	27
Figure 3.1 Slip behaviour for unwrapped specimens	31
Figure 3.2 Initial slip variation for unwrapped beam specimens.....	32
Figure 3.3 Final slip variation for unwrapped beam specimens.....	33
Figure 3.4 Typical slip-cycle variation for UW0 (F45-N-T0).....	34
Figure 3.5 Typical slip-cycle variation for UW5 (F45-N-T5).....	34
Figure 3.6 Typical slip-cycle variation for UW9 (F37-N-T9a).....	35
Figure 3.7 Phases of slip behaviour for FRP wrapped beam specimen.....	36
Figure 3.8 Initial slip variation for FRP wrapped specimens	37
Figure 3.9 Variation of D with the load range (FRP wrapped beams)	38
Figure 3.10 Typical slip-cycle variation for W0 (F65-W0-N0)	39
Figure 3.11 Typical slip-cycle variation for W5 (F50-W5-N5)	39
Figure 3.12 Typical slip-cycle variation for W9 (F55-W9-T9a).....	40
Figure 3.13 Bond stress versus slip (Harajli, Hamad and Rteil, 2004)	41
Figure 3.14 Experimental bond stress-slip variation versus model prediction (Unwrapped)	44
Figure 3.15 Experimental bond stress-slip variation versus model prediction (FRP wrapped)	44

Figure 3.16 Beam anchorage specimen.....	45
Figure 3.17 Stress-strain curve for concrete.....	46
Figure 3.18 Finite element mesh of the model.....	47
Figure 3.19 Finite element analysis for static bond stress-slip variation.....	48
Figure 3.20 Envelope for the cyclic bond stress-slip.....	49
Figure 3.21 Variation of A with the load range for different corrosion levels.....	50
Figure 3.22 Variation of B with the load range for different corrosion levels.....	51
Figure 3.23 Typical bond stress-slip variation for UW0 (F45-N-T0).....	52
Figure 3.24 Typical stress-slip variation for UW5 (F40-N-T5).....	52
Figure 3.25 Typical stress-slip variation for UW9 (F35-N-T9b).....	53
Figure 3.26 Variation of α with the load range for different corrosion levels.....	54
Figure 3.27 Variation of A with the load range for different corrosion levels.....	54
Figure 3.28 Variation of B with the load range for different corrosion levels.....	55
Figure 3.29 Typical bond stress-slip variation for W0 (F65-W0-T0).....	56
Figure 3.30 Typical bond stress-slip variation for W5 (F50-W5-T5).....	56
Figure 3.31 Typical bond stress-slip variation for W9 (F48-W9-T9).....	57
Figure 4.1 Forces acting on steel bar.....	58
Figure 4.2 Internal forces in uncracked reinforced concrete section.....	60
Figure 4.3 Bond stress-slip (u-s) model.....	63
Figure 4.4 Variation of the final slip with fatigue bond life.....	67
Figure 4.5 Model prediction of fatigue bond life for unwrapped beams.....	71
Figure 4.6 Model prediction of fatigue bond life for FRP wrapped beams.....	72
Figure B.1 Experimental and model results for unwrapped zero percent corrosion level.....	78
Figure B.2 Experimental and model results for unwrapped zero percent corrosion level (cont.).....	79
Figure B.3 Experimental and model results for unwrapped five percent corrosion level.....	80
Figure B.4 Experimental and model results for unwrapped nine percent corrosion level.....	81
Figure B.5 Experimental and model results for unwrapped nine percent corrosion level (cont.).....	82
Figure C.1 Experimental and model results for FRP wrapped zero percent corrosion level.....	83
Figure C.2 Experimental and model results for FRP wrapped five percent corrosion level.....	84
Figure C.3 Experimental and model results for FRP wrapped nine percent corrosion level.....	85
Figure D.1 Experimental and model results for unwrapped zero percent corrosion level.....	86
Figure D.2 Experimental and model results for unwrapped zero percent corrosion level (cont.).....	87
Figure D.3 Experimental and model results for unwrapped five percent corrosion level.....	88
Figure D.4 Experimental and model results for unwrapped nine percent corrosion level.....	89

Figure E.1 Experimental and model results for FRP wrapped zero percent corrosion level.....90
Figure E.2 Experimental and model results for FRP wrapped five percent corrosion level91
Figure E.3 Experimental and model results for FRP wrapped nine percent corrosion level.....92
Figure E.4 Experimental and model results for FRP wrapped nine percent corrosion level (cont.)93

Acknowledgements

I would like to state my sincere appreciation and humble thanks to my worthy research supervisor, Dr. Ahmad Rteil, for his invaluable guidance and supervision throughout this study. Due to his benign patronage and able coaching, I have been able to finish my MASc thesis successfully and it is my privilege to acknowledge his guidance.

The author gratefully acknowledges the input of Dr. Rehan Sadiq. Also, I would like to thank my committee members: Dr. Nemkumar Banthia, Dr. Abbas Milani and Dr. Lukas Bichler.

The author would like to thank the University of Engineering and Technology, Lahore, Pakistan for their financial support through merit scholarship “Faculty Development Program”.

At the end, I would acknowledge the contribution of my parents, brothers and sisters for their continuous support, enthusiasm, and encouragement.

Dedication

My past, present and future, all because of my mother's deep love!

Chapter 1: Introduction

1.1 Problem Statement

The performance of reinforced concrete (RC) members depends on the transfer of forces across the interface between concrete and steel reinforcing bars. This transfer of forces is accomplished through the bond forces between the steel and the concrete. The steel-concrete bond dictates the cracking behaviour and the ultimate strength of a RC member (Oh and Kim, 2007). The interruption of transfer of forces at the steel-concrete interface, due to the bond deterioration, results in an increased number of cracks and deflection. It may also lead to a brittle and abrupt failure of the concrete element (ACI 408, 2003). Therefore, a precise assessment of the bond between the steel and the concrete is important to determine the residual strength of RC structures (Oh and Kim, 2007; Rteil, 2007; Mor et al., 1992). Bond is affected by several factors such as the corrosion of the steel reinforcement, the presence of confinement, and the loading regime.

The corrosion of reinforcement in concrete structures is the most serious problem facing structural engineers. For example, corrosion caused the fall down of the Berlin Congress Hall and a parking garage in Minnesota, resulting in enormous casualties and damages (Isecke, 1982; Borgard et al., 1990). The principal cause of steel corrosion in reinforced concrete bridges, marine structures, and parking garages is the use of either chlorides as de-icing agents or the presence of chlorides in the environment. In addition to structural discrepancies, the deterioration of RC structures is also characterized by severe environmental conditions, inappropriate use of construction materials, and inadequate construction practices (Amleh, 2000). Approximately \$3 billion per year is the estimated cost required for the repair of corrosion damaged structures in Canada (David, 2000). Corrosion of reinforcement in RC structures cost the United States economy almost 1% of its gross domestic product (Whitmore and Ball, 2004).

The consequences of corrosion in RC structures are: 1) loss of reinforcing steel cross sectional area and 2) cracking of concrete cover which leads towards concrete spalling. The reduction in the area of the steel bars decreases the load carrying capacity of the RC structures. The cracking and spalling of the concrete cover, resulting from the splitting tensile forces acted by the rust volume on the concrete (ACI 222, 2001), lead to the deterioration of the bond due to

the loss of friction and mechanical anchorage provided by the ribs as well as the loss of concrete cover confinement.

Marine structures and bridges, which are prone to corrosion, are also subjected to cyclic loading. The live to dead load ratio is high in these structures due to the use of high strength material which reduces the dead load. Therefore, fatigue cyclic loading is becoming an important design criterion for these structures (ACI 215, 1974). The fatigue cyclic loading causes progressive damage in the form of increased number of cracks, crack width, and deflection, which affects the steel-concrete bond strength. The influence of fatigue cyclic load is characterized by an increased in slip between the reinforcing steel bar and the concrete. The slip response dictates the cracking and crushing behaviour of concrete in front of the steel bar lugs (Balazs, 1991; Lindorf et al., 2009).

Fibre reinforced polymer (FRP) system has achieved a worldwide acceptance over other strengthening systems due to its high strength to weight ratio, favourable behaviour in harsh environments, improved fatigue behaviour, ease of handling in application, and non corrosive nature (ACI 440, 2002). Also, the FRP repair system controls the corrosion activity and hence increases the strength of RC structures (El Maaddawy et al., 2005a and b). Research has also shown that FRP wrapping increases the bond strength by providing confinement to the concrete, which does not allow the cracks to propagate further (Kono et al., 1998, 1999; Hamad et al., 2004a, b, c; Harajli et al., 2004; Rteil et al., 2005).

Design equations that deal with the worst case loading scenarios of new construction and analysis of existing reinforced concrete (RC) structures are required in order to ensure their satisfactory performance during their service lives. The existing analytical bond models that deal with the corrosion of reinforcement, FRP confinement and cyclic loading are based on pullout a specimen, which does not capture the actual bond behaviour in order to assess the bond performance of RC structures. Some of these models consider the effect of repeated loading, while others consider the effect of corrosion. However, models that consider the combined effect of fatigue cyclic loading and the corrosion of reinforcement are lacking in the literature. In addition, the effect of FRP wrapping needs to be evaluated under these combined effects. The

present study is intended to propose a design equations and analysis techniques that would help the structural engineers in order to cope with the fatigue-corroded steel-bond problems.

1.2 Thesis Overview

This study aims to develop tools which examine the influence of the fatigue cyclic loading on the bond behaviour between the corroded steel reinforcement and carbon fibre reinforced polymer (CFRP) confined concrete. Chapter 2 reviews the available literature on the bond between concrete and steel. This chapter discusses the effect of corrosion, FRP confinement in the bond anchorage zone, and the cyclic loading on bond between the steel and the concrete. Based on the literature review, the research objectives and the methodology are presented. Numerical modeling of bond associated parameters is developed in Chapter 3. Chapter 4 presents the analytical derivation, based on the mechanics of bond, of the cyclic slip-development length relationship. Finite element simulation of static bond stress-slip relation for the beam anchorage specimen will also be presented. Chapter 5 presents the conclusions and the limitations of this study and provides future research recommendations.

Chapter 2: Literature Review and Research Objectives

2.1 Corrosion

2.1.1 Corrosion Process

Corrosion is the formation of a chemical compound due to deterioration of a metal by chemical reaction with environmental species. It is an electrochemical process at room temperature; i.e., the flow of an electric current takes place as a result of a chemical reaction (Choo and Newman, 2003).

Positive ions are formed when the free electrons leave the metal surface during the metal dissolution process. A chemical reaction that produces positive ions is called oxidation, and the site where oxidation takes place is called an anode (e.g., positive iron ions are formed due to iron oxidation). The reaction during which the negative ions are formed when the residual electrons are consumed in the metal by a chemical reaction called reduction. The site where reduction takes place is termed as cathode (e.g., negative hydroxyl ions are formed when oxygen is reduced). An oxidation and/or reduction process occurs on an electronic conductor called electrode (Glass and Buenfeld, 1998).

To avoid the accumulation of charges, an electronic and ionic current must flow between the cathode and the anode. Ionic conductor is an aqueous solution that consists of ions (Fe^{+2} , Na^+ , OH^- , Cl^-) and termed as electrolyte. Cations are positive ions and anions are negative ions. The metal acts as an electronic conductor. If there is no external source of battery (electron/power supply), the anodic and cathodic reactions occur in such a way that it prevents the build up of an electric charge (Glass and Buenfeld, 1998).

2.1.2 Concrete Environment

Concrete consists of aggregates and cement matrix. The cement matrix is basically calcium hydroxide and calcium silicate gel, which are the products of hydration reaction (Choo and Newman, 2003). An important characteristic of cement hydration is that the aqueous phase quickly attains a high pH (12-13) value. The reaction of this alkaline solution with steel results in

the formation of a thin, impenetrable, and dense film consisting of a metal oxide layer, forming on the steel (called passive layer) and protects it from further metal dissolution (Glass et al., 2000a).

As long as the reinforcing steel bar is in contact with the passive layer it will be secured from corrosion. However, many reinforced concrete structures are exposed to a variety of environments which may provide favourable surroundings for the initiation of corrosion.

2.1.3 Corrosion Initiation Process

Corrosion in RC structures is due to the entrance (through the cement pores) of destructive species (chlorides ions and carbon dioxide) into the cement paste (Choo and Newman, 2003). The transportation rate of the aggressive species is highly dependent on the permeability of concrete. This factor further depends on the cement type and its content, fineness of the cement, water/cement ratio (w/c), use of cementitious material (ground granulated blast furnace slag and silica fumes), and the compaction of concrete (Atkinson and Nickerson, 1984). Figure 2.1 shows the corroded steel reinforcement after the spalling of concrete.



Figure 2.1 Steel reinforcement corrosion in the concrete (Broomfield, 1997)

2.1.4 Carbonation Induced Corrosion

The reaction of alkaline hydroxide and carbon dioxide (CO_2) results in the formation of a carbonic acid (H_2CO_2). This will neutralize the alkaline solid phase and decreased the pH value of the concrete (Broomfield, 1997). The alkaline solid phase is depleted when a low pH zone extends inward from the concrete surface. This process is called carbonation. The passive layer becomes unstable and no longer exists if the pH value around the steel falls to 10 (Glass et al., 2000a).

The rate of carbonation depends on many factors related to both the concrete quality and the external environment. Concrete associated factors include the nature of porosity, the alkaline reserves of the cement hydration products, and the depth of the concrete cover. The carbonation rate increases with a high w/c ratio due to increase in the chemical porosity. The carbonation depth also increases in the presence of cracks (Glass et al., 1991). In addition, if the surrounding environment contains a high amount of carbon dioxide, it will significantly increase the rate of carbonation (Broomfield, 1997).

2.1.5 Chloride Induced Corrosion

Chloride ions act as a catalyst in the chloride-induced corrosion process. There are two possibilities for chloride ions to be in the concrete. The cast in chlorides which are present already in the concrete due to the use of set accelerators (calcium chloride), sea water or contaminated aggregates in the concrete. In addition, chloride ions can enter (diffuse) into the concrete from external sources. External sources for the chloride ions include sea salt (for structures near seas and oceans), and de-icing salts in cold geographic regions (Broomfield, 1997). The interaction of chloride ions with steel bar will lead to the initiation of corrosion based on one of the following theories. 1) According to oxide film theory, the chloride ions attack the protective layer (passive layer) surrounding the reinforcing steel bar and disturb the underneath iron. 2) The adsorption theory states that the chloride ions, hydroxyl ions, and the dissolved oxygen try to adsorb in the metal's surface. The interaction of chloride ions with the reinforcing steel bar increases the rate of elimination of the iron ions from the reinforcing steel bar into the solution. 3) The transitory complex theory states that the disturbance in passive layer takes place when the hydroxyl ions are replaced by the chlorides and forming a soluble iron chloride. Iron

chloride breaks into the chloride ion during migration from the anode. These free chloride ions then continue to react with the reinforcing steel bars (ACI 222, 2001).

2.1.6 Corrosion in Concrete

The mechanism of corrosion in concrete is the same whether it is carbonation induced or chloride induced. The corrosion mechanism in concrete is similar to an electrochemical reaction where the concrete matrix acts as an aqueous solution (electrolyte) and the reinforcing steel bar represent an electrical conductor (ACI 222, 2001). The schematic representation of the steel oxidation at the anode and the reduction at the cathode for the initiation of corrosion is shown in Figure 2.2.

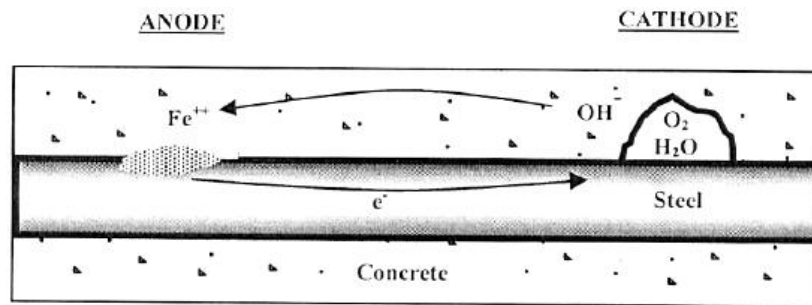


Figure 2.2 Corrosion mechanism in concrete (Broomfield, 1997)

The oxidation reaction at the anode results in the release of electrons. These electrons react with oxygen and water at the cathode resulting in the formation of hydroxide ions (Figure 2.2). Equation 2.1 and 2.2 shows the anodic and cathodic reactions respectively.



The stages for the formation of rust products are as follows: First, the iron ion (Fe^{+2}) reacts with the hydroxyl ions (OH) to form ferrous hydroxide [$Fe(OH)_2$] (Equation 2.3). The ferrous hydroxide further reacts with the available water and oxygen to form ferric hydroxide [$4Fe(OH)_3$] (Equation 2.4) and then hydrated ferric oxide (Equation 2.5) or rust [$Fe_2O_3 \cdot nH_2O$] (Broomfield, 1997).



Where 'n' in Equation 2.5 depends on the available oxygen and water.

2.1.7 Corrosion Effects on Concrete Structures

Corrosion causes a decrease in the cross sectional area of the reinforcing steel bar. This reduction in the steel area directly affects the deflection and the capacity of the RC element.

The formation and deposition of rust product on the reinforcing steel bars reduces the direct contact of between the reinforcing steel and the concrete; thus, decreasing the bond strength.

In addition, the volume of the rust products, which is many times higher than the parent reinforcing steel bars, exerts a tensile stresses on the surrounding concrete. Due to these tensile stresses, a radial crack initiates and may lead towards the spalling of the concrete cover (Figure 2.3) (Broomfield, 1997). In this case, a complete loss of bond takes place. As discussed in Section 2.4.1, the loss of steel-concrete bond interrupts the force transfer mechanism between these two materials (steel and concrete). Therefore, the member will behave like a plain concrete and will fail abruptly.

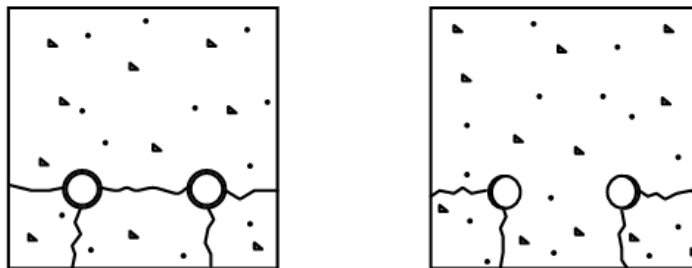


Figure 2.3 Cross sectional view of corrosion induced cracks

2.2 Fibre Reinforced Polymers

Fibre reinforced polymer (FRP) sheets have been widely used for rehabilitation (repair and strengthening) of deteriorated RC structures. Also they have been used to strengthen and upgrade existing structures against flexural, shear, and bond failures (Saadatmanesh and Malek, 1998; Pisani, 2005; El-Syed et al., 2007; Hamad et al., 2004). FRP sheets consist of high tensile strength fibres within a polymer matrix (ACI 440, 2002).

2.2.1 Fibres

Fibres provide the strength and the stiffness in the longitudinal direction in order to resist the applied load (ACI 440, 2002). The three types of fibres that are used in structural engineering applications are namely carbon, glass, and aramid (Figure 2.4).



Figure 2.4 Carbon and glass fibres

Carbon fibre reinforced polymer (CFRP) composites have many advantages such as high tensile strength, resistance to corrosion, low coefficient of thermal expansion, improved fatigue behaviour, high strength to weight ratio, and high stiffness. On the other hand, manufacturing cost of CFRP is high. Glass fibre reinforced polymer (GFRP) composites require less manufacturing cost relative to carbon fibres and have high tensile strength in comparison with steel, low electrical conductivity and high heat resistance properties. In comparison to carbon fibres, GFRPs have a lower stiffness. The generic name of aromatic polyamide is aramid.

Aramid fibres have more stiffness than GFRP and are cheaper to produce than CFRP. They have low density, non corrosive nature, excellent fatigue behaviour, and possess high strength (ACI 440, 1996).

2.2.2 Resin

The transfer of stresses between the fibres and between the fibers and concrete is accomplished through the use of polymer resin. There are two types of resins: thermoset and thermoplastic. Thermosetting resins are commonly used in structural applications. They include vinyl esters, epoxies, phenolics, and polyesters (ACI 440, 2007).

Thermosetting resins form a continuous 3-D network of covalent bond. These resins will not melt if heated but will soften and cannot be converted back into their original liquid form. They are good insulator of heat and electricity. The typical properties of thermosetting polymer resins are shown in Table 2.1.

Table 2.1 Thermosetting polymer resin properties (ACI 440, 2007)

Type	Density (g/cm ³)	Tensile modulus (MPa)	Tensile strength (MPa)	Maximum elongation (%)
Polyester	1.2	4.0	65	2.5
Epoxy	1.2	3.0	90	8
Vinylester	1.12	3.5	82	6

2.2.3 Properties of FRP

The stress-strain plots of different FRP systems shows that they can sustain higher stresses (up to 2500 MPa) in comparison with the reinforcing steel. Also, FRP systems show a linear stress-strain behaviour up to failure (Figure 2.5). It should be noted that FRPs have lower modulus of elasticity compared to steel and have no yielding and are highly unidirectional.

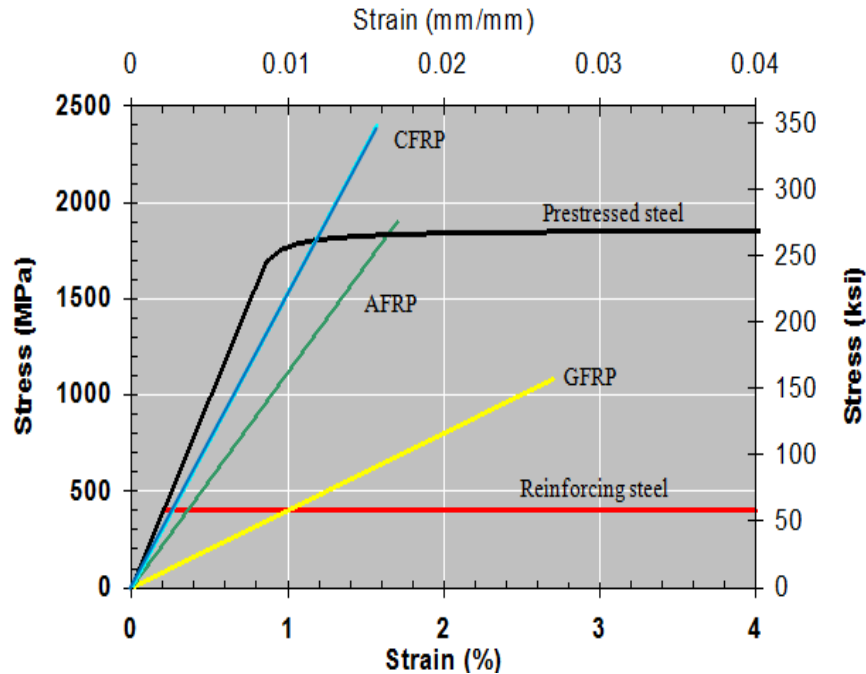


Figure 2.5 Stress-strain plots of FRP (ACI, 1996)

2.2.4 Construction Applications of FRP

Due to their properties, FRP composites are used in different applications in construction. The FRP wrapping of RC structures may increase the service life of the structures as they are more resistant to corrosion, and the easy and quick installation of FRP results in cheap construction cost (in terms of labour). The application of FRP composites in construction includes (ACI 440R-2007):

- Using FRP sheets and plates as a repair, rehabilitation and strengthening material for structural members (beams, columns, slabs and walls);
- Using FRP rods and rebars as an internal reinforcement;
- Using FRP prefabricated shapes as structural shapes like tube and channel sections.

2.3 Fatigue Failure in Reinforced Concrete Structures

Reinforced concrete (RC) bridges and marine structures are subjected to fatigue cyclic loading (repeated loading). During their service life, these structures can take up to 7×10^8 cycles (Tilly, 1979). The use of ultimate state design and high strength material resulted in a decrease in the

cross sectional dimension of the structural members, therefore the dead loads were decreased. At the same time, live loads are increasing (heavier trucks or more trucks on bridges). This resulted in higher live to dead load ratio. Due to this, higher stress ranges are acting on the structural members which give rise to fatigue problems. The cyclic loading affects the serviceability behaviour of the structures even if the fatigue failure does not take place. The fatigue loading results in an increased number of cracks and deflections. The design process of reinforced concrete structures should consider the effect of repeated cyclic loading criteria's in order to ensure a satisfactory performance (ACI 215, 1974).

Under repeated cyclic loading, cracks begin to propagate inside the concrete member. The fatigue crack may commences from the base of the ribs of the reinforcing steel bar or a void in the cement paste. Stress-strain behaviour of concrete becomes softer after the formation of excessive cracks with the increasing number of cycles (ACI 215, 1974).

Fatigue failure in RC structures may take place due to the accumulation of flexural, shear or bond stresses. According to ACI 215 (1974), a structure may have a fatigue life of up to ten million cycles if the concrete compressive strength is at least 50% higher than the concrete compressive stress range and steel stress range, S , is:

$$S \leq 161 - 0.33f_{smin} \leq 138 \text{ MPa} \quad \text{Equation 2.6}$$

Where f_{smin} is the minimum steel stress.

2.4 Bond between Steel and Concrete

The steel-concrete bond affects the performance of reinforced concrete structure (Amleh, 2000). Design equations in various codes are based on the assumption that a perfect bond exists between the concrete and the reinforcing steel bars in order to transfer the stresses between the two materials. Bond stress at the steel concrete interface is the shear stress which amend the steel stress along the length of the bar by transferring forces between the bar and the surrounding concrete (ACI 408, 2003). Due to this stress transfer mechanism between these two materials the steel and the concrete work as a composite material.

2.4.1 Bond Mechanism

The bond stresses developed between the concrete and the reinforcing steel bar are resisted by the chemical adhesion between the reinforcing steel bars and the concrete, the friction between the reinforcing steel and the concrete, and the mechanical anchorage provided by the reinforcing steel lugs against the concrete key, as illustrated in Figure 2.6 (ACI 408, 2003).

The vector addition of these forces results in a resultant force. The resultant force could be resolved into two components: the horizontal component called the bond force and vertical component called the bond splitting force (Figure 2.6).

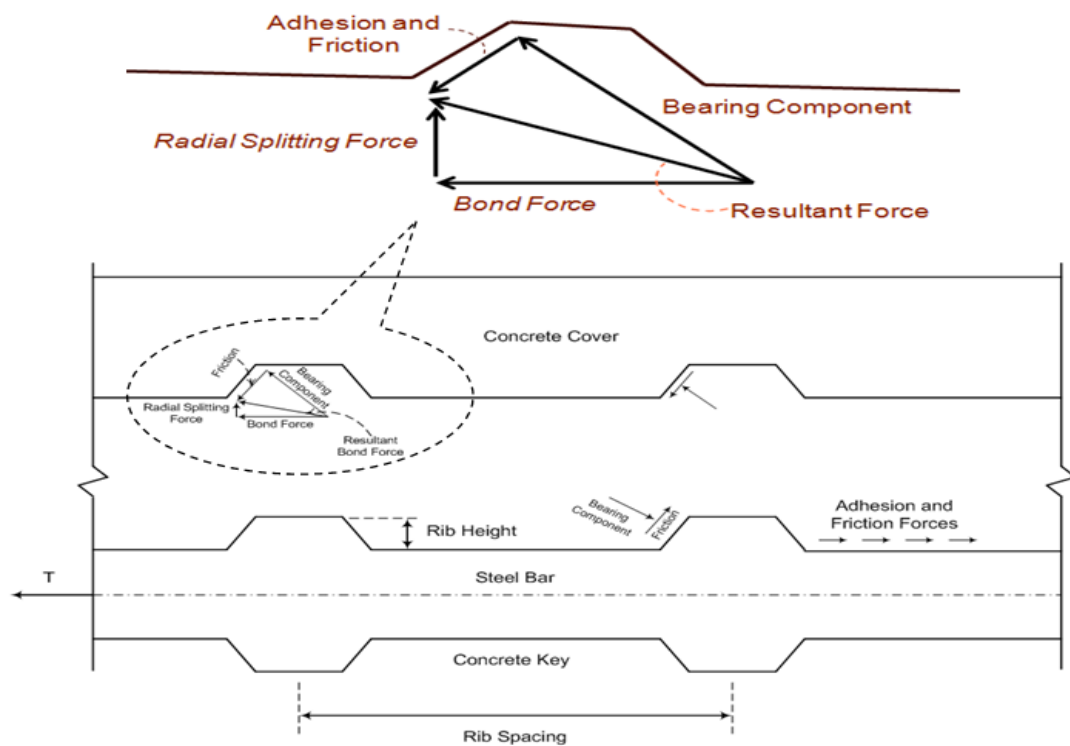


Figure 2.6 Bond force mechanism

Higher bond stresses (Figure 2.7) will cause the RC member to fail in bond by concrete splitting or by pull out failure. If the concrete cover and confinement are not adequate, the radial splitting forces cause the initiation and propagation of longitudinal and radial cracks from the steel bar to the concrete member surface. This will cause the concrete cover to split leading to splitting failure. However, if the concrete cover or the confinement is large enough, the radial splitting cracks need more energy in order to reach the concrete surface and the splitting failure

may be delayed or avoided. Therefore crack propagates along the longitudinal direction. This coupled with the increase in the shear component of the resultant bond force will result in shearing the concrete keys between the steel bar ribs off and causes the reinforcing steel bar to pullout. Splitting and pullout failure are both brittle failures. Once the force mechanism between steel and concrete is disturbed due to bond failure, the RC member will act as a plain concrete and will fail abruptly (ACI 408, 2003).

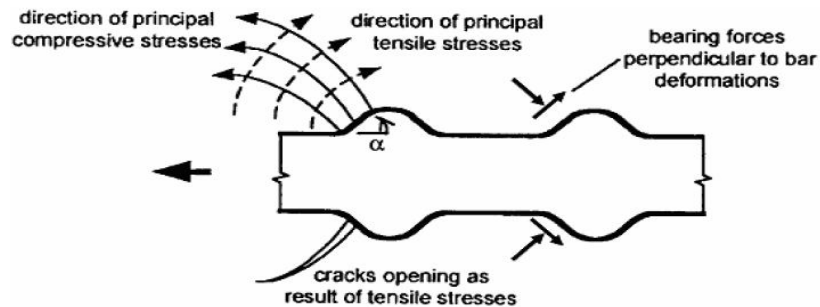


Figure 2.7 Forces and stresses in concrete (ACI 408, 2003)

2.4.2 Factors Affecting the Bond Behaviour

The behaviour of the bond between the steel and the concrete depends on many factors. The major ones are explained below.

Concrete Cover

The confinement provided by the concrete cover determines the bond failure mode (Eligehausen, 1979; Orangun, Jirsa and Breen, 1977; Tepfers, 1973). A splitting tensile failure will be more likely to occur in case of small concrete cover; while an adequate concrete cover for the same development length will result in pullout (bond shear) failure (ACI 408, 1992).

Development Length

Bond strength increases as the development length increases; however, it should be noted that the bond strength and the development length are not linearly proportional. This is because the bond stresses are not uniformly distributed along the development length. Bond stresses are concentrated close to the loaded end rather than the free end. With an increase in the development length, higher forces are required to induce bond failure in the RC member (ACI

408, 2003). Also, in the case of repeated loading, the fatigue bond life increases with increased development length (ACI, 408, 1992).

Compressive and Tensile Concrete Strength

In case of bond failure, the tensile strength of concrete is the more important parameter than the compressive strength because splitting and pullout failures are the result of tensile concrete failure (Orangun, Jirsa and Breen, 1977). The tensile (f_t) and compressive strength (f'_c) of concrete are proportional to each other (Carino and Lew, 1982). However, regression analysis on different experimental results showed that for bond failure a better correlation exists between the bond strength and $(f'_c)^{1/4}$ (ACI 408, 2003). This suggests that the bond failure is also related to the fracture energy of concrete (ACI 408, 2003).

Bar Size

Bar size is dependent on the development length in order to contribute towards the bond strength. For example, larger bar size increases the bond strength, but it requires larger development length in order to gain the same bond stresses, as in the case of small bar size (ACI 408, 2003).

Relative Rib Ratio (R_r)

Relative rib ratio is the ratio between the bearing area and the shearing area (Figure 2.8). “Bearing area is the area of ribs perpendicular to the bar axis and the shearing area is the surface area between the ribs” (ACI, 408, 1992). The bond behaviour is highly dependent on the relative rib ratio (R_r) (ACI 408, 1992). R_r values vary from 0.05 to 0.08 (ACI, 408, 1992).

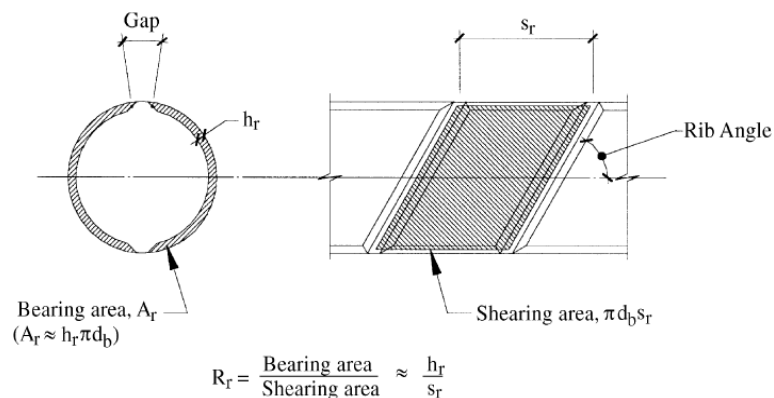


Figure 2.8 Relative rib ratio (R_r) (ACI 408, 2003)

The bond strength increases with an increase in R_r (Rehm and Eligehausen, 1979; Soretz and Holzenbeim, 1979; Balaazs, 1986; Eligehausen, 1977; Rehm and Eligehausen, 1977). In case of reverse cyclic loading, a reduction in the free end slip (50 to 70%) and loaded end slip (30 to 40 %) was observed if R_r increased from 0.085 to 0.119 (Zuo and Darwin, 2000). Also, R_r affects the bond fatigue performance (Zheng and Abel, 1998).

Bar Casting Position

In top cast bars, the direct contact between the steel bar and the concrete is reduced due to the accumulation of bleed water which results in lower bond strength compared to bottom cast bars (ACI 408, 2003).

Steel Strength

As the steel strength increases the bond strength increases. Due to higher steel strength, higher bond stresses are required in order to yield the bar (Equation 4.3) (ACI 408, 1992).

Confinement

Bond strength increases with the increase in the confinement level in the bond anchorage zone. Internal confinement includes transverse reinforcement (steel stirrups), fibres in the concrete mix and concrete cover. FRP wrapping is used as an external confinement which increases the bond stiffness and improves the post ductility failure. A sufficient level of confinement also affects the bond failure mode (Sections 2.4.1, 2.5 and 2.7).

Bar Surface Condition

The bar surface condition affects the frictional properties which ultimately contribute towards the bond strength. A decrease in the steel bar contact with the concrete will result if the steel bar surface is not clean from dust, mud or other non-metallic materials. Bar surface condition can be made non-favourable to corrosion by coating it with an epoxy coating. This will reduce the frictional component of the bond force and result in decreased bond strength (ACI 408, 2003).

2.4.3 Bond Test Specimens

Pull out and beam specimens (Figure 2.9) are commonly used in the experimental evaluation of the bond strength.

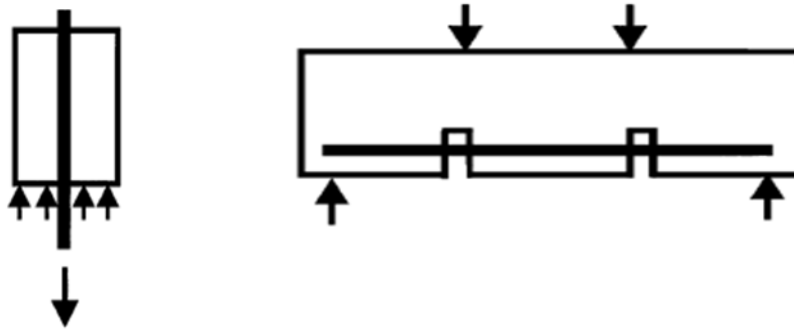


Figure 2.9 Pull out and beam specimen (ACI 408, 2003)

Pullout specimen does not capture the realistic bond behaviour and gives higher bond strength than the actual situation due to the following reasons; 1) the bearing of a big block on the surface prevents the splitting of the block due to its bigger size and the local bearing compression forces it produces; 2) pullout specimen does not consider the confinement effect of transverse reinforcement; and 3) the surrounding concrete around the reinforcing steel bar in case of a pullout specimen, is in compression (ACI 408, 2003). Therefore, specimens such as beam-end specimen, beam anchorage specimen and splice specimen gives a better representation of bond behaviour and bond strength (ACI 408, 2003).

2.5 Confinement of FRP in Bond Anchorage Zone

Various studies have been conducted in the past to observe the effect of FRP wrapping on the bond anchorage zone. All these studies concluded that FRP wrapping in the bond anchorage zone increased the bond strength by confining the concrete (Figure 2.10), which does not allow the cracks to propagate. Some of the previous studies are summarized below.

Kono et al. (1998) studied the effect of FRP confinement on the bond strength. They found an eighty percent increase in bond strength due to FRP wrapping (Kono et al., 1998). Also, in their study, the amount of FRP along the development length was evaluated. In another experimental study, Kono et al. (1999) concluded that the confinement provided by the FRP sheets increased the bond strength up to 115%. Hamad et al. (2004a, b, c) and Harajli et al. (2004) tested FRP confined bond beam specimens and proposed an equation for the additional bond strength provided by the FRP sheets. The FRP confinement also improved the post failure

ductility behaviour (Harajli et al., 2004; Hamad et al., 2005). Rteil et al. (2005) observed a 38% increase in bond strength due to CFRP wrapping in the bond critical region.

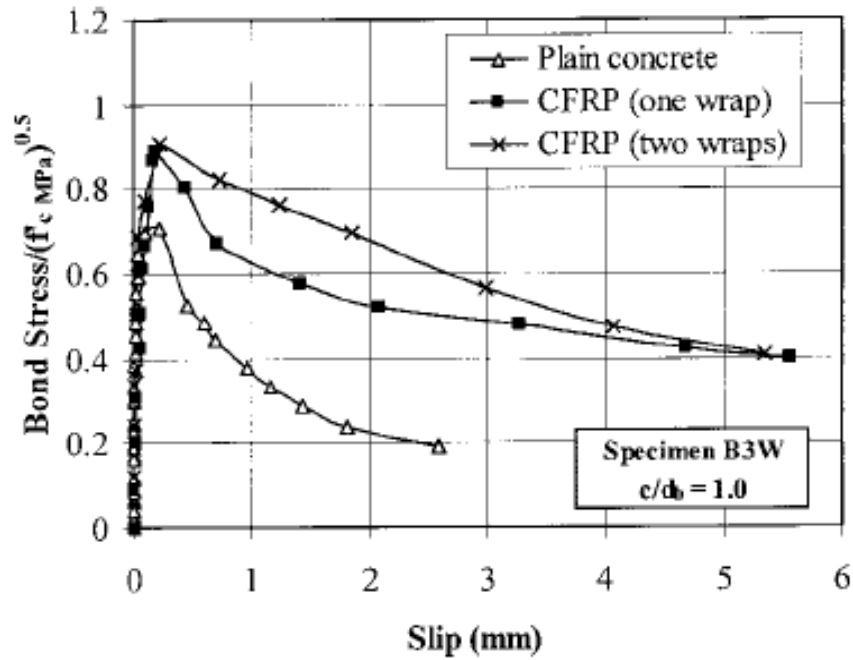


Figure 2.10 Effect of FRP confinement (Harajli et al., 2004)

In short, FRP sheets increased the bond strength due to an increase in the confinement forces that held the splitting cracks from opening further. Also, FRP sheets changed the bond stress-slip response due to improved bond ductility behaviour.

2.6 Effect of Corrosion on Bond

Experimental studies showed an increase in bond strength during the initial level of corrosion (Figure 2.11) (Al-Sulaimani et al., 1990; Almusallam et al., 1996; Mangat et al., 1999; Amleh and Mirza, 1999; Fang et al., 2004). This initial increase in bond strength was attributed to the formation of a firm layer of corrosion product that increased the confinement around the steel bar which results in an increased bond strength.

The bond strength decreased dramatically after the development of longitudinal corrosion cracks (Figure 2.11). This rapid decrease in bond strength was due to the loss of bearing component as the ribs of the reinforcing bars being reduced by corrosion, decrease in the frictional component of the bond force due to the deposition of the corrosion products, and

expansion of the longitudinal cracks that decreased the concrete confinement (Al-Sulaimani et al., 1990; Almusallam et al., 1996; Mangat et al., 1999; Amleh and Mirza, 1999; Fang et al., 2004).

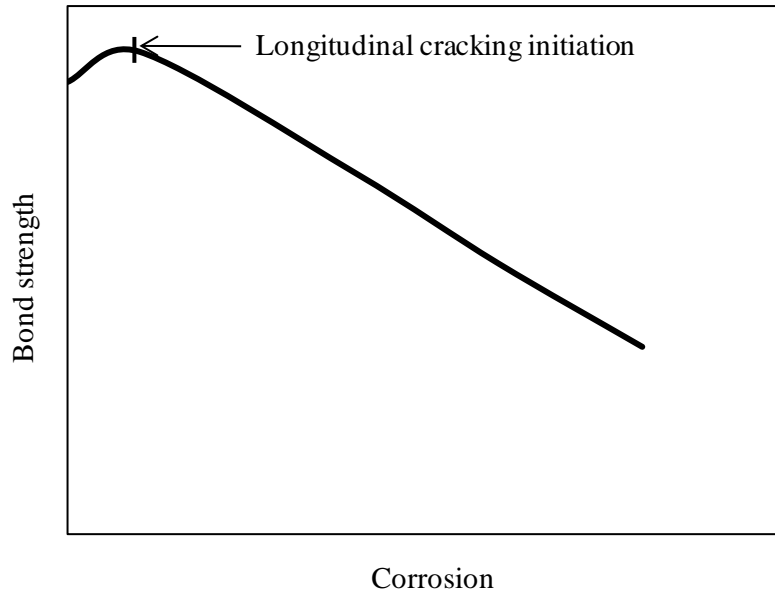


Figure 2.11 Schematic of the effect of corrosion on bond strength

Researchers used different analytical and numerical approaches in order to model the effect of reinforcement corrosion on bond between the reinforcing steel bar and the surrounding concrete (Berra et al., 2003; Fang et al., 2006; Amleh and Ghosh, 2006; Tastani et al., 2007). Most of these models were based on tests using pullout specimens.

2.7 Effect of FRP Confinement on the Bond Behaviour of Corroded Steel Bar

Wrapping the bond region of a corroded beam by FRP sheets increased the bond performance due to the prevention of further propagation of corrosion cracks by confining the concrete and increasing its transverse resistance, as seen in Figure 2.12 (Soudki and Sherwood, 2000, 2003). Experimental results also showed that the failure mode was affected by the FRP confinement. It changed splitting to pullout failure and splitting to flexure failure in pull out and beam specimens, respectively (Craig and Soudki, 2005).

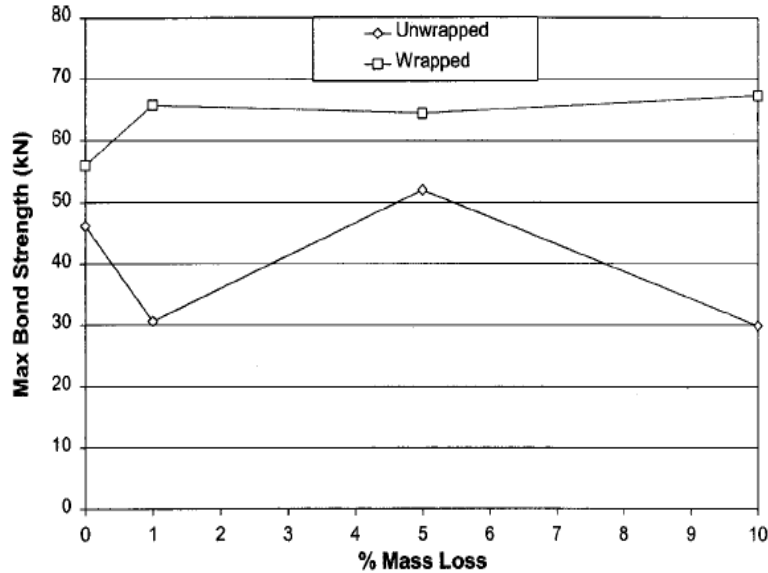


Figure 2.12 Bond strength under FRP confinement and corrosion (Soudki and Sherwood, 2003)

2.8 Bond Behaviour under Repeated Cyclic Loading

Cyclic loadings are classified into two categories. Loading which contains less than 100 cycles are termed as low cyclic loading. In low cyclic loading, the bond stress ranges are higher than 80% of the ultimate bond stress (ACI 408, 1992). Examples of low cyclic loading are seismic loading and high wind loadings. The second type of cyclic loading is called high cyclic loading, which is also referred to as fatigue loading. As the name indicates, the high cyclic loading contains millions of cycles, but has bond stresses that are less than 40% of the ultimate bond stress (ACI 408, 1992). Traffic loadings on bridges and structural member subjected to a continuous type of vibratory motion are examples of high cyclic loading. Fatigue loadings are problematic even at service loads (ACI 408, 1992).

The progressive deterioration of bond (due to cyclic loading) affects the serviceability of reinforced concrete structures and results in a bond fatigue failure. Experimental results showed that the serviceability and the fatigue strength of a reinforced concrete member is greatly dependant on the bond between the steel and the concrete (Mor et al., 1992; Bresler and Bertero, 1968; Balazs, 1991; Plizzari et al., 2002). The fatigue phenomena can be analyzed by observing the slip behaviour as the number of cycles of loading increases (Balazs, 1991). The following were the conclusions made from the previous studies on the bond under cyclic loading:

- The bond stresses were higher during the first cycle at the loaded ends of the specimen and gradually decreased to zero at the free end because there were no stress transfer in that region. When the concrete cracked, a redistribution of stresses took place (Bresler and Bertero, 1968).
- The peak bond stress was shifted, as the number of loading cycles increased, from the loaded to the free end. An increase in the bond stress (65% to 90%) was observed at the free end due to the reduction in the loaded end due to the application of repeated loading (Perry and Jundi, 1969).
- The slip behaviour of steel reinforcement was the primary factor responsible for the bond failure in case of cyclic loading. The variation of slip behaviour with the increased number of loading cycles is shown in Figure 2.13 (Balazs, 1991).

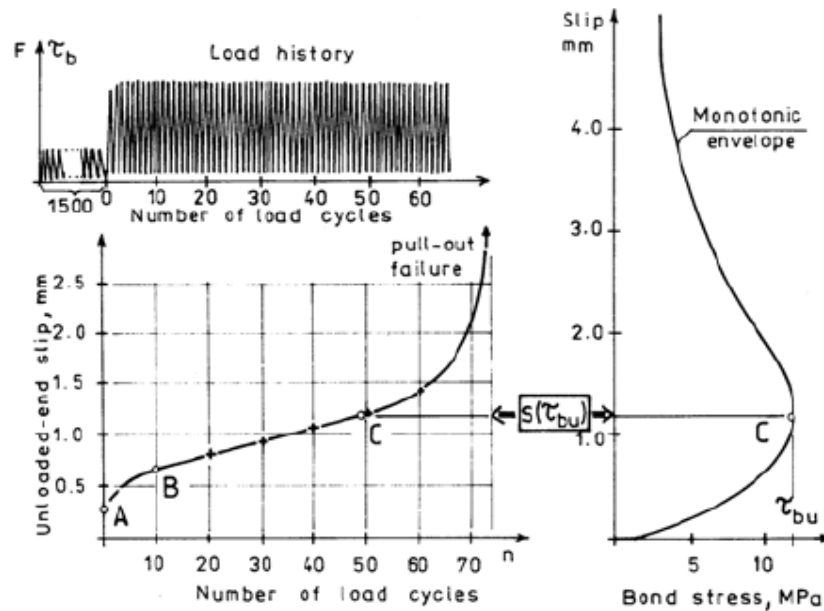


Figure 2.13 Reinforcing steel slip behavior under cyclic loading (Balazs, 1991)

- Specimens which failed in bond under static loading were more vulnerable to fatigue bond failure in cyclic loading. Concrete strength and development length were the main controlling factors under cyclic repeated loading (Verna and Stelson, 1962; Rehm and Elinghausen, 1979).

- The slip behaviour of steel reinforcement can be controlled by providing an internal (steel fibres, steel stirrups) or external confinement. This will increase the fatigue bond strength by reducing the splitting cracks and hence the reinforcing bars slip (Plizzari et al., 2002).

2.8.1 Oh and Kim Model

To the author's best knowledge, the only model in the literature includes the effect of fatigue loading was proposed by Oh and Kim (2007). In this model, the cyclic bond stress-slip relation was proposed based on the experimental data generated by the authors.

The cyclic slip (s_N) was expressed as a function of the initial slip (s_l) and the number of cycles (N) of loading as shown below:

$$s_N = s_1 N^b, \quad b = 0.098 \text{ from experimental data}$$

Similarly the residual slip was expressed as follows:

$$s_{rN} = s_{r1} N^{rb}, \quad b = b_r$$

Based on their experimental data Oh and Kim (2007), derived the residual slip as follows:

$$s_{r1} = s_1 [2(\mathcal{T}_{rep}/\mathcal{T}_{max}) - (\mathcal{T}_{rep}/\mathcal{T}_{max})^2], \quad s_{r0} = 0$$

Where s_l is the initial slip and $\mathcal{T}_{rep}/\mathcal{T}_{max}$ is the repeated bond stress level.

The bond stress-slip relation after N number of load cycles and fatigue bond life (N_f) model were proposed by Oh and Kim (2007) as follows:

$$\mathcal{T}_N = 0, \quad s < s_{r(N-1)}$$

$$\mathcal{T}_N = \mathcal{T}_{max} \left(\frac{s - s_{r(N-1)}}{s_{p1}} \right)^{\alpha_N}, \quad s \geq s_{r(N-1)}$$

$$\text{Where, } \alpha_N = \frac{\alpha_1}{N^{0.092} (\mathcal{T}_{rep}/\mathcal{T}_{max})}$$

Table 2.2 Details of experimental setup (Rteil, 2007)

Group		Corrosion level when FRP applied	Corrosion level when tested	Number of specimens	Remarks
		(Days)	(Days)		
Monotonic	M	No FRP	0	1	Control beams
		0	0	1	
Cyclic	UW0	No FRP	0	5 to 10	Specimen depends on different load ranges
	UW5	No FRP	50		
	UW9	No FRP	100 or 150		
	W0	0	0		
	W5	50	50		
	W9	100 or 150	100 or 150		

The experimental results showed that the corroded and uncorroded beam specimens failed due to the splitting of the concrete. In case of uncorroded unwrapped beams, the concrete cover was pushed away as the number of loading cycle increased (Figure 2.15). On the other hand, the confinement of FRP sheets changed the bond behaviour; the concrete in front of the steel bar lugs was crushed and the bottom cover was cracked (Figure 2.16). The increase in initial slip and failure slip was observed as the maximum load applied and the corrosion level increased (Rteil, 2007).



Figure 2.15 Unwrapped corroded beams (Rteil, 2007)

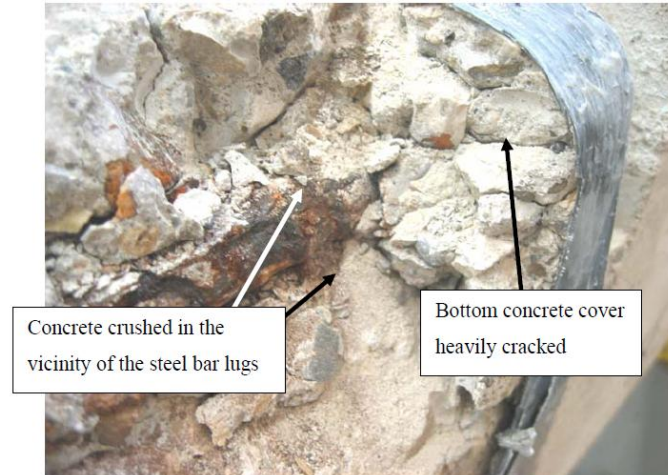


Figure 2.16 FRP wrapped corroded beams (Rteil, 2007)

It was observed by Rteil (2007) that the FRP wrapped beams had a smaller number of cracks than the unwrapped specimens. Also, FRP sheets increased the fatigue bond life compared to unwrapped specimens at all corrosion levels. The load range-fatigue bond life plots showed a linear behaviour on logarithmic scale (Rteil, 2007). The detailed experimental results of the fatigue bond life for both unwrapped and FRP wrapped beam specimens are shown in Appendix A.

In his study, Rteil (2007), measured the loaded end slip and the free end slip and it was observed that the loaded end slip was higher than the free end slip. This was due to the fact that the loaded end slip consists of rigid body motion, as well as the elastic and plastic elongation of the steel reinforcement bar. Experimental results showed that in case of unwrapped beam specimens the slip increased at a very low rate up to 85 to 95 percent of the beam's life and then a dramatic increase in slip was observed up to failure (Figure 2.17). Rteil (2007) explained this behaviour of slip as follows: initially the concrete in between the reinforcing bar ribs prevented the steel bar from slippage but when the tensile stresses increased sufficiently due to crack propagation, a decrease in the concrete confinement ability resulted in increased slip (Rteil, 2007).

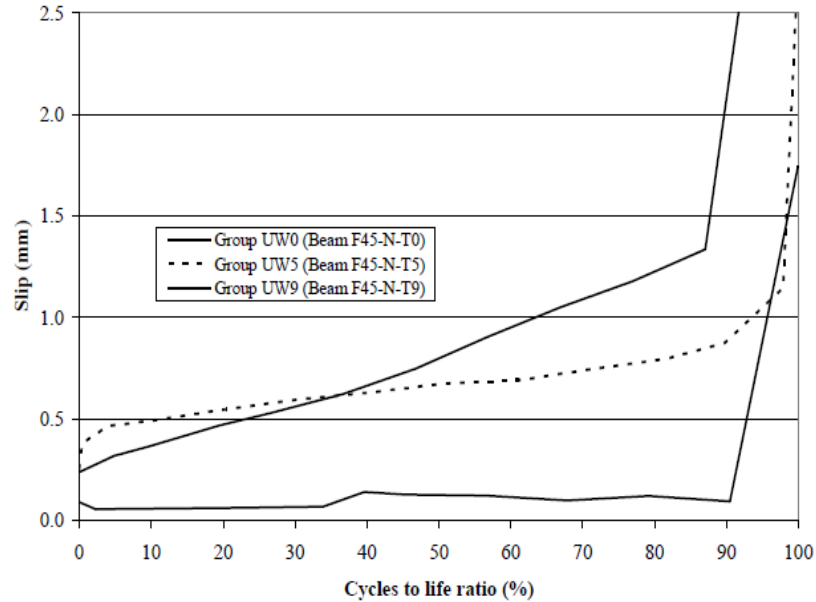


Figure 2.17 Slip behavior for unwrapped beam specimen (Rteil, 2007)

The confinement of FRP wrapping changed the initial behaviour of the slip. Rteil (2007) observed a high increase in slip during the first 5 to 10 percent of the beam's life (Figure 2.18) than the unwrapped beam specimens. This was explained as follows: at the start of the loading cycles, the confinement effect of FRP sheets was not fully utilized (shown from the FRP strain reading). The concrete cover was pushed away by the hoop stresses generated due to slip increased which pushed the concrete cover outward. Due to this, FRP sheet was under tensile stresses and bottom concrete cover was under compressive forces. Therefore, the concrete around the steel ribs was crushed and propagated the cracks along the reinforcing steel bar towards the concrete surface, which ultimately increased the stress in the FRP sheet. Due to this, the slip behaviour showed a constant increase up to 85 to 90 percent of the beam's life (Figure 2.18) due to the contribution of the FRP sheets which held the cracks from further propagation. The last 5 to 10 percent of the beam's life showed a dramatic increase in the slip (Rteil, 2007).

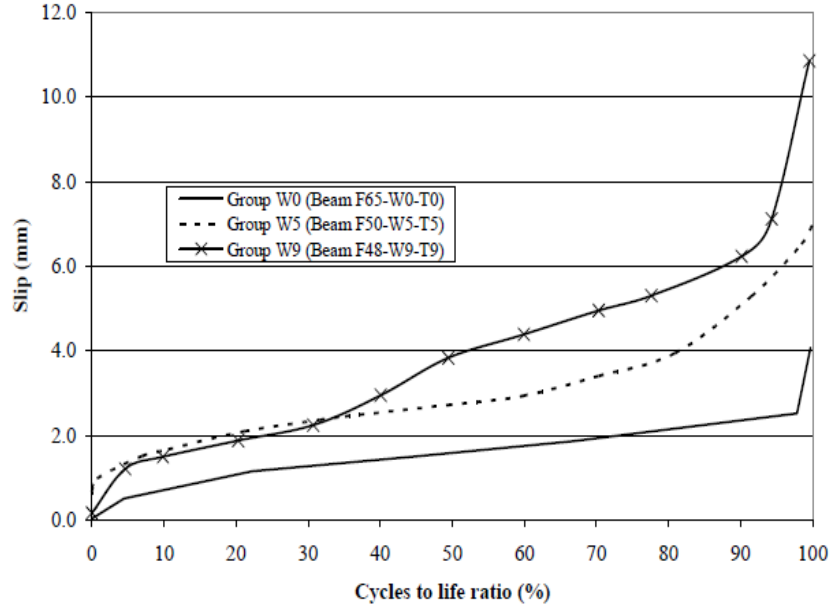


Figure 2.18 Slip behavior for FRP wrapped beam specimen (Rteil, 2007)

In his study, Rteil (2007) proposed a fracture mechanics model based on the fatigue crack-growth analysis. The slip in the steel bar was considered a damage criterion in this study. A bond stress intensity factor (K_{bond}) was proposed as follows:

$$K_{bond} = (u_{max}P)\sqrt{s}$$

Where u_{max} is the maximum static bond stress, P is the ratio of the maximum load applied to the static capacity, and s is the slip of reinforcing bar.

The relationship between the cyclic slip growth rate (ds/dN) and K_{bond} was proposed by Rteil (2007) as follows:

$$\frac{ds}{dN} = C(K_{bond})^m = C[(u_{max}P)\sqrt{s}]^m \quad \text{Equation 2.7}$$

In Equation 2.7, C and m are constants that depend on the corrosion level and the confinement. The fatigue bond life can be determined by integrating Equation 2.7 between initial slip (s_i) and final slip (s_f) as follows:

$$N_f = \frac{s_f^{1-m/2} - s_i^{1-m/2}}{C(u_{max}P)^m(1 - \frac{m}{2})} \quad \text{for } m \neq 2$$

The model proposed by Rteil (2007) was based on the scattered data therefore it is not reliable.

2.10 Research Motivation

It is evident from the literature presented that numerical and analytical modeling of the corroded steel-FRP confined concrete bond under fatigue cyclic loading is lacking. Also it is noted that only few researchers studied the theoretical aspects of the steel-concrete bond under different scenarios (corrosion, repeated loading and external confinement using FRP) where most of them used a pull out specimen (which does not capture the exact bond behaviour) for their experimental and analytical investigation.

Bond models based on beam specimens that considered the combined effect of corrosion of reinforcement, FRP confinement and fatigue cyclic loading are needed in order to evaluate the exact behaviour and performance of RC structures.

2.11 Research Objectives

Based on the literature review and the identified gaps, the following objectives were set for this study;

- To develop a numerical model for slip, which indicates the deterioration of bond after ‘ N ’ number of loading cycles with consideration of corrosion and loading ranges as well as the FRP wrapping. This will help in understanding the performance of reinforced concrete (RC) structures under adverse environmental and loading conditions.
- Development of static and cyclic bond stress-slip ($u-s$) model in order to analyze cracks, as well as to determine the deflection and the ultimate capacity of RC members.
- Analytical derivation of cyclic slip versus development length that will provide an assessment tool for structural engineers. This model will be used to predict the fatigue bond life of RC structures.

Chapter 3: Numerical Modeling

3.1 General

The bond between steel and concrete dictates the performance of reinforced concrete (RC) structures at service and ultimate loads. Therefore, bond should be considered in the design of new structures and in the analysis of existing structures in order to evaluate the exact behaviour of RC structures subjected to static or cyclic loading. In this chapter, a numerical modeling of the bond associated parameters will be discussed. These models are based on the experimental results of Rteil (2007). Two models have been developed: 1) slip-fatigue (s-N) model, and 2) bond stress-slip (u-s) model. These models consider the effect of steel corrosion, the fatigue cyclic loading and the external confinement provided by FRP sheets. The slip-fatigue relationship was obtained by using non-linear regression analysis on the experimental data. Slip-fatigue model can be used in finite element method (numerical method) in order to define the bond properties for the bond element. The bond stress versus slip modeling under cyclic loading was performed by modifying the bond stress-slip law that was proposed by Harajli et al. (2004) for static loading. This modification was done in order to consider the effect of reinforcement corrosion and fatigue cyclic loading. Bond stress-slip model will be used in developing the analytical relationship between the cyclic slip and the development length needed for the steel reinforcement in order to avoid bond failure (Section 4.2). These models will be used to predict the fatigue bond life.

3.2 Slip-Fatigue Model

Under fatigue cyclic loading, bond deterioration results in longitudinal cracking and crushing of the concrete in front of the steel reinforcing bar ribs which caused the bar to slip. Therefore, bond deterioration can be measured by observing the slip increase (Rteil, 2007; ACI 408, 2003). In this study, free end slip was considered in order to only take the effect of the rigid body motion of the steel bar.

3.2.1 For Unwrapped Beam Specimen

The slip behaviour for unwrapped beam specimens was categorized into two phases. Phase 1 shows a constant behaviour of slip, and in the second phase, a dramatic increase in the slip was observed up to failure, as illustrated by Rteil's (2007) experimental study (Section 2.9). The schematic representation of the slip behaviour for unwrapped beam specimens is shown in Figure 3.1. ' S_i ' is the initial slip (free end slip at the maximum load of first cycle); ' S_f ' is the final slip (indicates the complete loss of steel-concrete bond); and ' N_f ' is the fatigue bond life. From the experimental results (Rteil, 2007) it was shown that the slip-cycle relationship is dependent on the corrosion level (a), initial slip (S_i) and final slip (S_f). The length of Phase 1 and 2 (Figure 3.1) depends on the loading range applied. The duration of Phase 1 is higher (about 90% of the specimen life) for specimens subjected to a lower loading range. When the beams were subjected to a high loading range, then the duration of Phase 1 decreased to about 30% of the beam's life (Rteil, 2007).

From the experimental results (Rteil, 2007), it was concluded that initial slip and final slip were dependent on the load range applied, as well as the corrosion level. Also, a linear relationship was suggested by the experimental results (Rteil, 2007) between the initial slip (and final slip) and the applied load range as illustrated by Figure 3.2 and Figure 3.3 for each corrosion level.

Accordingly, the following equation was proposed to model the slip-fatigue behaviour.

$$S_N = S_i + \frac{S_f N^a}{N^a + (0.95N_f)^a} \quad \text{Equation 3.1}$$

Where ' S_N ' is the slip after ' N ' number of cycles and ' a ' is the corrosion dependent variable (Table 3.1).

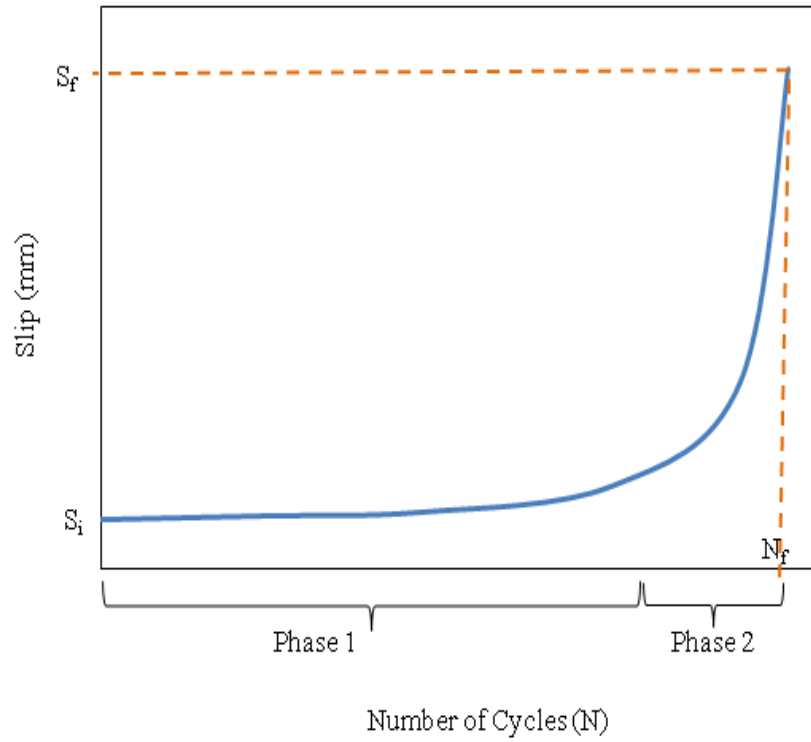


Figure 3.1 Slip behaviour for unwrapped specimens

The initial (S_i) and final slip (S_f), which were found to be a function of the loading range (P) and corrosion level, were modeled by a linear relationship on a semi logarithmic scale.

$$S_i = f \text{Log} P - g \quad \text{Equation 3.2}$$

$$S_f = h \text{Log} P - l \quad \text{Equation 3.3}$$

Where f , g , h and l are corrosion dependent variables (Table 3.1). P is the applied load range in percentage of the specimen's static capacity. Figure 3.2 and Figure 3.3 show the model prediction (Equations 3.2 and 3.3) and the experimental values of the initial and final slip for unwrapped beam specimens for 0%, 5% and 9% corrosion level respectively.

Table 3.1 Corrosion dependent variables for unwrapped beam specimen

Factors	Corrosion level (%)		
	Zero	Five	Nine
f	0.40	0.50	12
g	0.63	0.60	18.50
h	52	15	40
l	82	19	58
a	26	10	30

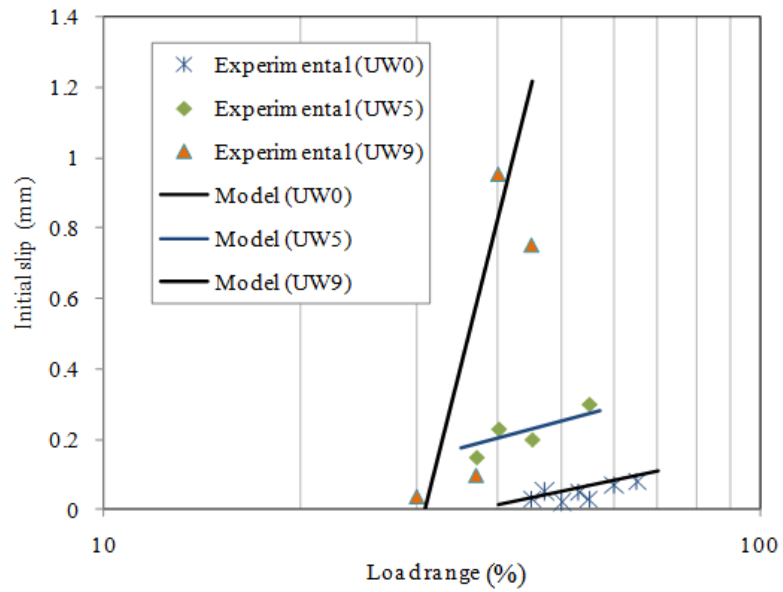


Figure 3.2 Initial slip variation for unwrapped beam specimens

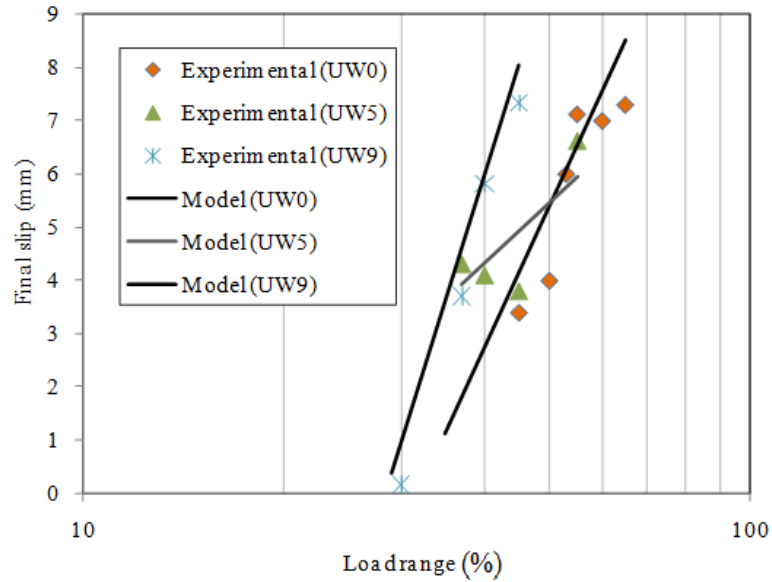


Figure 3.3 Final slip variation for unwrapped beam specimens

Model Implementation

Figure 3.4, Figure 3.5, and Figure 3.6 show a typical slip variation with number of cycles predicted from Equation 3.1 plotted against the experimental results. Complete plots for all the tested specimens are in Appendix B. The ratio of predicted values from Equation 3.1 and the experimental slip ($S_{model} / S_{experimental}$) was 1.11, 1.02, and 0.84 for zero, five, and nine percent corrosion levels respectively. The standard deviation for 0%, 5%, and 9% corrosion levels were 0.16, 0.034, and 0.14 for unwrapped beam specimens respectively. The correlation coefficient for the experimental slip and the slip that was predicted from the model (Equation 3.1) was 0.86, 0.94 and 0.85 for 0%, 5% and 9% corrosion level respectively. At 95% of confidence interval, the average ratio $S_{model}/S_{experimental}$ varied from 0.97 to 1.26, 0.98 to 1.06 and 0.68 to 1.0 for 0%, 5% and 9% corrosion level respectively. The model (Equation 3.1) satisfactorily predicts the experimental behaviour (Figure 3.4, Figure 3.5 and Figure 3.6).

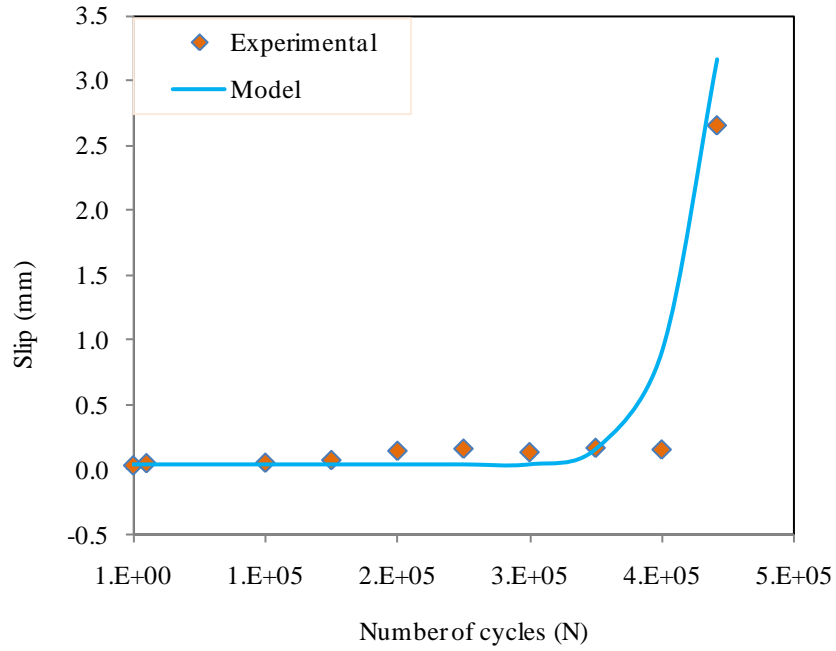


Figure 3.4 Typical slip-cycle variation for UW0 (F45-N-T0)

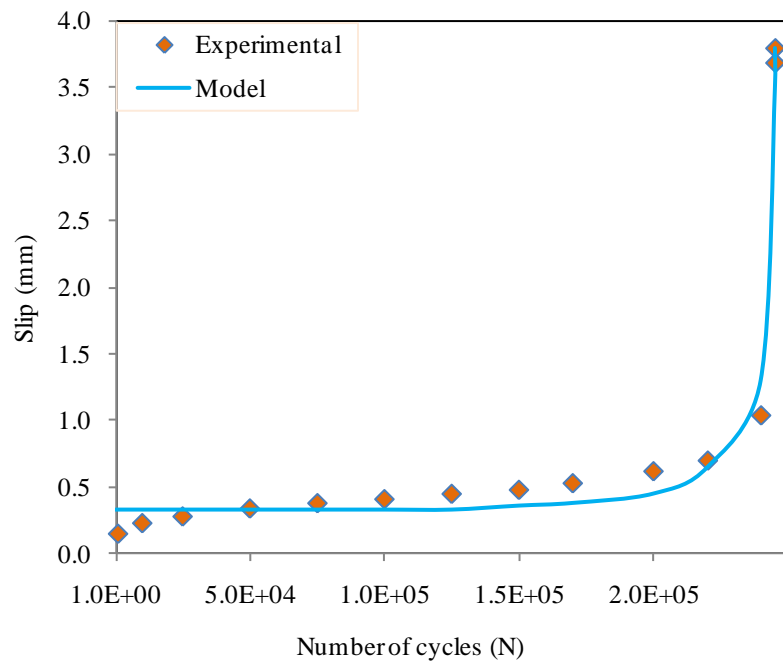


Figure 3.5 Typical slip-cycle variation for UW5 (F45-N-T5)

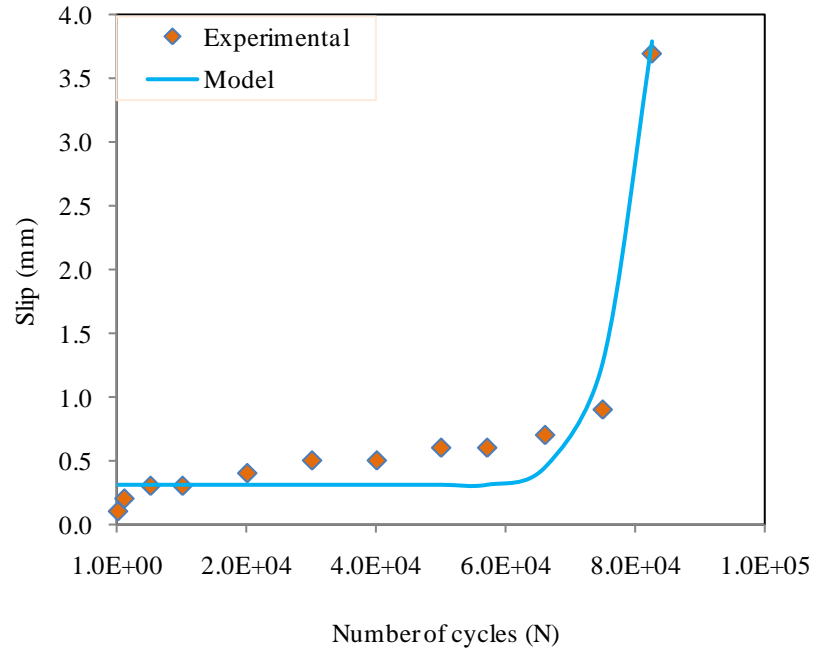


Figure 3.6 Typical slip-cycle variation for UW9 (F37-N-T9a)

It should be noted that the initial slip of the corroded unwrapped beams was higher than their uncorroded counterparts (Figure 3.5 and Figure 3.6) because the concrete was already cracked due to corrosion before the application of cyclic loads.

3.2.2 FRP Wrapped Beam Specimen

Rteil (2007) observed that the slip behaviour for FRP wrapped beam specimens followed a three phase process (Figure 3.7). The slip increased exponentially in the first phase (5 to 10% of the beam's life) due to the application of higher load range as compared with the unwrapped tested specimens. Phase 2 showed a continuous increase in the slip (85 to 90% of the beam's life) but at a very low rate (Figure 3.7). During this phase, the confinement effect of FRP sheets was utilized. A rapid increase in slip was observed during the 3rd phase leading to failure (Section 2.9). The duration of each phase was dependent on the load range applied and the corrosion level (Rteil, 2007).

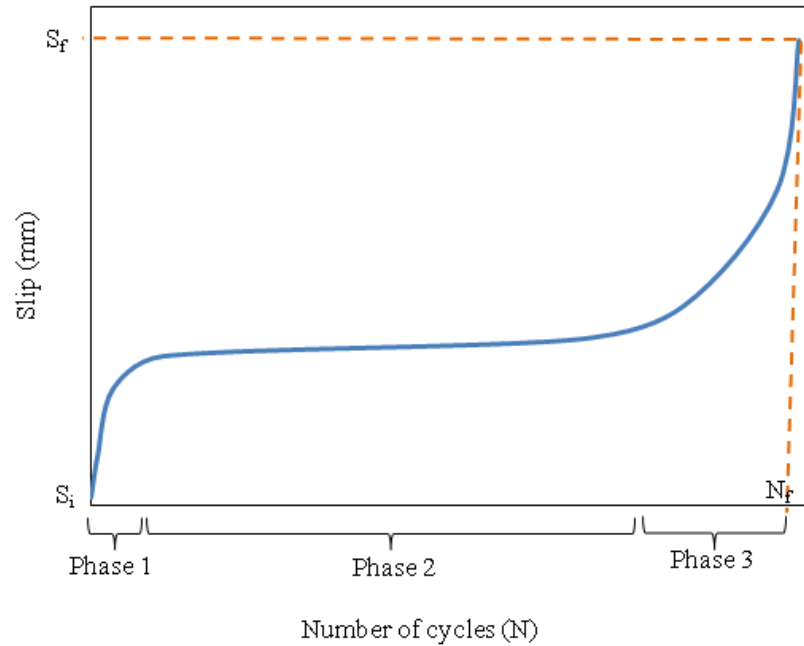


Figure 3.7 Phases of slip behaviour for FRP wrapped beam specimen

As with the unwrapped specimens, experimental results for FRP wrapped specimens (Rteil, 2007) showed that the slip-fatigue relation is a function of the initial slip, the loading range, the corrosion level, and the fatigue bond life in the case of FRP wrapped beam specimens. Accordingly, the slip-fatigue for FRP wrapped case was modeled as follows.

$$\frac{S_N}{PS_{max}} = S_i + C_1 \left(\frac{N}{N_f}\right)^3 - C_2 \left(\frac{N}{N_f}\right)^2 + D \left(\frac{N}{N_f}\right) \quad \text{Equation 3.4}$$

Where S_{max} is the maximum slip under static loading (calculated using Equation 3.12), P is the applied loading range in percentage of static capacity, C_1 and C_2 are corrosion dependant constant (Table 3.2), (N/N_f) is the percentage of cycle to life ratio and D is a variable which depends on the corrosion level and the applied loading range (P).

In case of FRP wrapped specimens, the initial slip ' S_i ' was higher than the corresponding unwrapped beam specimen because the FRP wrapped specimens were tested at a higher load range than the unwrapped ones. Also, just like the unwrapped specimens, the initial slip varies as the corrosion level changed (Rteil, 2007). Therefore, the initial slip ' S_i ' was modeled (Equation 3.5) as a function of the loading range and the corrosion level using a linear relationship on a

semi logarithmic scale. Also, in order to calculate the value of ‘ D ’ in Equation 3.4, a linear relationship on a semi logarithmic scale was proposed (Equation 3.6).

$$S_i = m \text{Log} P - n \quad \text{Equation 3.5}$$

$$D = p - q \text{Log} P \quad \text{Equation 3.6}$$

Where m , n , p and q are corrosion dependent variables (Table 3.2). Figure 3.8 shows a good correlation between the predicted initial slip (Equation 3.5) and the experimental values. Figure 3.9 shows the general trend of the values of D for 0%, 5% and 9% corrosion level respectively for FRP wrapped beam specimen.

Table 3.2 Corrosion dependent variable for FRP wrapped beam specimen

Factors	Corrosion level (%)		
	Zero	Five	Nine
m	0.70	0.70	0.70
n	1.15	1.02	1.02
p	1.50	0.90	2.50
q	0.76	0.39	1.32
C_1	1.5×10^{-5}	3.0×10^{-5}	2.5×10^{-5}
C_2	2.0×10^{-3}	4.2×10^{-3}	4.0×10^{-3}

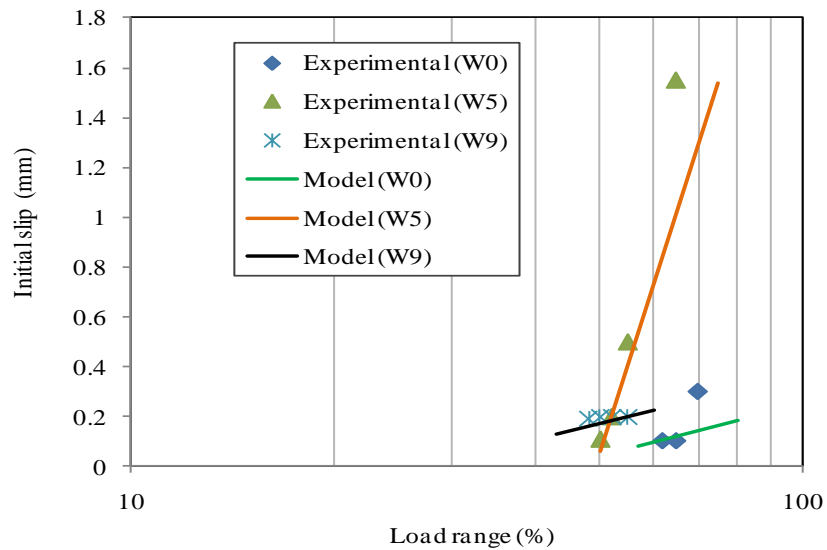


Figure 3.8 Initial slip variation for FRP wrapped specimens

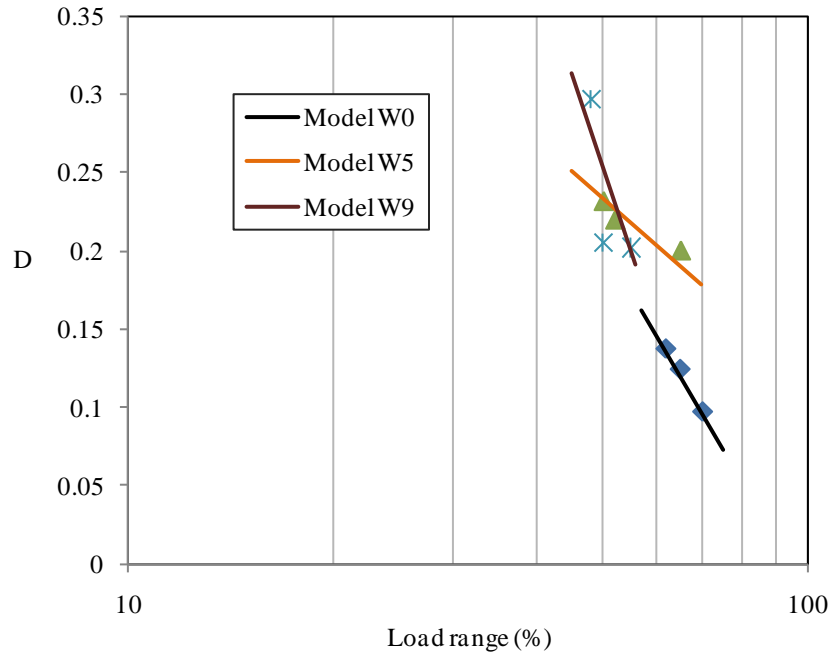


Figure 3.9 Variation of D with the load range (FRP wrapped beams)

Model Implementation

Figure 3.10, Figure 3.11, and Figure 3.12 compare the experimental results versus the predictions from Equation 3.4 for a typical specimen with zero, five, and nine percent corrosion levels respectively. All plots of FRP wrapped tested beams are in Appendix C. The ratio $S_{\text{model}}/S_{\text{experimental}}$ was 0.90, 0.85, and 0.80 for zero, five, and nine percent corrosion level respectively. The standard deviations were 0.067, 0.10, and 0.13 for 0%, 5%, and 9% corrosion level respectively, in case of FRP wrapped beam specimens. The correlation coefficient for the experimental slip and the slip that was predicted from the model (Equation 3.4) was 0.98 for all levels of corrosion. At 95% of confidence interval, the average ratio $S_{\text{model}}/S_{\text{experimental}}$ varied from 0.86 to 0.94, 0.94 to 1.04 and 0.71 to 0.89 for 0%, 5% and 9% corrosion level respectively. For FRP wrapped case, as shown by Figure 3.10, Figure 3.11 and Figure 3.12, the experimental results are in good correlation with the model prediction (Equation 3.5).

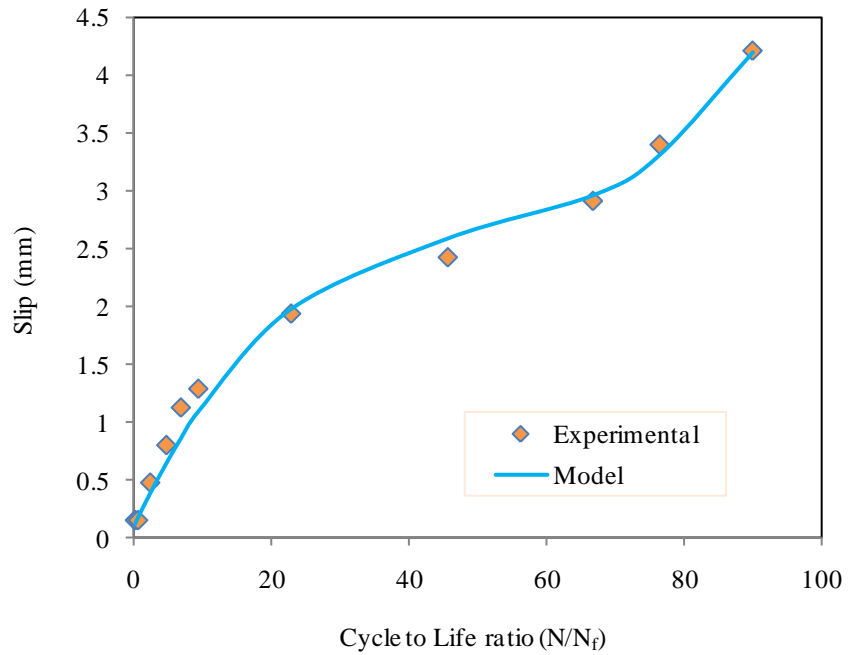


Figure 3.10 Typical slip-cycle variation for W0 (F65-W0-N0)

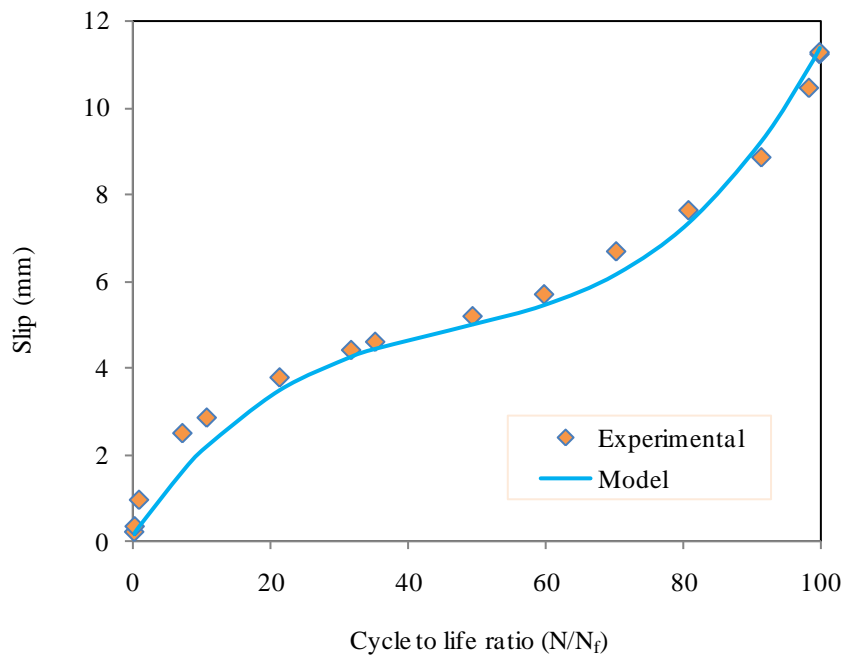


Figure 3.11 Typical slip-cycle variation for W5 (F50-W5-N5)

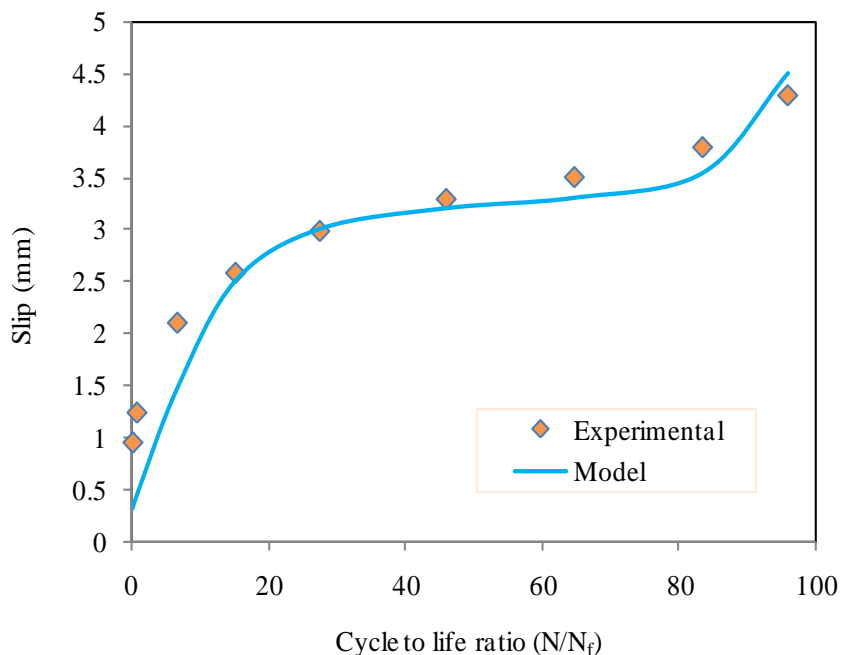


Figure 3.12 Typical slip-cycle variation for W9 (F55-W9-T9a)

3.3 Bond Stress-Slip Model

Bond stress is defined as the shear stress in the direction of steel bar which changes the steel stress by transferring the forces between the steel and the concrete (ACI 408, 1992). In this study, an average bond stress was considered along the steel-concrete interface. The bond stress-slip relation is important in RC structures in order to analyze cracks, as well as to determine the deflection and the ultimate capacity of RC members (Oh and Kim, 2007; Mor et al., 1992; Bresler and Bertero, 1968; Balazs, 1991; Plizzari et al., 2002). Bond stress-slip ($u-s$) relation could be thought of as the constitutive relation for the bond, which is equivalent to stress-strain curve for other materials. As such, it can be used to define the material properties for the bond element in the finite element simulation (Section 3.3.2). Also, the proposed bond stress-slip model will be incorporated in the analytical modeling (Section 4.2) in order to formulate the cyclic slip and the development length relationship.

3.3.1 Bond Stress-Slip under Static Load

In this study, the bond stress-slip law that was proposed by Harajli et al. (2004) for the static loading was used in order to model the bond stress-slip behaviour for the unwrapped and FRP wrapped beam specimen under static loading.

Figure 3.13 shows the bond stress-slip envelope for the pull out and the splitting failure. The splitting failure envelope consists of four phases that explain the bond behaviour during static loading. As loads are applied, the initial stiffness of the bond in a splitting bond failure is similar to that of a pullout failure. The first phase ends when an increase in the residual stress component of the bond force results in the development of splitting tensile cracks. Once a splitting crack develops the behaviour of the bond stress-slip relation deviates from the pull out behaviour due to the decrease in the bond stiffness as the crack propagates in the concrete cover. The second phase ends when the crack has expanded to the surface and the splitting of the concrete cover takes place. This indicates a complete deterioration of the bond (s_{max} , u_{max}). The third phase of the bond behaviour shows a dramatic drop in the bond stress (Figure 3.13). This decrease in bond stress continues until the equilibrium is developed between the post splitting tensile forces in the concrete and the bond forces (s_{ps} , u_{ps}). At this point, the fourth phase begins and ends at zero bond due to the expansion of the splitting cracks in the concrete (Harajli et al., 2004).

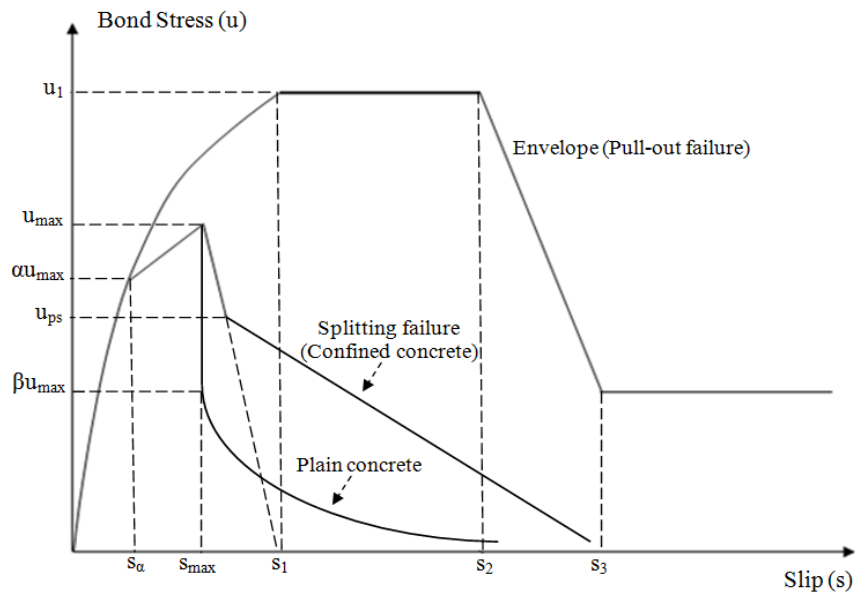


Figure 3.13 Bond stress versus slip (Harajli, Hamad and Rteil, 2004)

This expansion of splitting cracks can be controlled by providing external confinement (FRP wrapping) or internal confinement (steel stirrups). FRP wrapping confines the concrete and improves the post failure behaviour. This model was described mathematically by Harajli et al. (2004) as follows.

$$\left.
\begin{aligned}
u &= u_1 \left(\frac{s}{s_1}\right)^{0.3} && \text{for } s < s_\alpha \\
u &= u_{max} \left[\left(\frac{s - s_\alpha}{s_{max} - s_\alpha}\right) (1 - \alpha) + \alpha \right] && \text{for } s_\alpha < s < s_{max} \\
u &= u_{max} \left[1 + \left(\frac{s_{max} - s}{s_1 - s_{max}}\right) \right] && \text{for } s_{max} < s < s_{ps} \\
u &= u_{ps} \left[1 - \left(\frac{s - s_{ps}}{s_3 - s_{ps}}\right) \right] && \text{for } s_{ps} < s < s_3
\end{aligned}
\right\} \text{Equation 3.7}$$

Where ‘ u ’ is the bond stress (MPa); ‘ s ’ is the slip (mm); ‘ u_1 ’ is the maximum bond stress; and ‘ s_1 ’ is the slip for a pullout failure corresponding to ‘ u_1 ’. The following are the set of equations that define the different parameters of the bond stress-slip law (Harajli et al., 2004)

$$u_1 = 2.57\sqrt{f'_c} \quad \text{Equation 3.8}$$

$$s_1 = 0.15c_o \quad \text{Equation 3.9}$$

$$s_\alpha = s_1 \left(\frac{\alpha u_{max}}{u_1}\right)^{1/0.3} \quad \text{Equation 3.10}$$

$$u_{max} = A\sqrt{f'_c} \left(\frac{c+K_c}{d_b}\right)^{2/3} \leq u_1 \quad \text{Equation 3.11}$$

$$s_{max} = s_1 e^{\left(\frac{1}{0.3}\right)\ln\left(\frac{u_{max}}{u_1}\right)} + s_o \ln\left(\frac{u_1}{u_{max}}\right) \quad \text{Equation 3.12}$$

$$u_{ps} = u_{max}(B + K_{cs}) \leq u_{max} \quad \text{Equation 3.13}$$

$$s_{ps} = \left[\left(\frac{u_{max}-u_{ps}}{u_{max}}\right)(s_1 - s_{max}) + s_{max}\right] \left(\frac{K_c}{2}\right) \leq s_1 \quad \text{Equation 3.14}$$

Where c_o is the clear distance between the ribs of the reinforcing bar (s_3 is equal to c_o), f'_c is the concrete compressive strength, c is the clear concrete cover, d_b is the diameter of the steel bar, and s_o is a constant depending on the confinement level.

The confinement provided by steel stirrups and FRP sheets can be calculated by using the factors K_c and K_{cs} as follows (Harajli et al., 2004):

$$K_c = \frac{7A_{tr}}{sn} + \frac{28r_e A_{frp}}{sn} \quad \text{Equation 3.15}$$

$$K_{cs} = \frac{7.5A_{tr}}{snc} + \frac{28r_e A_{frp}}{snc} \quad \text{Equation 3.16}$$

Where s is the spacing between stirrups or FRP sheets; n is the number of reinforcing bars; A_{tr} and A_{frp} are the areas of steel stirrups and FRP sheets respectively; and r_e is the ratio of modulus of elasticity of FRP sheets to modulus of elasticity of steel.

Implementation of the Bond Stress-Slip Model

Table 3.3 shows the parameters used in this study related to the test specimen and their values for the unwrapped and FRP wrapped cases. The parameters α , A and B in Equations 3.10, 3.11, and 3.13 are constants based on the experimental results. The values of these parameters (α , A and B), found from the experimental results of Rteil (2007), for the calculation of bond stress-slip behaviour for the unwrapped and FRP wrapped beam specimen are shown in Table 3.4.

Table 3.3 Specimen parameters for bond stress slip relation

Constants	Unwrapped specimen	FRP wrapped specimen
c_o	10	10
f'_c	42	42
c	32.5	32.5
d_b	20	20
s_o	0.15	0.3

Table 3.4 Bond stress-slip relation parameters

Constants	Unwrapped specimen	FRP wrapped specimen
α	0.9	0.97
A	0.6	0.8
B	0.85	0.8

Figure 3.14 and Figure 3.15 shows the comparison of the predicted bond stress-slip variation from Equation 3.7 and the experimental results for unwrapped and FRP wrapped beam specimen respectively. The model gives a good prediction of the experimental results.

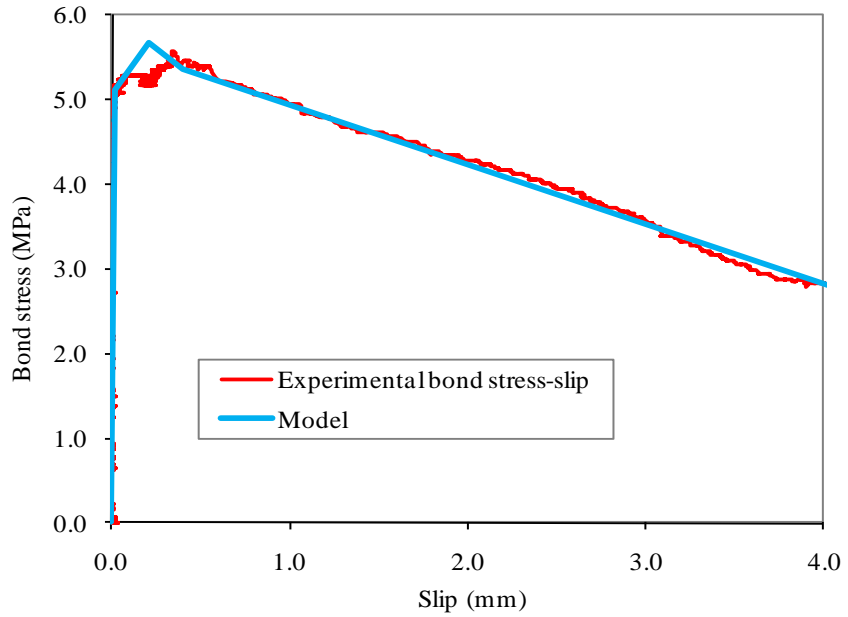


Figure 3.14 Experimental bond stress-slip variation versus model prediction (Unwrapped)

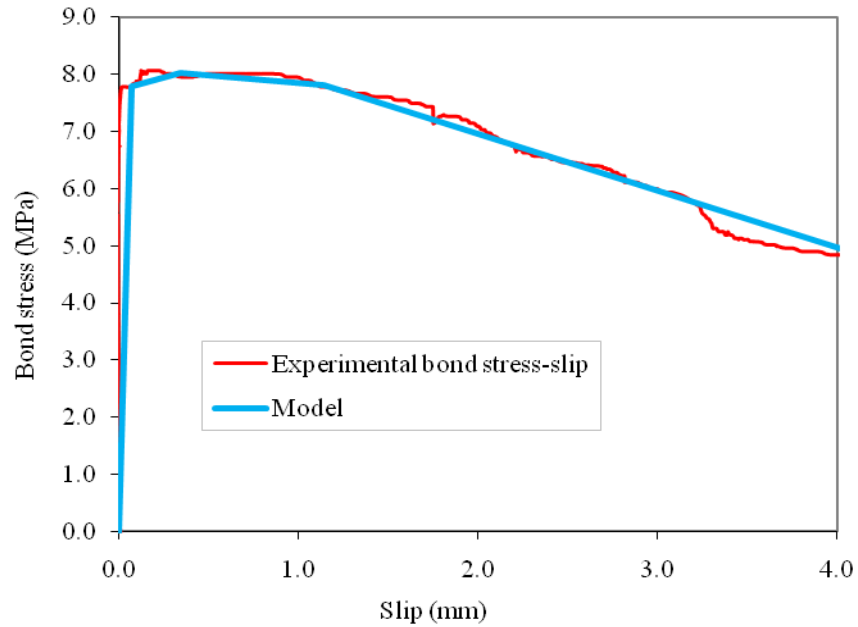


Figure 3.15 Experimental bond stress-slip variation versus model prediction (FRP wrapped)

3.3.2 Finite Element Analysis

In order to verify the proposed static bond stress-slip model (Equation 3.7), a finite element analysis was carried out.

In this study, beam anchorage specimen was modeled using a commercial non linear finite element package “ABAQUS” for the simulation of monotonic bond stress-slip model, for unwrapped and FRP wrapped beam specimen, proposed above (Section 3.3.1). The following are the geometrical and material properties for the model.

Geometrical Properties

A two dimensional (2-D) beam has been modeled in “ABAQUS”. The beam was 2000 mm in length and 250 mm deep. The beam was partitioned into three elements namely; concrete, steel reinforcement and bond element (Figure 3.16).

All the elements of the beam anchorage specimen were modeled using a 2-D plane strain solid element. The loading span was 1800 mm and the distance between the two point loading was 600 mm. The length of bond element (bonded length) was 250 mm as used in the experimental work of Rteil (2007).

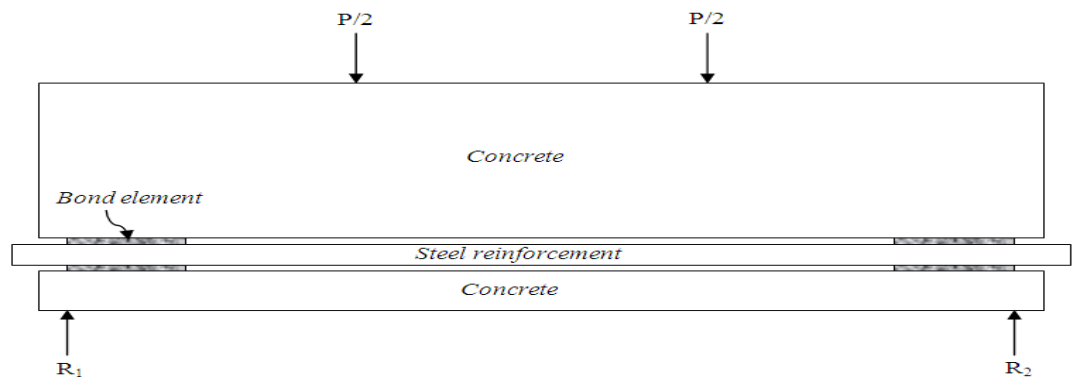


Figure 3.16 Beam anchorage specimen

Material Properties

The behaviour of the concrete was modeled using the “Concrete” material properties available in Abaqus. In this study, a concrete smeared crack approach was used. This approach smeared out the deformation at each crack (Amleh and Ghosh, 2006). The reversible behaviour of concrete

after cracking is explained by the oriented damage elasticity concept of the concrete smeared crack model. When the compressive stresses are dominant, a hardening yield surface, which is isotropic, becomes active. Due to this, the points which failed by cracking are determined by a crack detection surface (Abaqus/CAE User's manual, 6.9).

For defining the stress-strain curve of concrete (in compression), this study used the Collins and Mitchell (1997) model (Figure 3.17):

$$\frac{f_c}{f'_c} = \frac{n \left(\frac{\epsilon_c}{\epsilon_o} \right)}{n-1 + \left(\frac{\epsilon_c}{\epsilon_o} \right)^{nk}} \quad \text{Equation 3.17}$$

Where f'_c is the concrete compressive strength.

$$n = \text{curve fitting factor} = 0.8 + \frac{f'_c}{17}$$

$$\epsilon_o = \text{concrete strain at } f'_c = \frac{f'_c}{E_c} \frac{n}{n-1}$$

$$k = \text{is the stress decay factor} = 0.67 + \frac{f'_c}{62} > 1.0$$

$E_c = \text{modulus of elasticity} = (3300\sqrt{f'_c} + 6900) \left(\frac{\gamma_c}{2300} \right)$ for concrete density $1500 \leq \gamma_c \leq 2500 \text{ Kg / m}^3$.

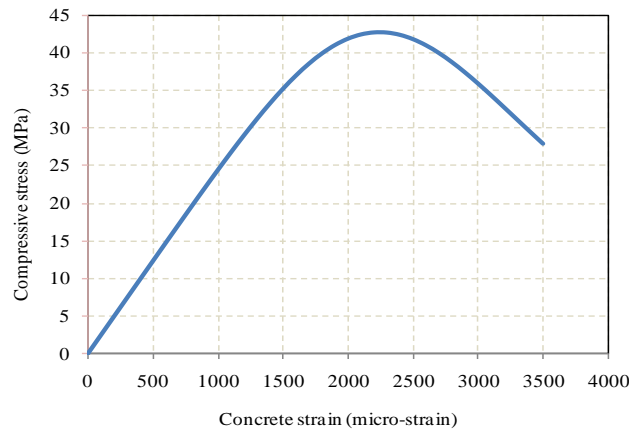


Figure 3.17 Stress-strain curve for concrete

For the steel reinforcement, the modulus of elasticity and yield strength were 200 GPa and 400 MPa respectively.

Bond Element

Bond element is the linkage between steel and concrete. Bond stress-slip relation (Equation 3.7) was employed in order to define the material properties for the bond element. Just like the stress-strain relationship in case of concrete and steel, bond stress versus slip can be used as the constitutive relationship for the bond element.

Meshing

The different part of the beam was meshed by using the module “mesh” in ABAQUS/CAE. The top down meshing technique (Free meshing), a more flexible method, was used in this study. A 3-node linear plane strain triangle element (CPE3) was defined for the concrete, steel reinforcing bar, and bond element (Figure 3.18). Finer meshing was used near the bond element as shown in Figure 3.18.

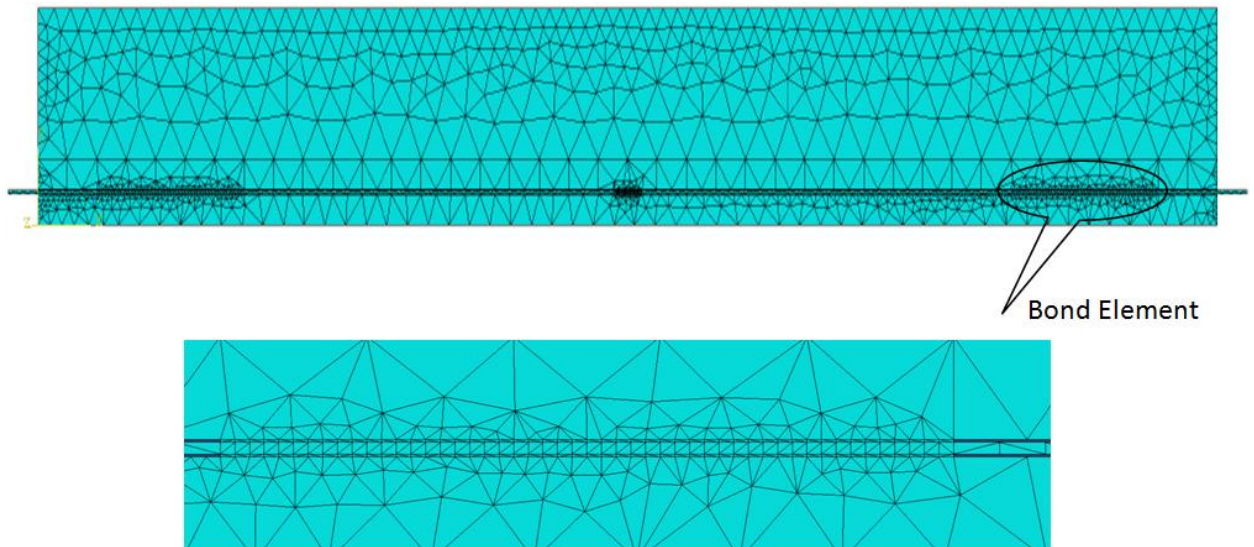
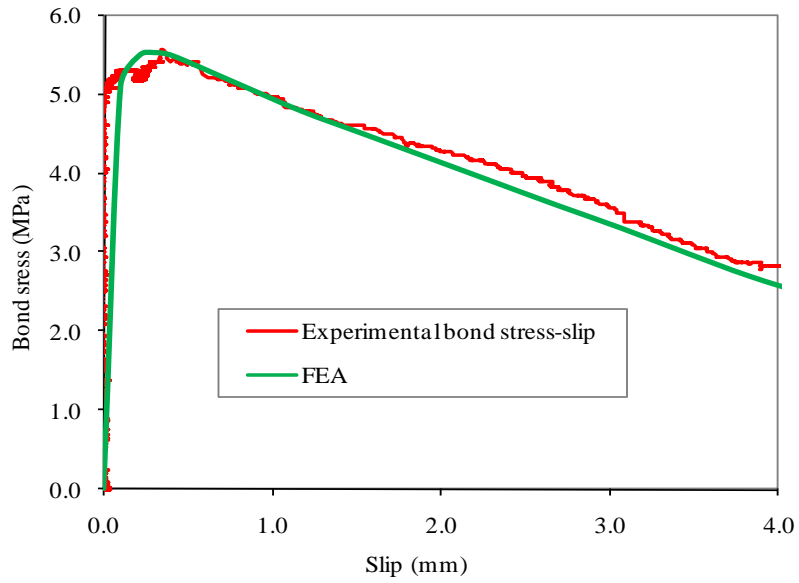


Figure 3.18 Finite element mesh of the model

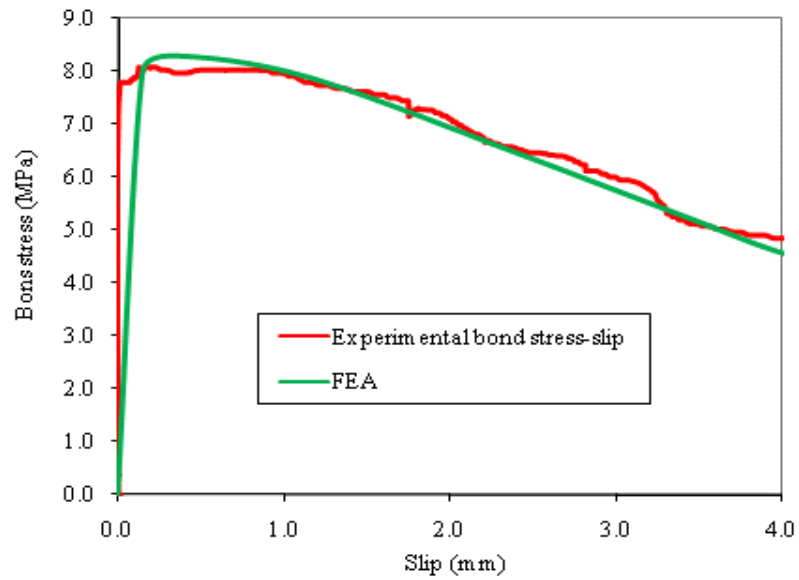
Results

Figure 3.19 compares the experimental results versus the finite element results for the static bond stress-slip behaviour for the unwrapped and FRP wrapped beam specimen respectively. The

finite element analysis satisfactory simulates the experimental behaviour (Figure 3.19) and verifies the proposed bond stress-slip relation (Equation 3.7).



a) Unwrapped



b) FRP wrapped

Figure 3.19 Finite element analysis for static bond stress-slip variation

3.3.3 Bond Stress-Slip under Cyclic Load

In this study, the bond stress-slip hysteresees for each cycle were plotted. It was observed that the peak bond stress-slip values follow the exact behaviour of the monotonic bond stress-slip model, which acts as an upper envelope for these hysteresis loops (Figure 3.20). Further, it was noticed that the cyclic envelope can be modeled as a reduced monotonic envelope (the envelope which is lower than the actual monotonic envelope due to the application of lower applied loading range than its static capacity). Therefore, the bond stress-slip law proposed by Harajli et al. (2004) for the static loading was modified and used to track the hysteresis envelope of the bond stress-slip response under cyclic loading. The model proposed by Harajli et al. (2004) was modified in order to account for the cyclic loading and the corrosion of reinforcement.

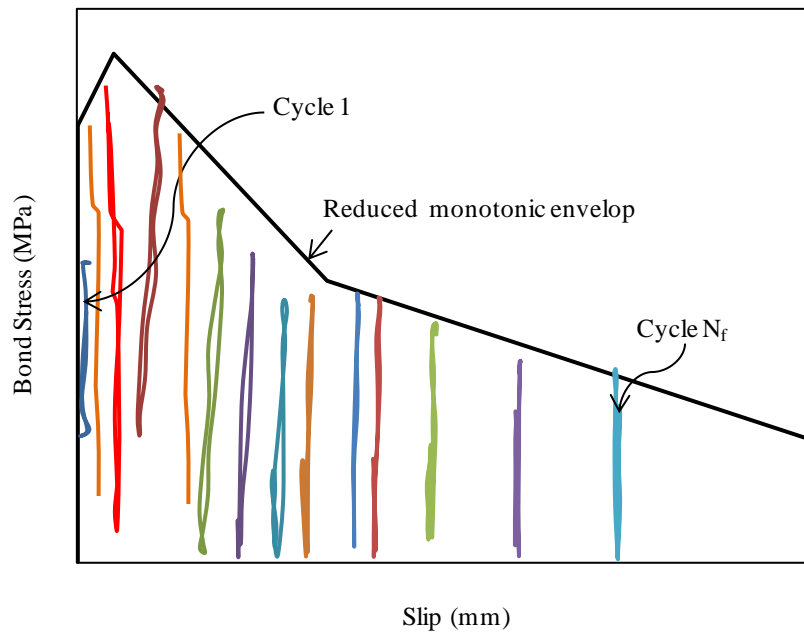


Figure 3.20 Envelope for the cyclic bond stress-slip

Unwrapped Beam Specimens

In case of unwrapped specimens, the value of ' α ' was assumed as constant. This assumption was made due to the initial constant behaviour of the slip (Rteil, 2007) and the crack propagation. The values for A and B (Rteil, 2007) were modeled as a function of the loading range and the corrosion level (Figure 3.21 and Figure 3.22) as follows.

$$A = q_1 \text{Log}P - t_1 \quad \text{Equation 3.18}$$

$$B = q_2 \text{Log}P - t_2 \quad \text{Equation 3.19}$$

Where P is the percentage of applied loading, q_i and t_i ($i = 1, 2$) are the constants that depend on the corrosion level. Figure 3.21 and Figure 3.22 show the plots of A and B versus loading range (P) for 0%, 5%, and 9% corrosion level respectively. The values of q_i and t_i for the calculation of A and B for different corrosion levels (Equation 3.17 and 3.18) are shown in Table 3.5.

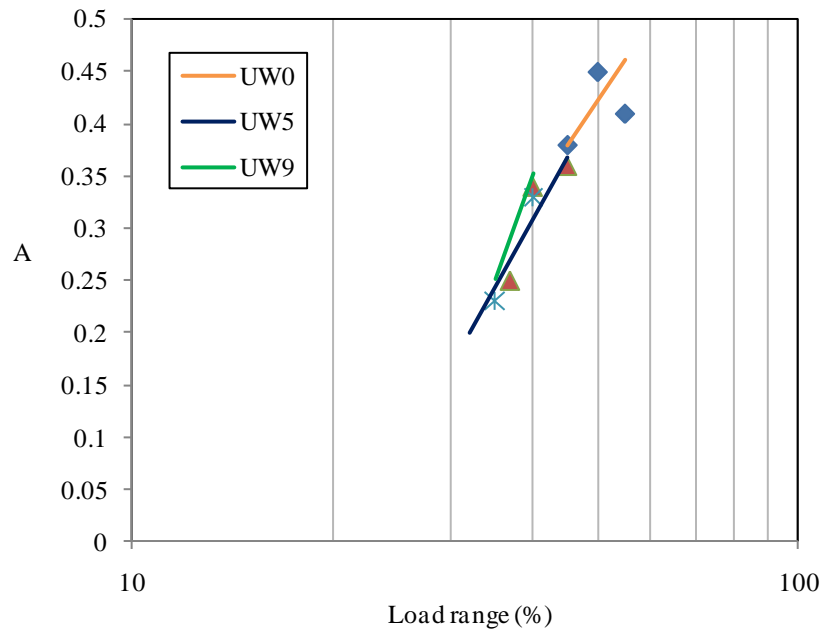


Figure 3.21 Variation of A with the load range for different corrosion levels

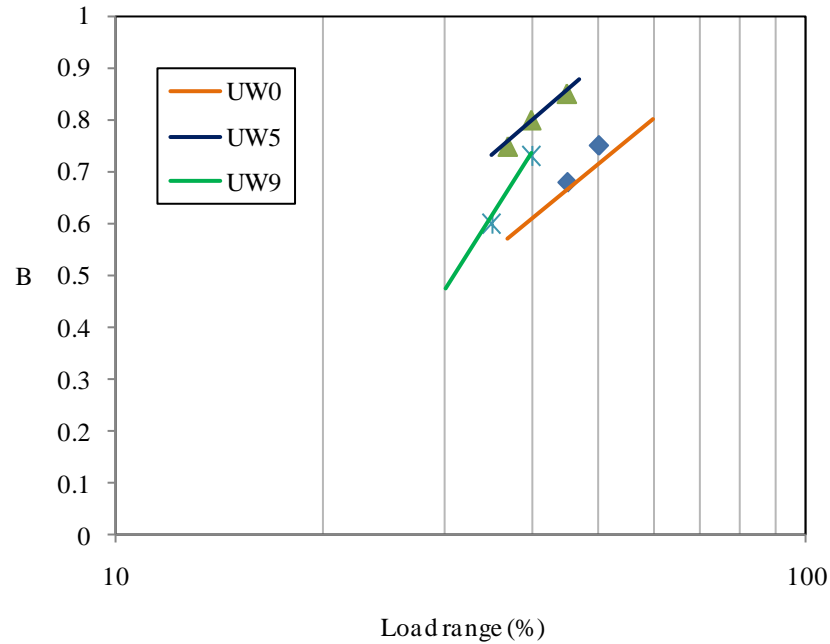


Figure 3.22 Variation of B with the load range for different corrosion levels

Table 3.5 Proposed values for q_i and t_i for different corrosion level

Parameters		Corrosion Level (%)		
		Zero	Five	Nine
A	q_1	0.94	1.22	1.72
	t_1	1.175	1.65	2.42
B	q_2	1.15	1.16	2.25
	t_2	1.25	1.065	2.87

Figure 3.23, Figure 3.24, and Figure 3.25 shows a typical bond stress-slip envelope predicted by Equation 3.7 for the cyclic bond stress-slip relation for the zero, five, and nine percent corrosion level (see Appendix D for complete plots). In these figures, the solid line shows the model prediction while the individual points indicate the experimental maximum value of the bond stress for each cycle corresponding to their slip. For simplicity, the maximum values of the bond stress corresponding to each cycle were plotted instead of a full loop (hysteresis). The proposed model shows that the cyclic bond stress-slip response track the experimental bond stress-slip envelope.

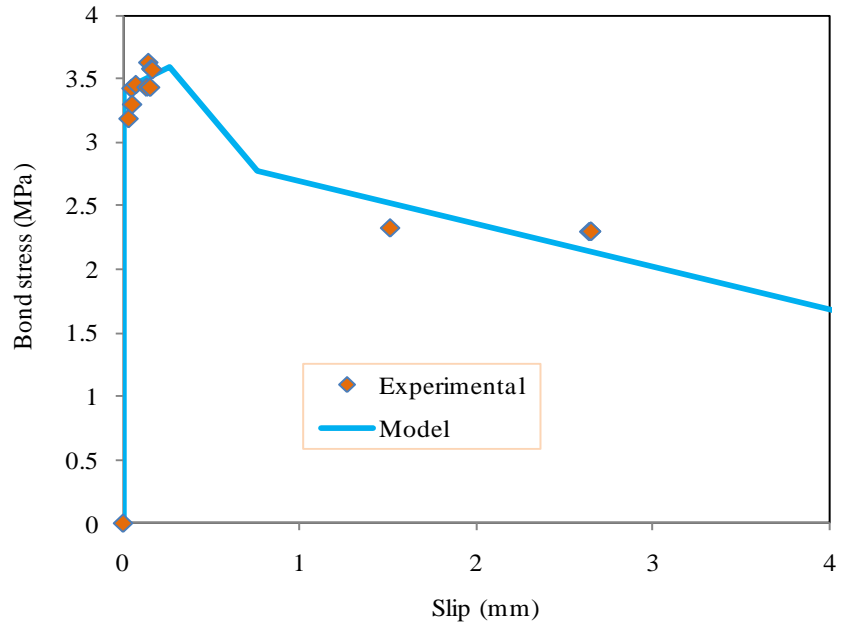


Figure 3.23 Typical bond stress-slip variation for UW0 (F45-N-T0)

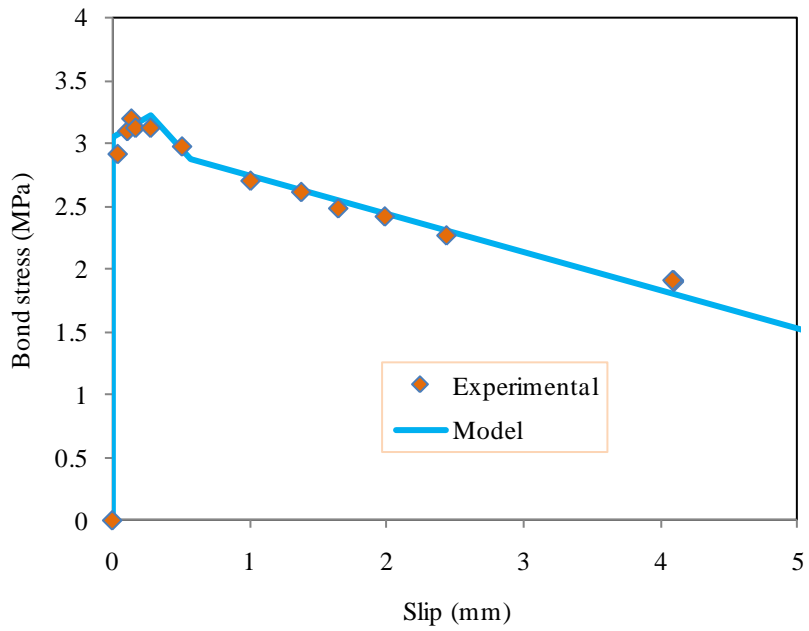


Figure 3.24 Typical stress-slip variation for UW5 (F40-N-T5)

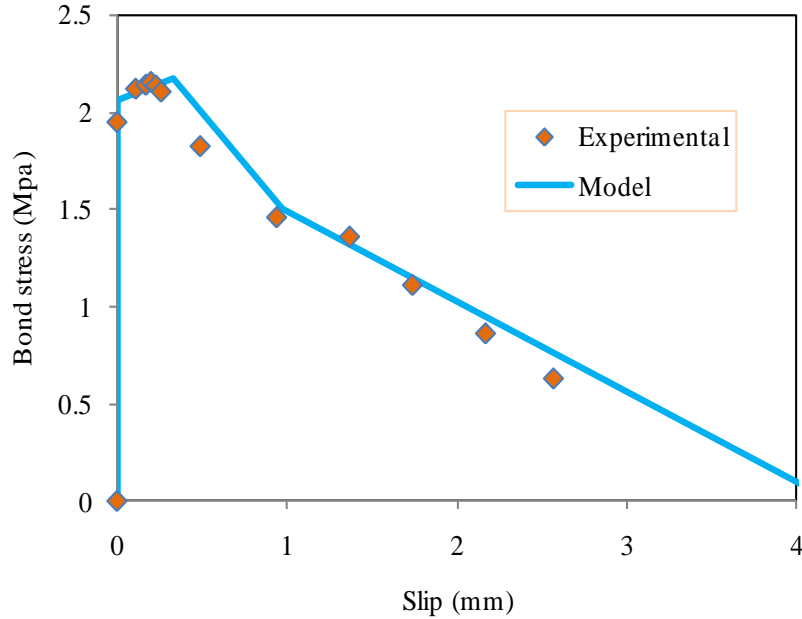


Figure 3.25 Typical stress-slip variation for UW9 (F35-N-T9b)

FRP Wrapped Beam Specimen

The values of α , A and B were modeled based on the experimental behaviour (Rteil, 2007) for the cyclic bond stress-slip relation as shown by Equations 3.19, 3.20, and 3.21 respectively.

$$\alpha = m_1 P + n_1 \quad \text{Equation 3.20}$$

$$A = m_2 P + n_2 \quad \text{Equation 3.21}$$

$$B = m_3 P + n_3 \quad \text{Equation 3.22}$$

Where P is the ratio of the applied loading to the static capacity in percentage, m_i and n_i ($i = 1, 2$ and 3) are constants that depends on the corrosion level. Figure 3.26, Figure 3.27, and Figure 3.28 show the plot between α , A and B versus the load range (P) for 0%, 5%, and 9% corrosion levels respectively for FRP wrapped beam specimens. The values of m_i and n_i for the calculation of α , A and B (Equations 3.19, 3.20 and 3.21) are shown in Table 3.6.

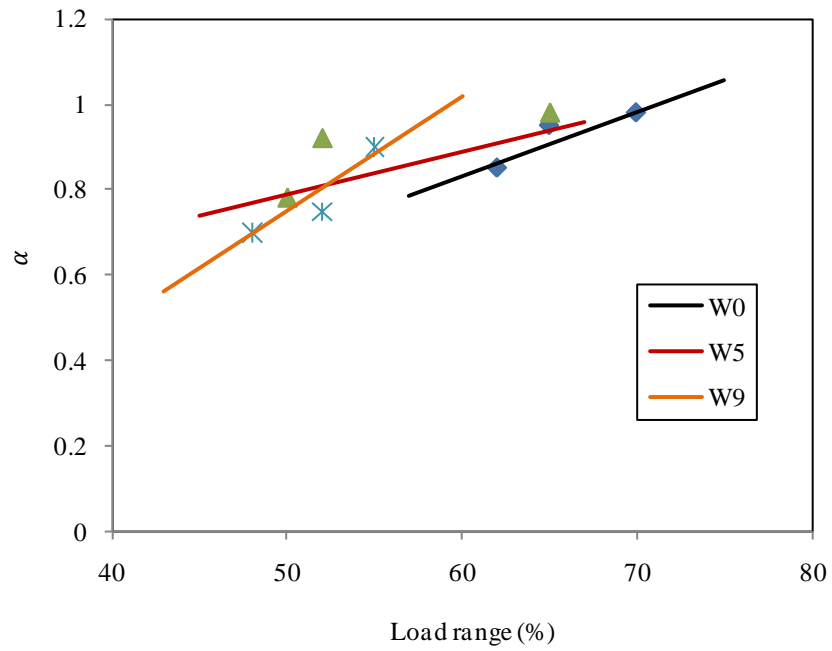


Figure 3.26 Variation of α with the load range for different corrosion levels

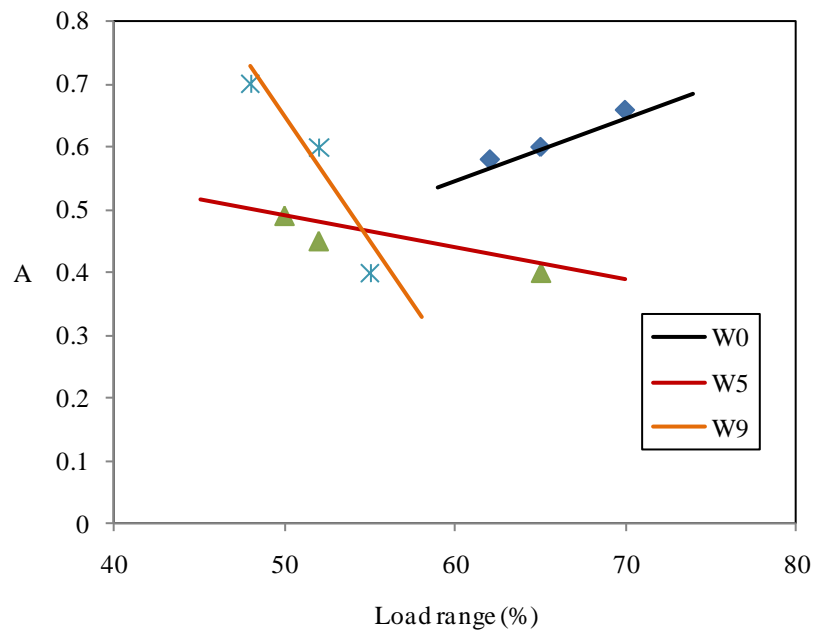


Figure 3.27 Variation of A with the load range for different corrosion levels

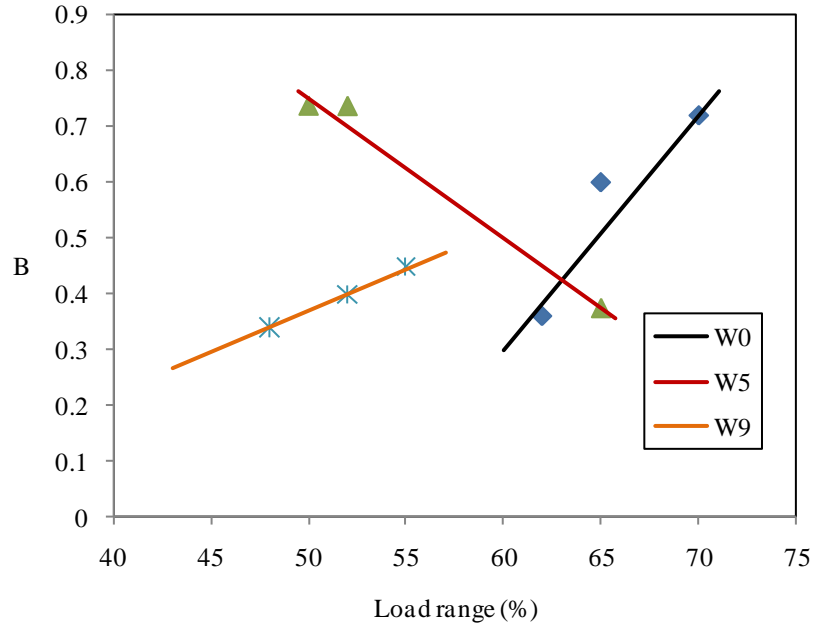


Figure 3.28 Variation of B with the load range for different corrosion levels

Table 3.6 Proposed values for m_i and n_i for different corrosion level

Parameters		Corrosion Level (%)		
		Zero	Five	Nine
α	m_1	0.015	0.01	0.027
	n_1	-0.07	0.29	-0.6
A	m_2	0.01	-0.005	-0.04
	n_2	-0.055	0.74	2.65
B	m_3	0.042	-0.025	0.015
	n_3	-2.22	2	-0.38

Figure 3.29, Figure 3.30, and Figure 3.31 show the typical model implementation of the cyclic bond stress-slip relation for zero, five, and nine percent corrosion level respectively (complete plots are in Appendix E). Model prediction shows that the cyclic bond stress-slip behaviour follows the monotonic bond stress-slip envelope and satisfactorily track the experimental behaviour.

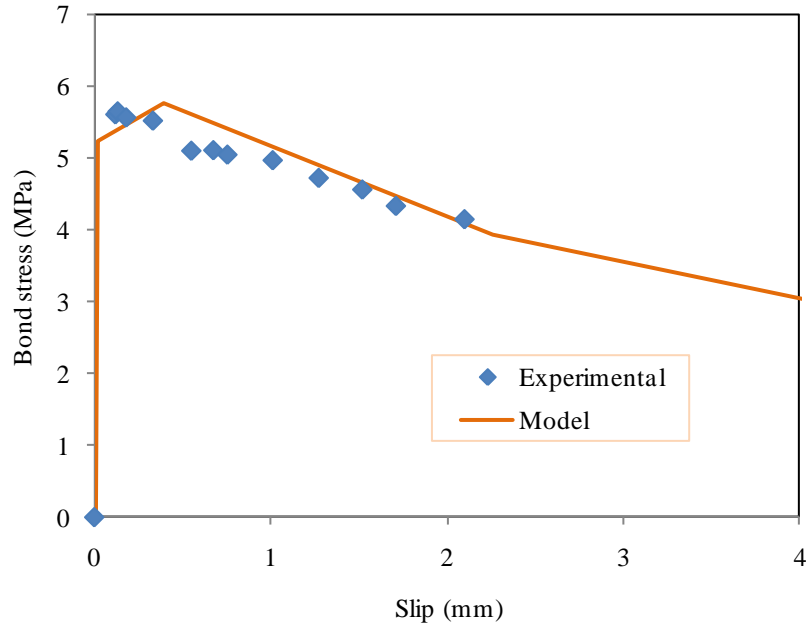


Figure 3.29 Typical bond stress-slip variation for W0 (F65-W0-T0)

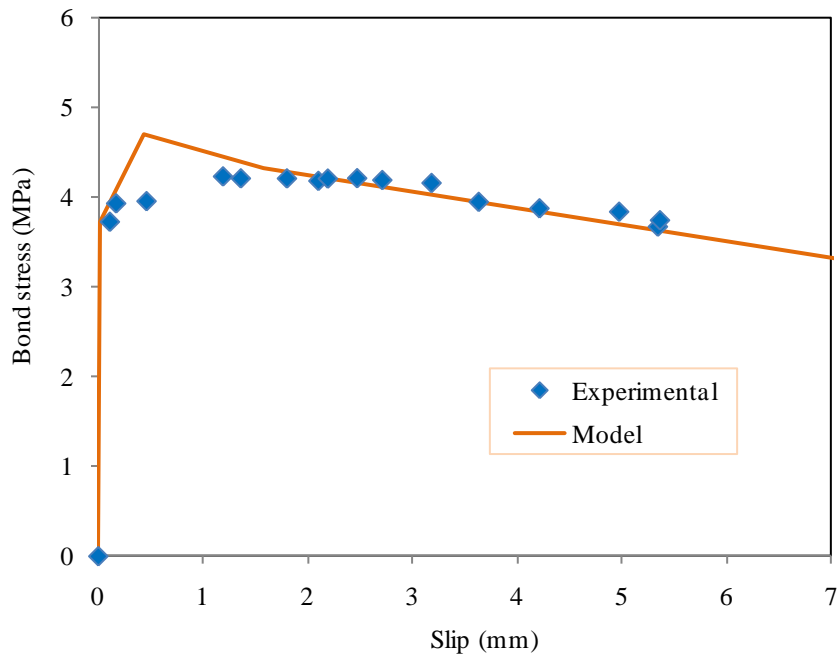


Figure 3.30 Typical bond stress-slip variation for W5 (F50-W5-T5)

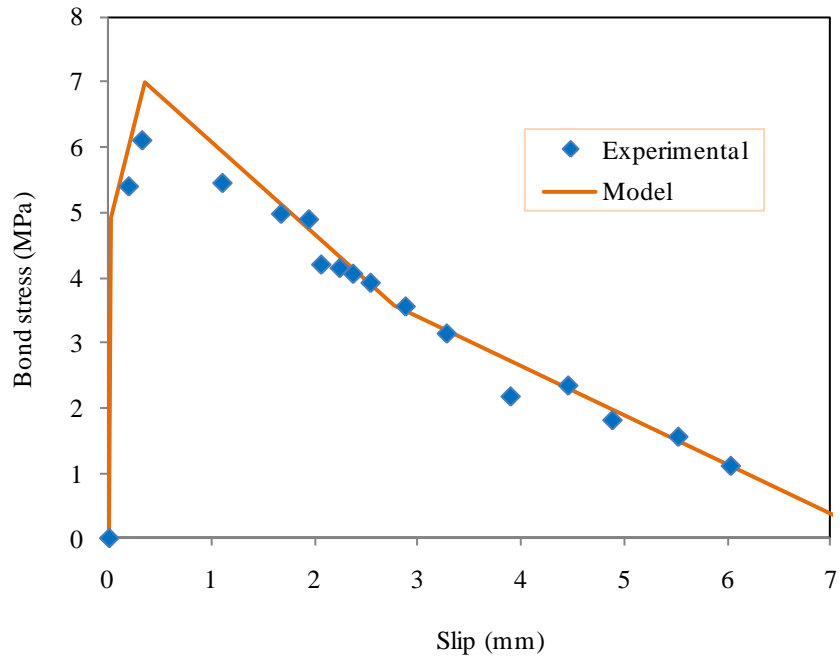


Figure 3.31 Typical bond stress-slip variation for W9 (F48-W9-T9)

Chapter 4: Analytical Modeling

4.1 General

In this chapter, an analytical model will be developed which will relate the slip at cycle 'N' to the required development length ' l_d ' of steel reinforcement in order to prevent bond failure. This model is based on the mechanics of bond forces and will use the bond stress-slip model developed in Chapter 3 (Section 3.3).

4.2 Slip-Development Length Model

Development length is an important design consideration that defines the bond failure pattern and improves the structural capacity of RC members. Consider a steel reinforcing bar with length ' dx ' having a diameter ' d_b ' on which the shear stress ' u ' is acting. The equilibrium of the forces acting on the steel reinforcing bar results in (Figure 4.1):

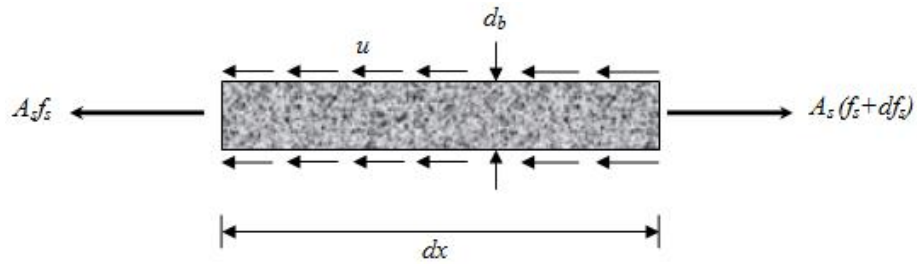


Figure 4.1 Forces acting on steel bar

$$u (\pi d_b dx) = A_s (f_s + d f_s) - A_s f_s \quad \text{Equation 4.1}$$

$$u (\pi d_b dx) = A_s d f_s \quad \text{Equation 4.2}$$

$$u = \frac{A_s d f_s}{\pi d_b dx} = \frac{d_b d f_s}{4 dx} \quad \text{Equation 4.3}$$

Where A_s is the area of steel and f_s is stress in the steel bar.

The slip $S(x)$ at a distance ' x ' is defined as the relative displacement between the steel and the concrete at the level of steel reinforcement.

$$S(x) = S_s(x) - S_{ct}(x) \quad \text{Equation 4.4}$$

Where $S_s(x)$ and $S_{ct}(x)$ are the displacement of the steel and the concrete (in tension) at a distance 'x' respectively.

Differentiating Equation 4.4 gives;

$$\frac{dS(x)}{dx} = \varepsilon_s(x) - \varepsilon_{ct}(x) \quad \text{Equation 4.5}$$

Where ε_s and ε_{ct} are the steel and the concrete tensile strains at the level of the steel reinforcement, respectively. Assuming a linear elastic behaviour in concrete and steel, the relationship between the stresses and the strain can be written as follows

$$f_s = E_s \varepsilon_s \Rightarrow \varepsilon_s = \frac{f_s}{E_s} \quad \text{Equation 4.6}$$

$$f_{ct} = E_c \varepsilon_{ct} \Rightarrow \varepsilon_{ct} = \frac{f_{ct}}{E_c} \quad \text{Equation 4.7}$$

Where E_s and E_c are the modulus of elasticity of the reinforcing steel bar and the concrete respectively. f_s and f_{ct} are the tensile stresses in the steel and in the concrete at the level of steel reinforcement, respectively. Substitute Equations 4.6 and 4.7 in Equation 4.5.

$$\frac{dS(x)}{dx} = \frac{f_s}{E_s} - \frac{f_{ct}}{E_c}$$

$$\frac{dS(x)}{dx} = \frac{f_s}{E_s} \left[1 - \frac{f_{ct}/f_s}{E_c/E_s} \right] = \frac{f_s}{E_s} \left[1 - n \frac{f_{ct}}{f_s} \right] \quad \text{Equation 4.8}$$

$$\text{Where } n = \frac{E_s}{E_c}$$

In order to determine f_{ct} and f_s the equilibrium of the reinforced concrete cross section was used. For equilibrium, tension forces (T) should be equal to the compressive force (C) (Figure 4.2).

$$T = C$$

$$f_s A_s + f_{ct} A_{ct} = f_{cc} A_{cc}$$

Equation 4.9

Where f_{cc} is the compressive stress in concrete; A_{ct} and A_{cc} are the areas of concrete in tension and compression respectively.

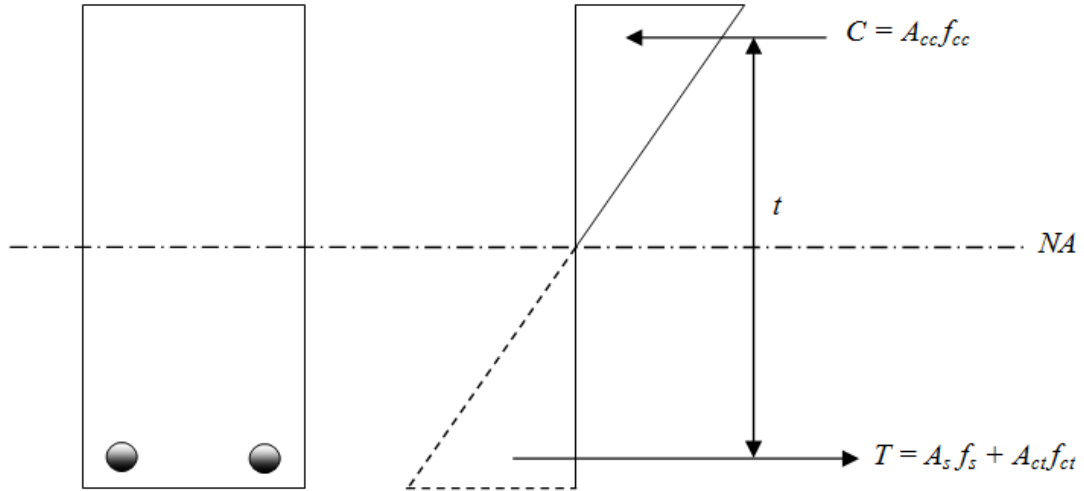


Figure 4.2 Internal forces in uncracked reinforced concrete section

Also, for equilibrium to hold, the internal moments should be equal to the external moments;

$$M_{int.} = M_{ext.}$$

$$A_{cc} f_{cc} t = M_s$$

where t is the lever arm (Figure 4.2) and M_s is the moment due to the applied service loads

$$f_{cc} = \frac{M_s}{t A_{cc}} \quad \text{Equation 4.10}$$

Substituting Equation 4.10 in 4.9 results;

$$f_s A_s + f_{ct} A_{ct} = \frac{M_s}{t} \quad \text{Equation 4.11}$$

Diving both sides of Equation 4.11 by $\left(\frac{f_s}{A_{ct}}\right)$ and after rearranging;

$$\frac{f_{ct}}{f_s} = \left(\frac{M_s}{t f_s A_{ct}} - \frac{A_s}{A_{ct}} \right) \quad \text{Equation 4.12}$$

Substituting Equation 4.12 in 4.8;

$$\frac{dS(x)}{dx} = \frac{f_s}{E_s} \left[1 - n \left(\frac{M_s}{t f_s A_{ct}} - \frac{A_s}{A_{ct}} \right) \right] \quad \text{Equation 4.13}$$

Differentiating Equation 4.13 with respect to 'x'

$$\frac{d^2S(x)}{dx^2} = \frac{df_s}{E_s dx} - \frac{n f_s}{t f_s A_{ct} E_s} \left(\frac{dM_s}{dx} \right) + \frac{n A_s f_s}{A_{ct} E_s} \quad \text{Equation 4.14}$$

Multiplying the right side of Equation 4.14 by $\left(\frac{4d_b}{4d_b} \right)$

$$\frac{d^2S(x)}{dx^2} = \left[\frac{df_s}{E_s dx} - \frac{n f_s}{t f_s A_{ct} E_s} \left(\frac{dM_s}{dx} \right) + \frac{n A_s f_s}{A_{ct} E_s dx} \right] \left(\frac{4d_b}{4d_b} \right)$$

The rearrangement of the above equation results;

$$\frac{d^2S(x)}{dx^2} = \left(\frac{4}{d_b E_s} \right) \left(\frac{d_b df_s}{4 dx} \right) + \left(\frac{4n A_s}{E_s A_{ct} d_b} \right) \left(\frac{df_s d_b}{4 dx} \right) - \left(\frac{dM_s}{dx} \right) \left(\frac{4n d_b f_s}{4 t f_s A_{ct} d_b E_s} \right)$$

But; $u = \left(\frac{d_b df_s}{4 dx} \right)$ from Equation 4.3 and $V = \left(\frac{dM_s}{dx} \right) = \text{shear force}$

Therefore,

$$\frac{d^2S(x)}{dx^2} = \left(\frac{4}{d_b E_s} \right) u + \left(\frac{4n A_s}{E_s A_{ct} d_b} \right) u - V \left(\frac{4n}{4 t A_{ct} E_s} \right)$$

But; $n = \frac{E_s}{E_c}$

$$\frac{d^2S(x)}{dx^2} = \left(\frac{4}{d_b E_s} + \frac{\pi d_b}{E_c A_{ct}} \right) u - \left(\frac{V}{t A_{ct} E_c} \right)$$

Multiplying the first term of the right hand side of the above equation by $\left(\frac{A_s}{A_s} \right)$

$$\frac{d^2S(x)}{dx^2} = \left(\frac{4}{d_b E_s} \left(\frac{A_s}{A_s} \right) + \frac{\pi d_b}{E_c A_{ct}} \right) u - \left(\frac{V}{t A_{ct} E_c} \right)$$

$$\frac{d^2S(x)}{dx^2} = \left(\frac{\pi d_b}{E_s A_s} + \frac{\pi d_b}{E_c A_{ct}} \right) u - \left(\frac{V}{t A_{ct} E_c} \right)$$

Where $E_s A_s$ and $E_c A_{ct}$ are the axial stiffness coefficients for steel and concrete in tension respectively.

$$\frac{d^2S(x)}{dx^2} = \pi d_b \left(\frac{1}{E_s A_s} + \frac{1}{E_c A_{ct}} \right) u - \left(\frac{V}{t A_{ct} E_c} \right)$$

$$\frac{d^2S(x)}{dx^2} = k_1 u - k_2 \quad \text{Equation 4.15}$$

$$\text{Where, } k_1 = \pi d_b \left(\frac{1}{E_s A_s} + \frac{1}{E_c A_{ct}} \right) \text{ and } k_2 = \left(\frac{V}{t A_{ct} E_c} \right)$$

Equation 4.15 was derived based on the equilibrium of forces. This relationship should hold at any cycle 'N' during the fatigue cycles assuming elastic behavior. Therefore, in order to consider the cyclic loading the terms, 'S' and 'u' were replaced by ' S_N ' and ' u_N ' respectively. Where S_N and u_N are the slip and bond stress at any cycle N. Equation 4.15 becomes;

$$\frac{d^2S_N(x)}{dx^2} = k_1 u_N - k_2 \quad \text{Equation 4.16}$$

The initial (first) phase of the bond stress-slip law ($u < \alpha u_{max}$; Section 3.3) was ignored in this study as the slip of rebars in this phase is very small in comparison with the second phase. The bond stress in the bond splitting phase (Phase 2) can be written as in Equation 4.17 (Figure 4.3).

$$u_N = E_b S_N \quad , S_\alpha \leq S_N \leq S_{max} \quad \text{Equation 4.17}$$

$$\text{Where, } E_b = \frac{(u_{max} - \alpha u_{max})}{(S_{max} - S_\alpha)}$$

The values of u_{max} , s_{max} and s_α can be calculated using Equations 3.11, 3.12, and 3.10 respectively (Section 3.3.1).

Incorporating the bond stress-slip relationship (Equation 4.17) into Equation 4.16:

$$\frac{d^2 S_N(x)}{dx^2} = k_1(E_b S_N) - k_2$$

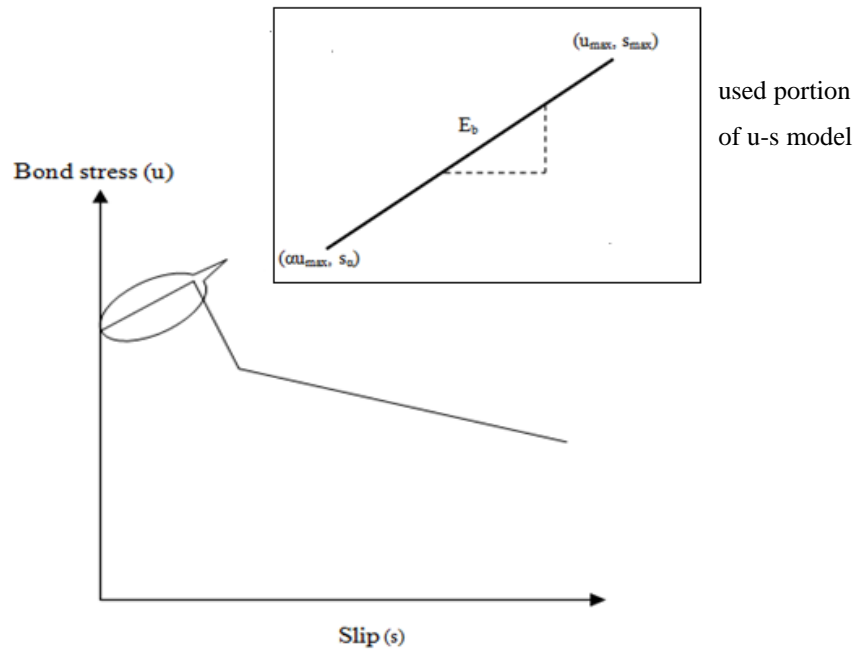


Figure 4.3 Bond stress-slip (u-s) model

Assume that $q = \sqrt{k_1 E_b}$

$$\frac{d^2 S_N(x)}{dx^2} = q^2 S_N(x) - k_2 \quad \text{Equation 4.18}$$

Equation 4.18 is the form of $\frac{d^2 y}{dx^2} = c^2 y - f(x)$, which is a second order non homogenous differential. Where 'y' is a function of 'x'; 'c' is a constant and $f(x)$ is not zero.

The solution of Equation 4.18 is the sum of the complementary function and the particular integral as given by Equation 4.19.

$$S_N = c_1 e^{qx} + c_2 e^{-qx} + \frac{k_2}{q^2} \quad \text{Equation 4.19}$$

Where c_1 and c_2 are the constants of integration to be determined by applying the boundary conditions.

Substitute Equation 4.19 in 4.17.

$$u_N = E_b \left(c_1 e^{qx} + c_2 e^{-qx} + \frac{k_2}{q^2} \right)$$

$$u_N = \frac{(u_{max} - \alpha u_{max})}{(S_{max} - S_{\alpha})} \left(c_1 e^{qx} + c_2 e^{-qx} + \frac{k_2}{q^2} \right) \quad \text{Equation 4.20}$$

Differentiating Equation 4.19 twice results:

$$\frac{d}{dx} [\varepsilon_s(x) - \varepsilon_{ct}(x)] = c_1 q^2 e^{qx} + c_2 q^2 e^{-qx} \quad \text{Equation 4.21}$$

Applying the boundary (initial) conditions:

At $x = 0$

$$M = 0 \Rightarrow f_s = f_{ct} = 0$$

Equation 4.21 becomes;

$$0 = c_1 q^2 e^{q(0)} + c_2 q^2 e^{-q(0)}$$

$$c_2 = -c_1 \quad \text{Equation 4.22}$$

At $x = l_d$

The differentiation of Equation 4.19 results;

$$\varepsilon_s(x) - \varepsilon_c(x) = c_1 q e^{qx} - c_2 q e^{-qx}$$

$$\frac{f_s}{E_s} - \frac{f_{ct}}{E_c} = c_1 q e^{q(l_d)} - c_2 q e^{-q(l_d)} \quad \text{Equation 4.23}$$

Substituting Equation 4.22 in Equation 4.23.

$$\frac{f_s}{E_s} - \frac{f_{ct}}{E_c} = c_1 q e^{q l_d} - (-c_1) q e^{-q l_d}$$

$$\frac{f_s}{E_s} \left(1 - n \frac{f_{ct}}{f_s} \right) = c_1 q e^{q l_d} + c_1 q e^{-q l_d} \quad \text{Equation 4.24}$$

Substitute Equation 4.12 in 4.24

$$\frac{f_s}{E_s} \left(1 - n \left(\frac{M_s}{t f_s A_{ct}} - \frac{A_s}{A_{ct}} \right) \right) = c_1 q e^{q l_d} + c_1 q e^{-q l_d}$$

$$\frac{f_s}{E_s} \left(1 - n \left(\frac{M_s}{t f_s A_{ct}} - \frac{A_s}{A_{ct}} \right) \right) = c_1 (q e^{q l_d} + q e^{-q l_d})$$

Rearranging the above equation results,

$$c_1 = \frac{1}{E_s (q e^{q l_d} + q e^{-q l_d})} \left[1 - n \left(\frac{M_s}{t f_s A_{ct}} - \frac{A_s}{A_{ct}} \right) \right] f_s$$

But $\frac{f_{ct}}{f_s} = \left(\frac{M_s}{t f_s A_{ct}} - \frac{A_s}{A_{ct}} \right)$, from Equation 4.12

Therefore,

$$c_1 = \frac{1}{q E_s (e^{q l_d} + e^{-q l_d})} \left[1 - n \left(\frac{f_{ct}}{f_s} \right) \right] f_s \quad \text{Equation 4.25}$$

Substitute Equation 4.25 in 4.22 results;

$$c_2 = -\frac{1}{q E_s (e^{q l_d} + e^{-q l_d})} \left[1 - n \left(\frac{f_{ct}}{f_s} \right) \right] f_s \quad \text{Equation 4.26}$$

Substituting the values of c_1 and c_2 from Equations 4.25 and 4.26 to Equation 4.19;

$$S_N = \left\{ \frac{1}{q E_s (e^{q l_d} + e^{-q l_d})} \left[1 - n \left(\frac{f_{ct}}{f_s} \right) \right] \right\} f_s e^{q x} + \left\{ -\frac{1}{q E_s (e^{q l_d} + e^{-q l_d})} \left[1 - n \left(\frac{f_{ct}}{f_s} \right) \right] \right\} f_s e^{-q x} + \frac{k_2}{q^2}$$

In order to prevent the bond failure, the anchorage length should be enough to minimize the bond stresses. Therefore, in above equation the value of 'x' was substituted by 'l_d'.

$$S_N = \left\{ \frac{1}{q E_s (e^{q l_d} + e^{-q l_d})} \left[1 - n \left(\frac{f_{ct}}{f_s} \right) \right] \right\} f_s e^{q(l_d)} - \left\{ \frac{1}{q E_s (e^{q l_d} + e^{-q l_d})} \left[1 - n \left(\frac{f_{ct}}{f_s} \right) \right] \right\} f_s e^{-q(l_d)} + \frac{k_2}{q^2}$$

$$S_N = \frac{1}{qE_s} \left[1 - n \left(\frac{f_{ct}}{f_s} \right) \right] \left[\frac{e^{ql_d} - e^{-ql_d}}{e^{ql_d} + e^{-ql_d}} \right] f_s + \frac{k_2}{q^2}$$

$$\text{But, } \tanh(ql_d) = \frac{e^{ql_d} - e^{-ql_d}}{e^{ql_d} + e^{-ql_d}} = \text{hyperbolic tangent}$$

$$S_N = \frac{\tanh(ql_d)}{qE_s} \left[1 - n \left(\frac{f_{ct}}{f_s} \right) \right] f_s + \frac{k_2}{q^2} \quad \text{Equation 4.27}$$

Equation 4.27 gives the relationship between the cyclic slip and the development length of steel reinforcing bars.

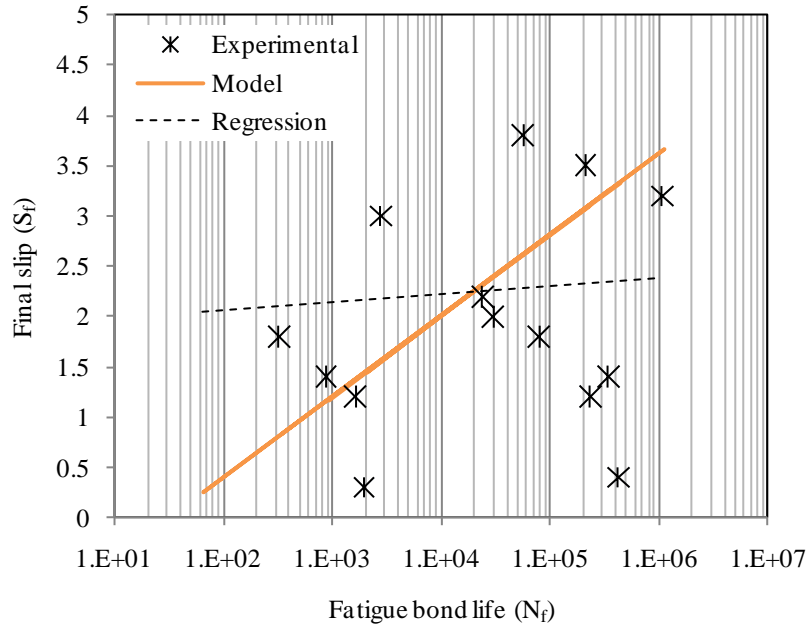
4.3 Final Slip-Fatigue Bond Life

From the experimental results (Rteil, 2007), it was concluded that the fatigue life was higher at a higher final slip value. Therefore, the following equations based on the regression analysis were proposed for unwrapped and FRP wrapped beam specimens in order to calculate the final slip.

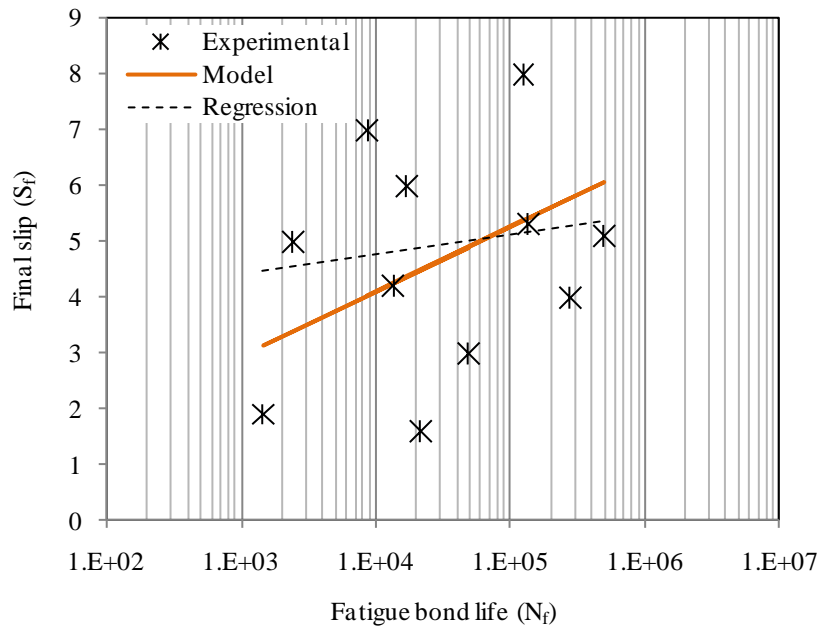
$$S_f = 0.35 \ln N_f - 1.2 \quad \text{for Unwrapped case} \quad \text{Equation 4.28}$$

$$S_f = 0.5 \ln N_f - 0.5 \quad \text{for FRP wrapped case} \quad \text{Equation 4.29}$$

Where S_f is the final slip and N_f is the fatigue bond life. Figure 4.4 shows the prediction of final slip from Equations 4.28 and 4.29 for the unwrapped and FRP wrapped beam specimens respectively. In Figure 4.4, the dashed line represents the regression fit of the experimental data and the solid line is the proposed model for the final slip. The proposed models (Equations 4.28 and 4.29) were the modified form of the regression model. This modification was necessary to better predict the experimental fatigue bond life ' N_f ' (Section 4.4).



a) Unwrapped specimens



b) FRP wrapped specimens

Figure 4.4 Variation of the final slip with fatigue bond life

4.4 Design Considerations

For design engineers, it is important to calculate the required development length of the steel reinforcement at 'N' number of cycles in order to resist the bond failure or the evaluation of fatigue bond life at any particular development length of the steel reinforcement bar. This will ensure the efficient performance of reinforced concrete structures.

The fatigue bond life for a particular development length of steel reinforcement in case of unwrapped and FRP wrapped beams, can be determined by equating Equation 4.27 with 4.28 and 4.29 as follows.

$$0.35 \ln N_f - 1.2 = \frac{\tanh(ql_d)}{qE_s} \left[1 - n \left(\frac{f_{ct}}{f_s} \right) \right] f_s + \frac{k_2}{q^2} \quad \text{Equation 4.30}$$

$$0.5 \ln N_f - 0.5 = \frac{\tanh(ql_d)}{qE_s} \left[1 - n \left(\frac{f_{ct}}{f_s} \right) \right] f_s + \frac{k_2}{q^2} \quad \text{Equation 4.31}$$

The ratio $\left(\frac{f_{ct}}{f_s} \right)$ is very small for all practical purposes therefore, for simplicity it can be ignored without losing accuracy. Rearranging Equations 4.30 and 4.31 result in:

$$\ln(N_f) = \frac{1}{0.12} \left(\frac{\tanh(ql_d)}{qE_s} f_s + \frac{k_2}{q^2} \right) + 1.2 \quad \text{Equation 4.32}$$

$$\ln(N_f) = \frac{1}{0.5} \left(\frac{\tanh(ql_d)}{qE_s} f_s + \frac{k_2}{q^2} \right) + 1 \quad \text{Equation 4.33}$$

Finally, Equation 4.32 and 4.33 relates the fatigue bond life and the development length of steel reinforcement for unwrapped and FRP wrapped beam specimens respectively.

Where;

$$q = \text{constant} = \sqrt{k_1 E_b}; \quad k_1 = \pi d_b \left(\frac{1}{E_s A_s} + \frac{1}{E_c A_{ct}} \right) \quad \text{and} \quad E_b = \frac{(u_{max} - \alpha u_{max})}{(S_{max} - S_\alpha)}$$

$$u_{max} = A \sqrt{f'_c} \left(\frac{c + K_c}{d_b} \right)^{2/3} \leq u_1, \quad \text{from Equation 3.11}$$

$$K_c = \frac{7A_{tr}}{sn} + \frac{28r_e A_{frp}}{sn}$$

$$s_{max} = s_1 e^{\left(\frac{1}{0.3}\right) \ln\left(\frac{u_{max}}{u_1}\right)} + s_o \ln\left(\frac{u_1}{u_{max}}\right), \text{ from Equation 3.12}$$

$$s_1 = 0.15c_o$$

$$u_1 = 2.57\sqrt{f'_c}$$

$$s_\alpha = s_1 \left(\frac{\alpha u_{max}}{u_1}\right)^{1/0.3}, \text{ from Equation 3.10}$$

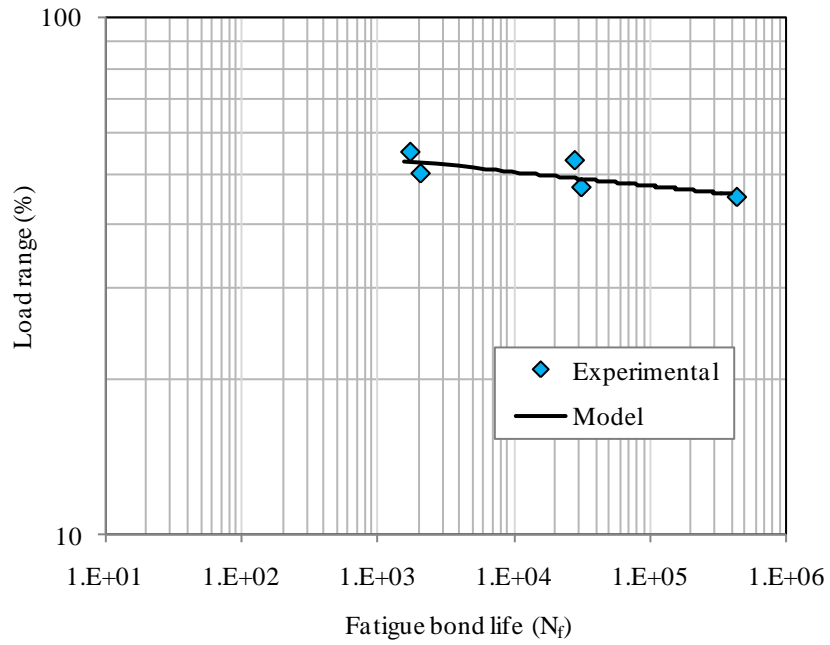
$$k_2 = \text{constant} = \left(\frac{V}{tA_{ct}E_c}\right)$$

4.4.1 Implementation of Model

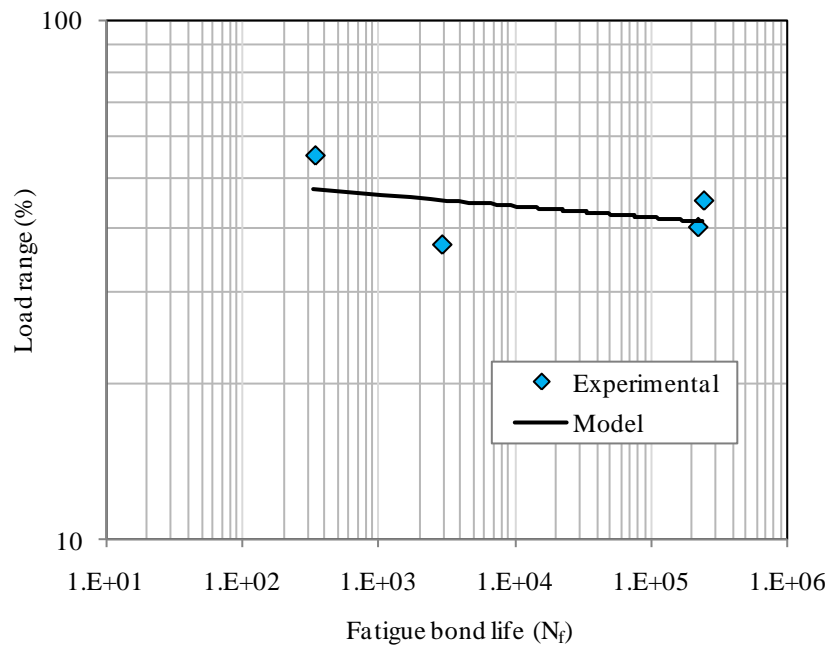
Figure 4.5 and Figure 4.6 show the model prediction (Equation 4.32 and 4.33) versus the experimental results for unwrapped and FRP wrapped beam specimens. The model satisfactorily predicts the experimental results.

In case of unwrapped beam specimens, the average ratio of experimental fatigue bond life and predicted fatigue bond life ($N_m/N_{exp.}$) was 0.89, 0.90 and 0.87 for 0%, 5% and 9% corrosion levels respectively. The correlation coefficient was 0.98 for all the corrosion levels. The standard deviations were 0.055, 0.074 and 0.076 for 0%, 5% and 9% corrosion level respectively. At 95% of confidence interval, the average $N_m/N_{exp.}$ varied between 0.85 to 0.94, 0.83 to 0.97 and 0.80 to 0.93 for 0%, 5% and 9% corrosion level respectively for unwrapped beam specimens.

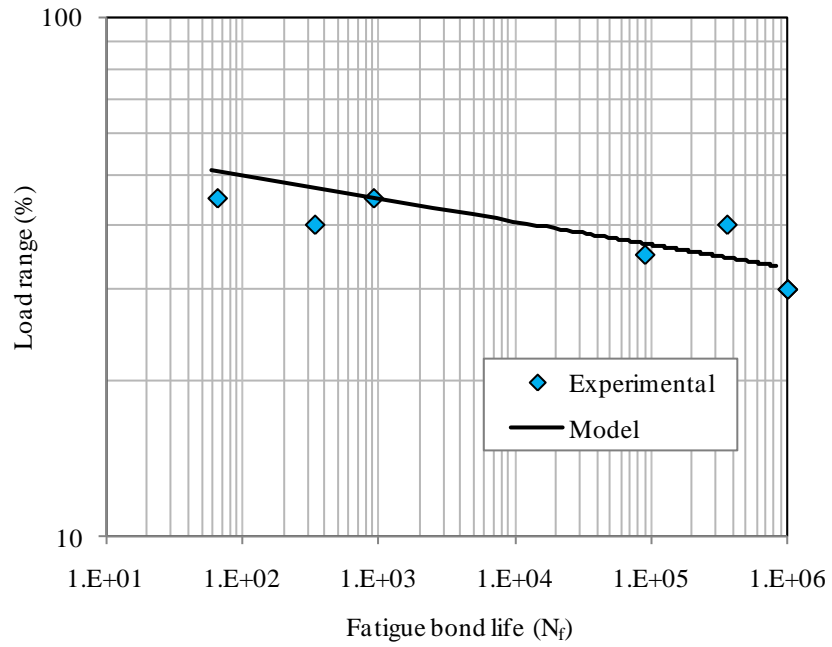
For FRP wrapped beam specimens, the average ratio of experimental fatigue bond life and predicted fatigue bond life ($N_m/N_{exp.}$) was 0.84, 0.97 and 1.06 for 0%, 5% and 9% corrosion levels respectively. The correlation coefficient was 0.98 for all the corrosion levels. The standard deviations were 0.055, 0.074 and 0.076 for 0%, 5% and 9% corrosion level respectively. At 95% of confidence interval, the average $N_m/N_{exp.}$ varied between 0.71 to 0.97, 0.96 to 0.98 and 0.42 to 1.72 for 0%, 5% and 9% corrosion level respectively for FRP wrapped beam specimens.



a) Zero percent corrosion level

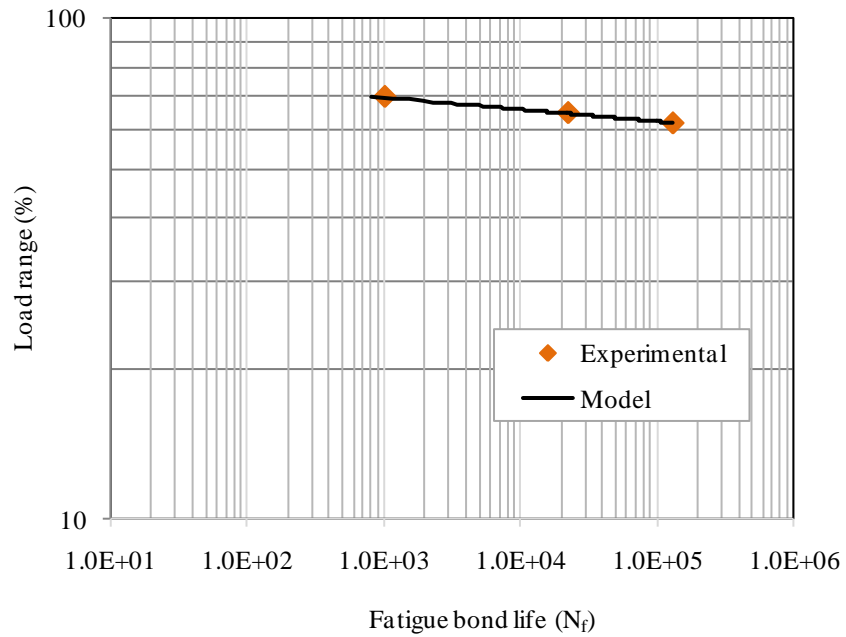


b) Five percent corrosion level

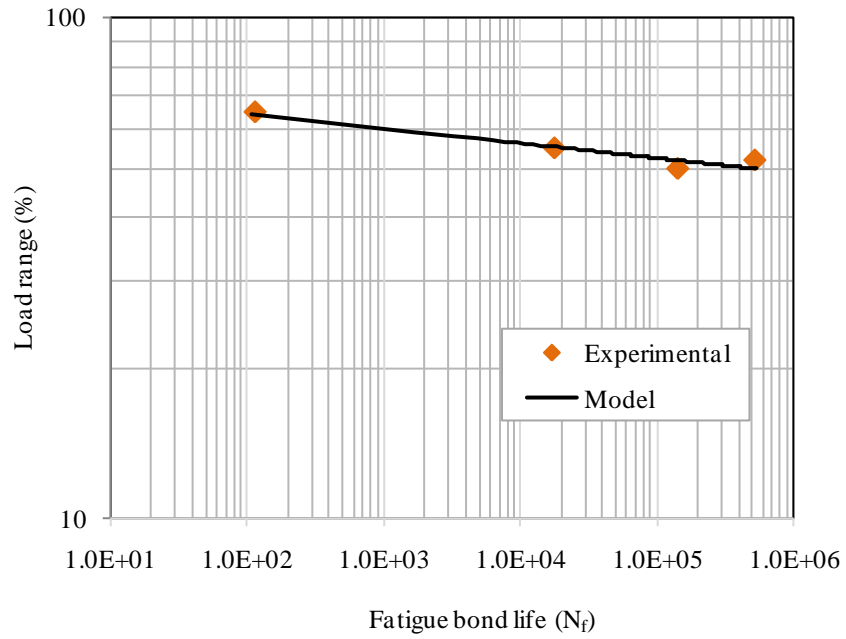


c) **Nine percent corrosion level**

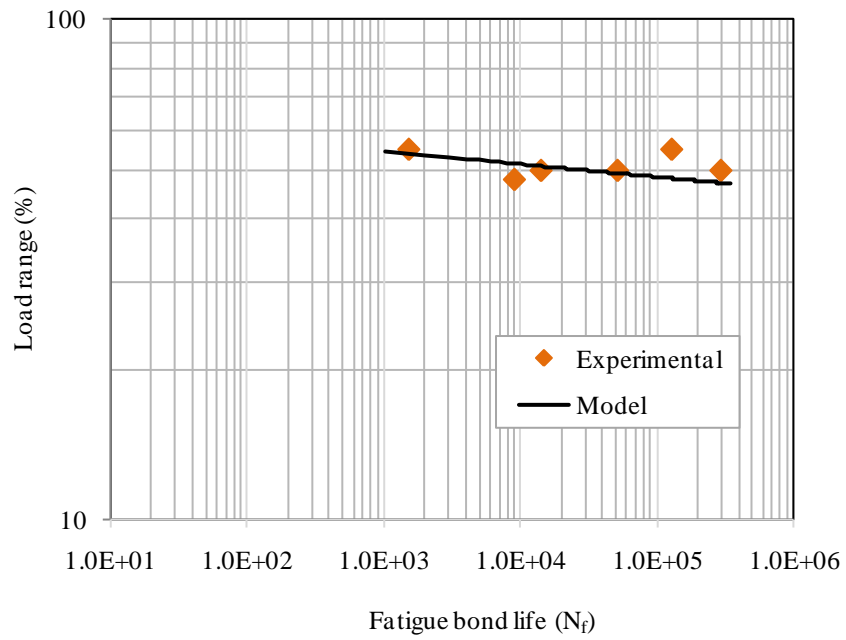
Figure 4.5 Model prediction of fatigue bond life for unwrapped beams



a) **Zero percent corrosion level**



a) Five percent corrosion level



a) Nine percent corrosion level

Figure 4.6 Model prediction of fatigue bond life for FRP wrapped beams

Chapter 5: Conclusions and Future Recommendations

5.1 Summary and Conclusions

The objectives of this study were to establish a design equation for new construction and analysis techniques for existing structures in order to evaluate the steel-concrete bond performance. The bond deterioration can be assessed by observing the slip of the reinforcement relative to concrete. Slip-fatigue model, based on the experimental results of Rteil (2007), was developed using non linear regression analysis. This model accounts for the different levels of corrosion and the FRP confinement. Harajli et al. (2004) static bond stress-slip law was modified in order to track the hysteresis envelope for the fatigue cyclic loading. An analytical relationship between the cyclic slip and the development length was formulated based on the mechanics of bond forces and considering the tension stiffening properties of the concrete. This relationship was equated with the final slip-fatigue model in order to predict the fatigue bond life. Finite element analysis was carried out in order to simulate the static bond stress-slip relationship. The following conclusions can be drawn from the present study;

- The slip-fatigue model was able to predict the initial constant rate increase in the slip and dramatic increase in the second phase for unwrapped beam specimens, as predicted by the experimental results of Rteil's (2007). The ratio $S_{model} / S_{experimental}$ was 1.11, 1.02, and 0.84 and the standard deviations were 0.16, 0.034, and 0.14 for zero, five, and nine percent corrosion level respectively for unwrapped beam specimens. The correlation coefficient for the experimental slip and the slip that was predicted from the model (Equation 3.1) was 0.86, 0.94 and 0.85 for 0%, 5% and 9% corrosion level respectively.
- For the FRP wrapped beam specimen, the slip after ' N ' number of cycles was modeled to predict all three phases of the experimental slip behaviour (Rteil, 2007). The $S_{model} / S_{experimental}$ ratio was 0.90, 0.85, and 0.80 and the standard deviations were 0.067, 0.10, and 0.13 for zero, five and nine percent corrosion level respectively, in case of FRP wrapped beam specimens. The correlation coefficient for the experimental slip and the slip that was predicted from the model (Equation 3.4) was 0.98 for all levels of corrosion.

- The cyclic bond stress-slip behaviour followed the reduced envelope of the monotonic bond stress-slip relation.
- The bond stress-slip relationship for the static as well as the cyclic loading was modeled by modifying the bond stress-slip law proposed by Harajli et al. (2004) for the static loading.
- A design equation that relates the fatigue bond life (N_f) and the development length (l_d) was proposed. This equation was derived based on the mechanics of bond forces and stresses, using the proposed cyclic bond stress-slip relation and assuming an uncracked linear elastic concrete section.
- The predicted fatigue bond life from the proposed design equation was in good correlation with the experimental values. The average ratio $N_m/N_{exp.}$ was 0.89, 0.90 and 0.87 for 0%, 5% and 9% corrosion levels respectively in case unwrapped beam specimens. For FRP wrapped beam specimens, the average ratio $N_m/N_{exp.}$ was 0.84, 0.97 and 1.06 for 0%, 5% and 9% corrosion levels respectively.
- Finite element analysis (FEA) was carried out in order to verify the static bond stress-slip behaviour. The analysis results satisfactory explain the experimental response.

In short, the present study provided a tool for the structural engineers in order to analyze the corroded steel-FRP confined concrete bond associated parameters for efficient performance of the reinforced concrete structures under fatigue cyclic loading.

5.2 Limitations and Future Research Recommendations

The present study was based on the experimental results of Rteil (2007). This study only investigated a very limited number of parameters namely corrosion level measured as percentage of mass loss, confinement using FRP and load range. Also, the induced corrosion technique (laboratory controlled) was used in this experimental work in order to initiate the corrosion in reinforced concrete bond beam specimens. Therefore, the proposed models are only applicable to those variables and within the used ranges. In addition, it should be noted that the experimental results were scattered and provided limited number of data. Therefore, it is suggested that more

experimental tests and analytical verification be conducted before the use of proposed models in design applications. Accordingly, it is suggested that the following future research topic be conducted:

- More experimental work is required on bond-corrosion-repeated loading problem in order to refine the presented models.
- Vary the corrosion level beyond 9%.
- The effect of concrete compressive strength, bar type, and concrete cover should be studied and their role in the design equation should be verified.
- Finite element validation of slip-fatigue model. Application of fatigue cyclic loading (up to 10^6 cycles) in finite element in order to verify the experimental prediction of bond stress versus slip for each cycle.

Appendix A

Table A.1 Fatigue bond life for unwrapped beam specimens (Rteil, 2007)

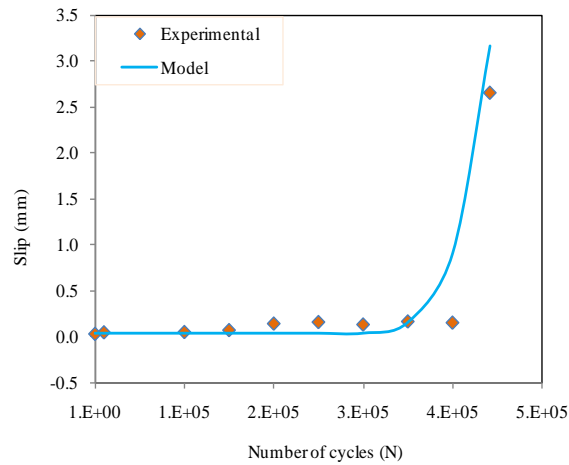
Group	Beams	Corrosion level when FRP applied (Days)	Corrosion level at test (Days)	Load ranges (%)	Fatigue bond life (N_f)
UW0	F45-N-T0	No FRP	0	45	442,134
	F47-N-T0			47	31,423
	F50-N-T0			50	2,041
	F53-N-T0			53	25,052
	F55-N-T0			55	1,714
UW5	F37-N-T5	No FRP	50	37	2,912
	F40-N-T5			40	222,263
	F45-N-T5			45	245,318
	F50-N-T5			50	0.5
	F55-N-T5			55	340
UW9	F30-N-T9a	No FRP	100	30	999,263
	F35-N-T9a			35	1,116,795
	F37-N-T9a			37	82,690
	F40-N-T9a			40	342
	F45-N-T9a			45	66
	F35-N-T9b	No FRP	150	35	89,887
	F37-N-T9b			37	59,568
	F40-N-T9b			40	360,156
	F42-N-T9			42	0.5
	F45-N-T9b			45	923

Table A.2 Fatigue bond life for FRP wrapped beam specimens (Rteil, 2007)

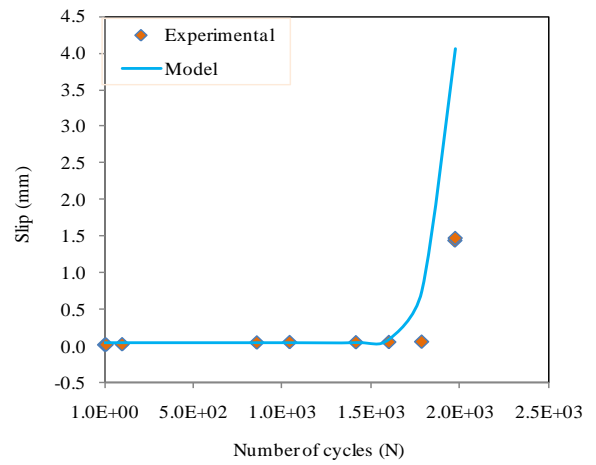
Group	Beams	Corrosion level when FRP applied (Days)	Corrosion level at test (Days)	Load range (%)	Fatigue bond life (N _f)
W0	F62-W0-T0	0	0	62	131,046
	F65-W0-T0			65	22,487
	F70-W0-T0			70	1,030
W5	F50-W5-T5	50	50	50	142,208
	F52-W5-T5a			52	523,270
	F52-W5-T5b			52	1,950
	F55-W5-T5			55	17,731
	F65-W5-T5			65	113
W9	F48-W9-T9	100	100	48	9,027
	F50-W9-T9a			50	51,319
	F52-W9-T9a			52	2,529
	F55-W9-T9a			55	1,523
	F50-W9-T9b	150	150	50	14,145
	F50-W9-T9c			50	293,023
	F52-W9-T9b			52	8,742
	F55-W5-T9			55	441,586
	F58-W5-T9a			58	351,582
	F58-W5-T9b			58	238,532
	F60-W5-T9			60	8,956

Appendix B

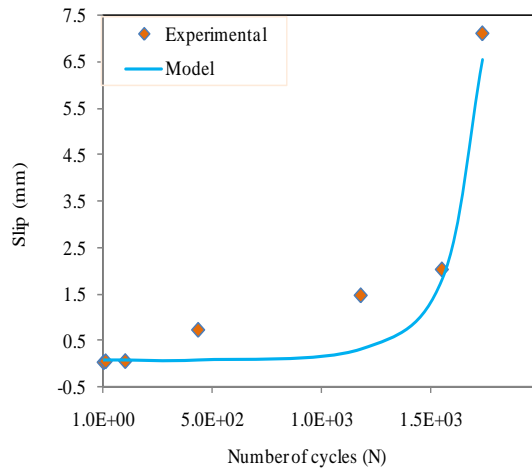
Slip versus Number of Cycles for Unwrapped Specimens



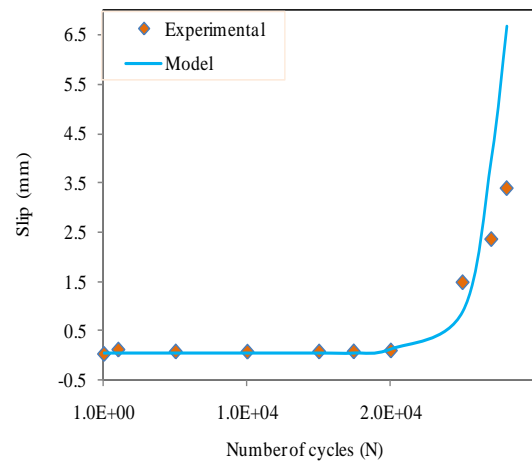
a) F45-N-T0



b) F50-N-T0

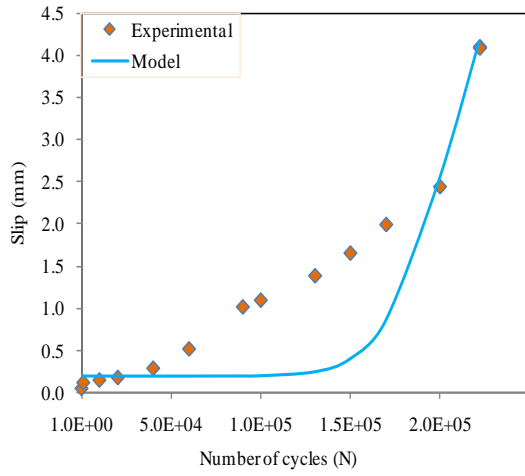


c) F55-N-T0

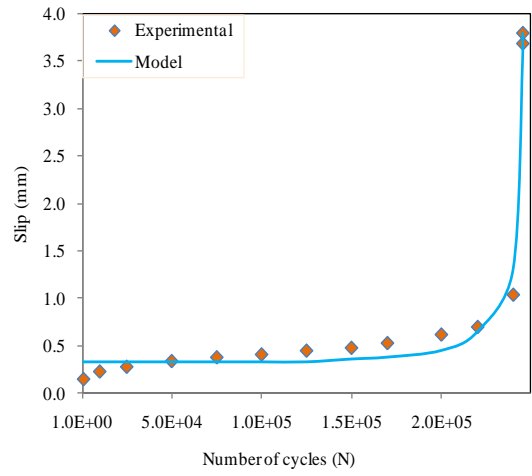


d) F53-N-T0

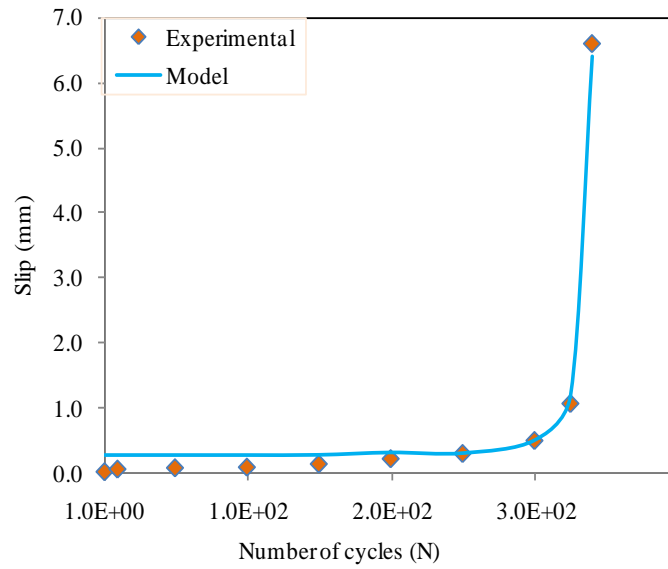
Figure B.1 Experimental and model results for unwrapped zero percent corrosion level



a) F40-N-T5

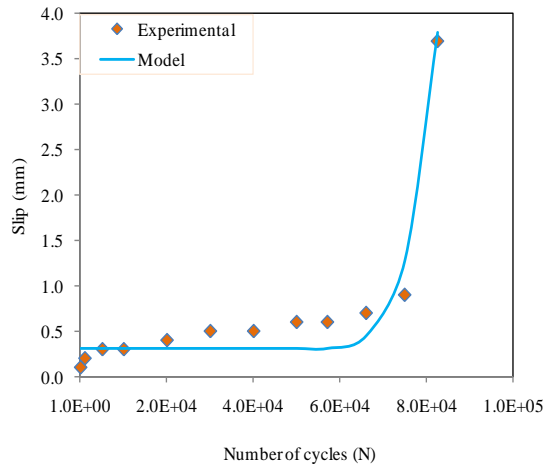


b) F45-N-T5

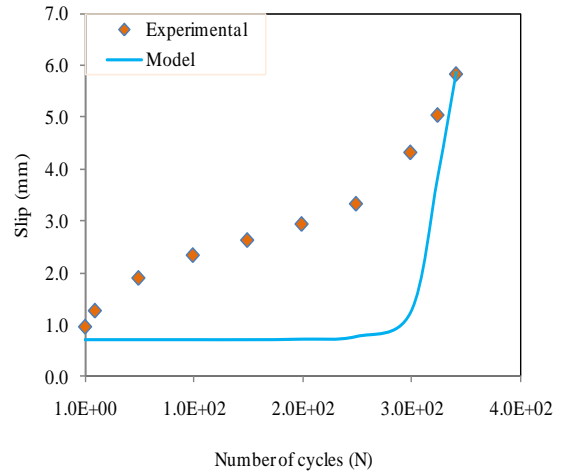


c) F55-N-T5

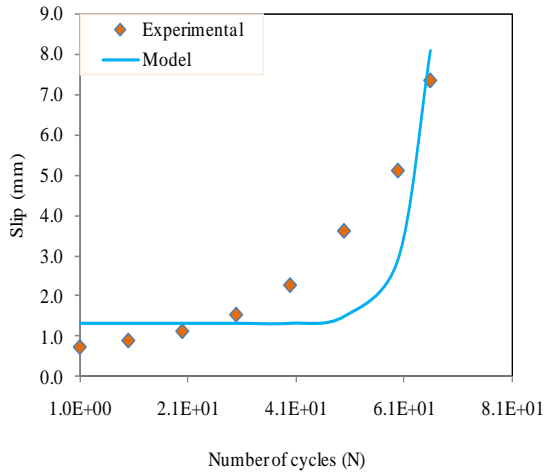
Figure B.3 Experimental and model results for unwrapped five percent corrosion level



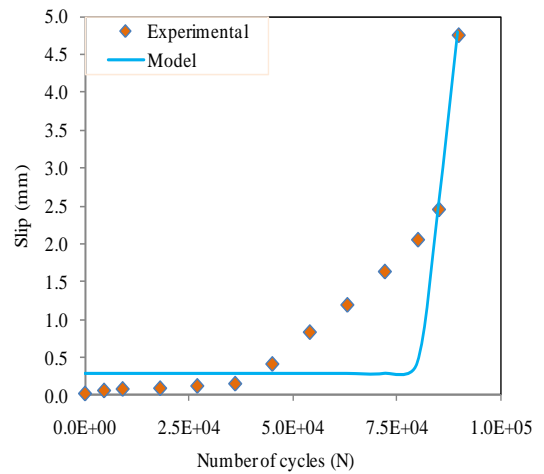
a) F37-N-T9a



b) F40-N-T9a

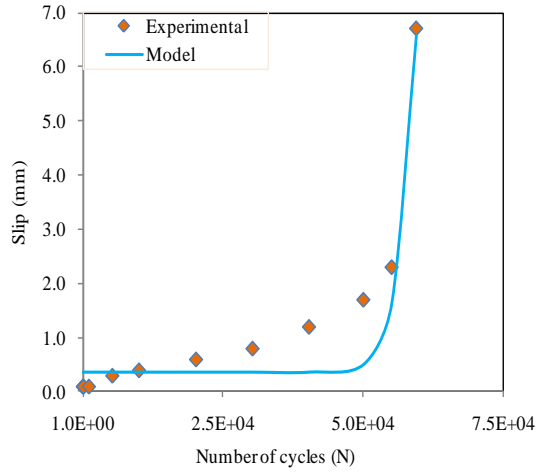


c) F45-N-T9a

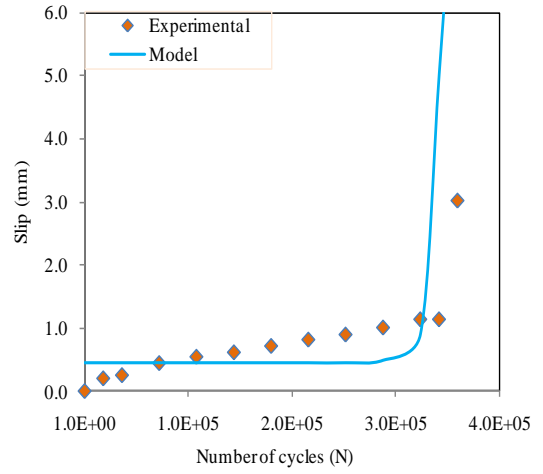


d) F35-N-T9b

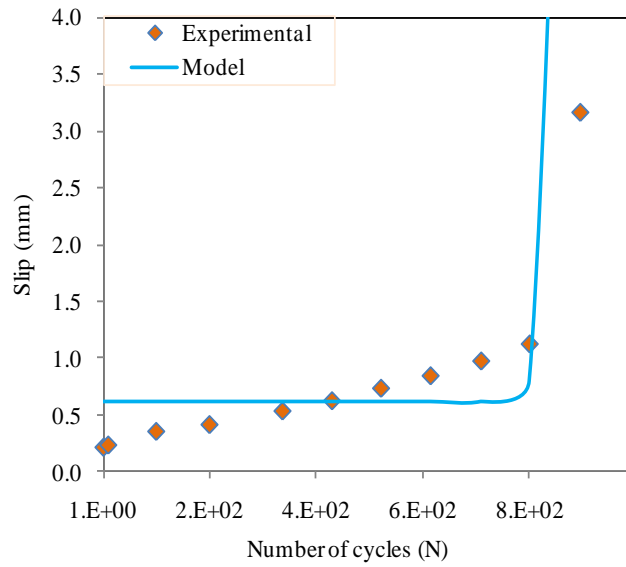
Figure B.4 Experimental and model results for unwrapped nine percent corrosion level



e) F37-N-T9b



f) F40-N-T9b

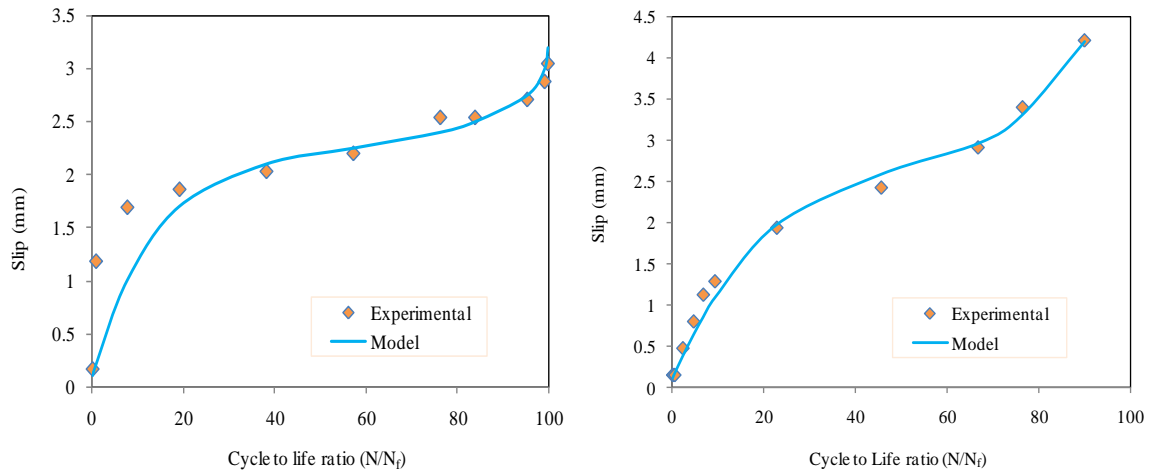


g) F45-N-T9b

Figure B.5 Experimental and model results for unwrapped nine percent corrosion level (cont.)

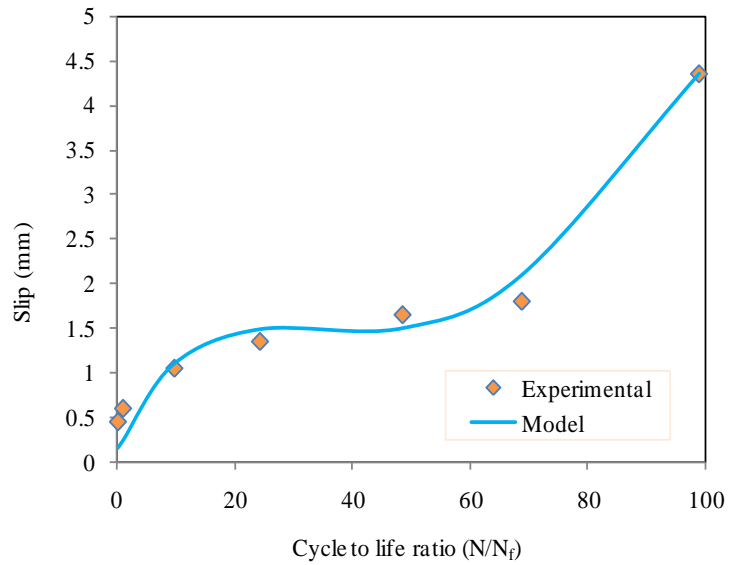
Appendix C

Slip versus Number of Cycles for FRP wrapped Specimens



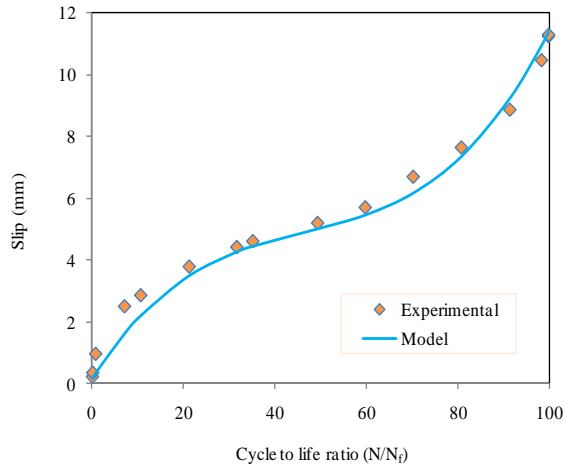
a) F62-W0-T0

b) F65-W0-T0

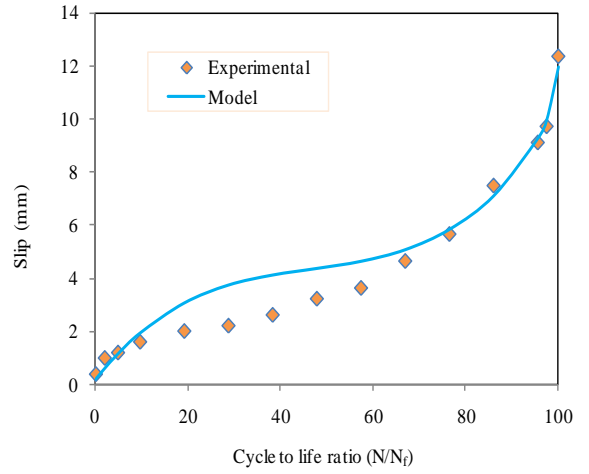


c) F70-W0-T0

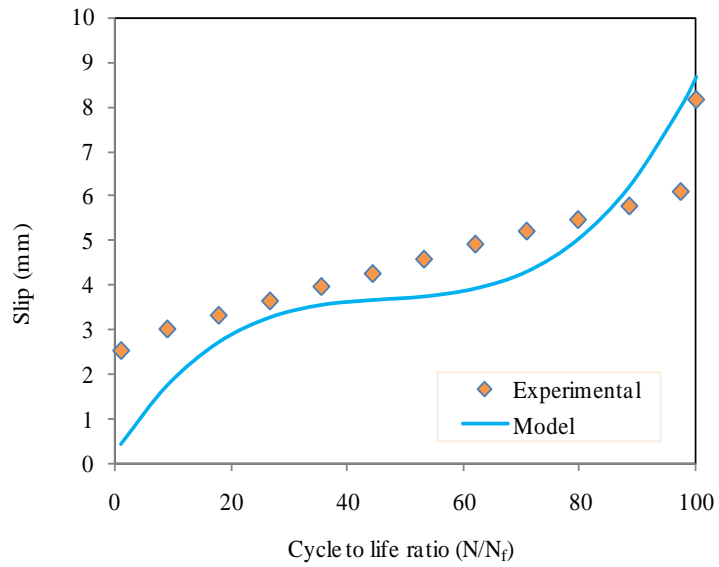
Figure C.1 Experimental and model results for FRP wrapped zero percent corrosion level



a) F50-W5-T5

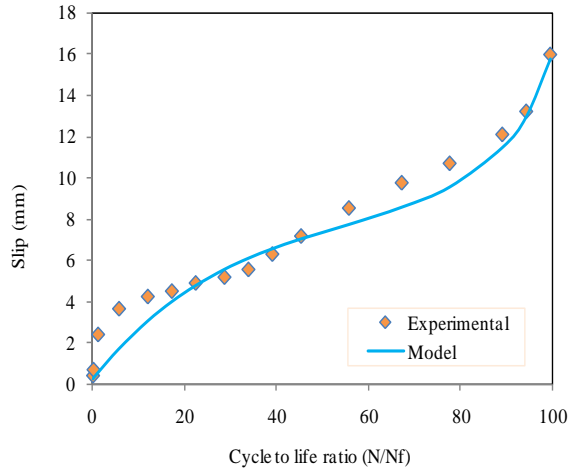


b) F52-W5-T5

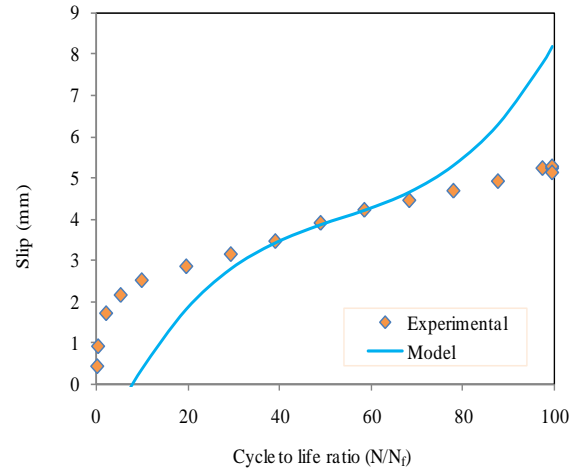


c) F65-W5-T5

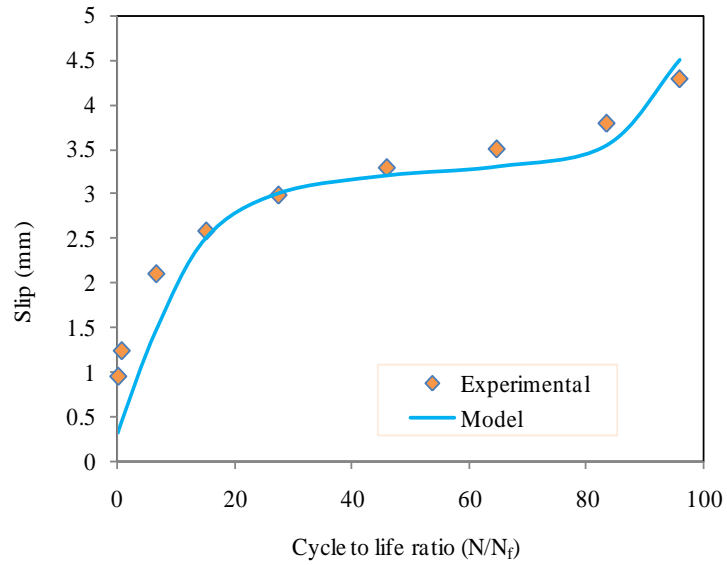
Figure C.2 Experimental and model results for FRP wrapped five percent corrosion level



a) F48-W9-T9a



b) F50-W9-T9a

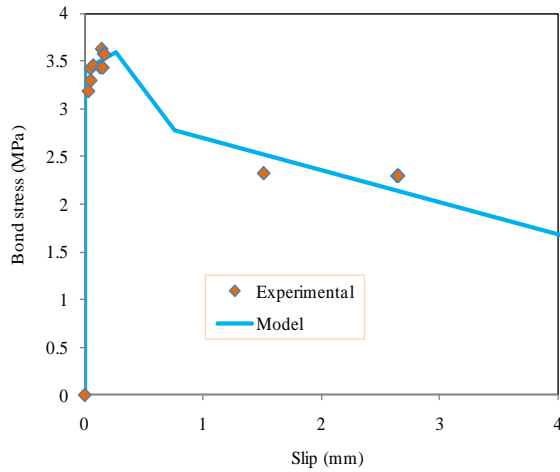


c) F55-W9-T9a

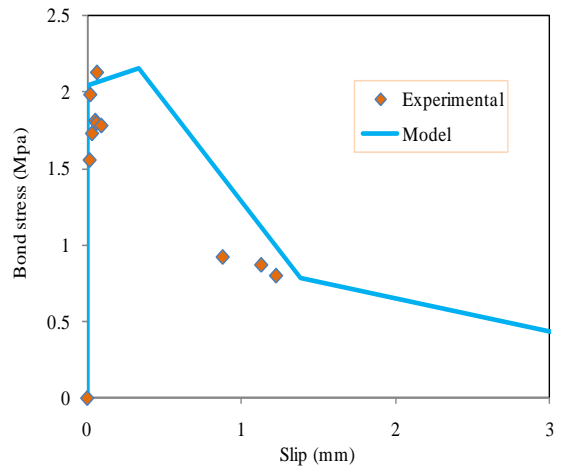
Figure C.3 Experimental and model results for FRP wrapped nine percent corrosion level

Appendix D

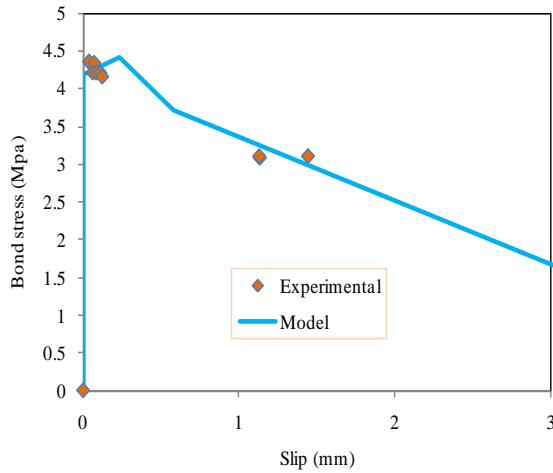
Cyclic Bond Stress-Slip for Unwrapped Specimens



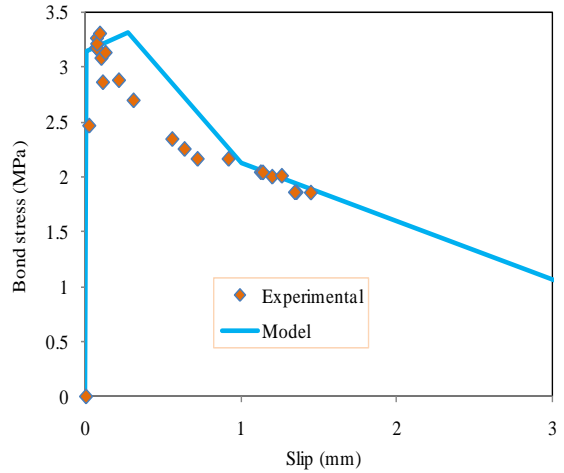
a) F45-N-T0



b) F47-N-T0

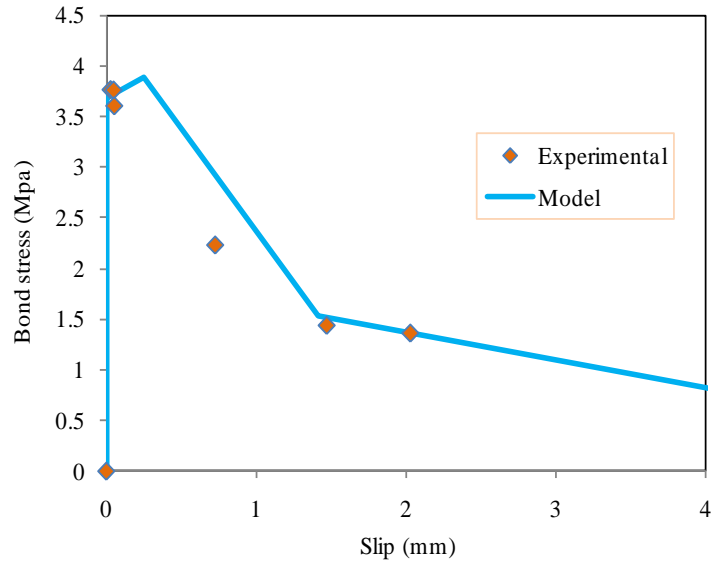


c) F50-N-T0



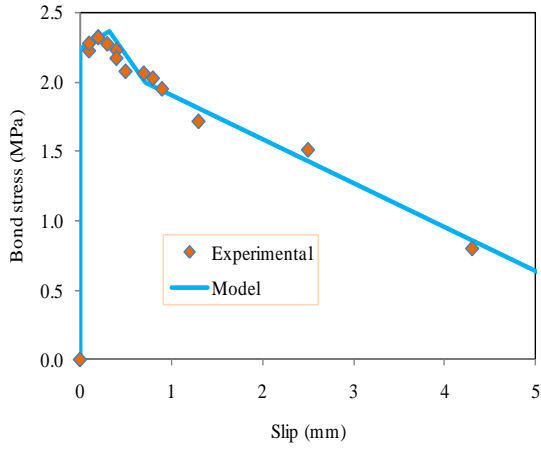
d) F53-N-T0

Figure D.1 Experimental and model results for unwrapped zero percent corrosion level

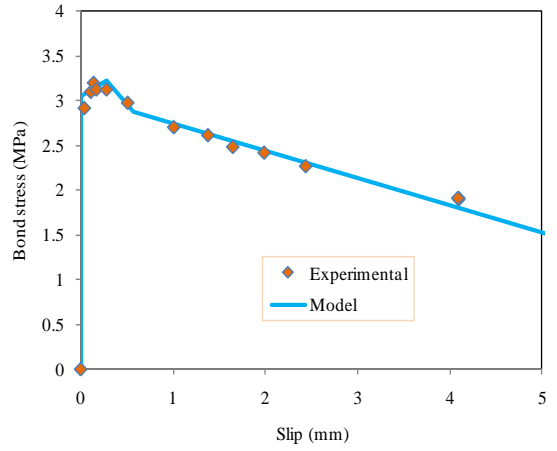


e) F55- N-T0

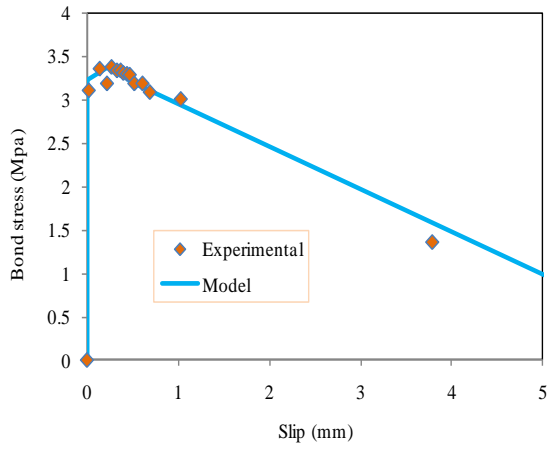
Figure D.2 Experimental and model results for unwrapped zero percent corrosion level (cont.)



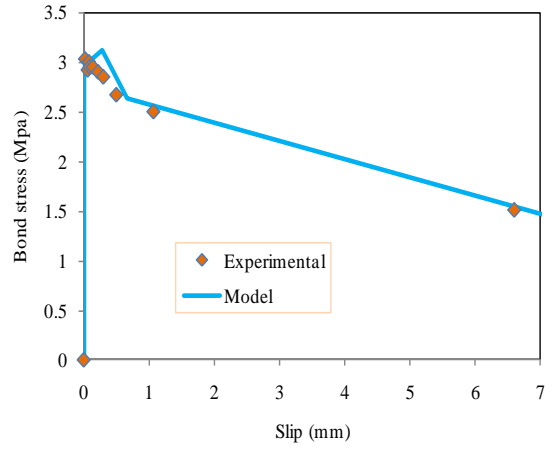
a) F37-N-T5



b) F40-N-T5

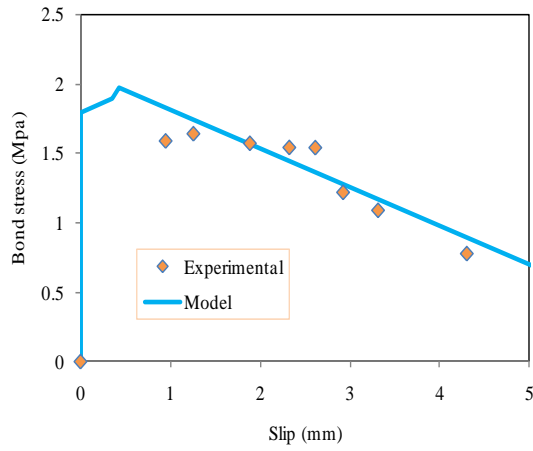


c) F45- N-T5

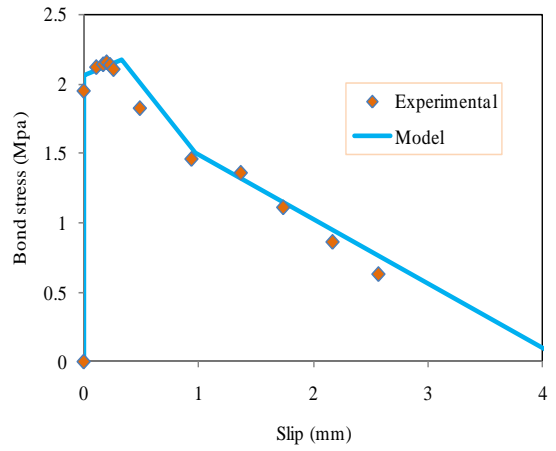


d) F55- N-T5

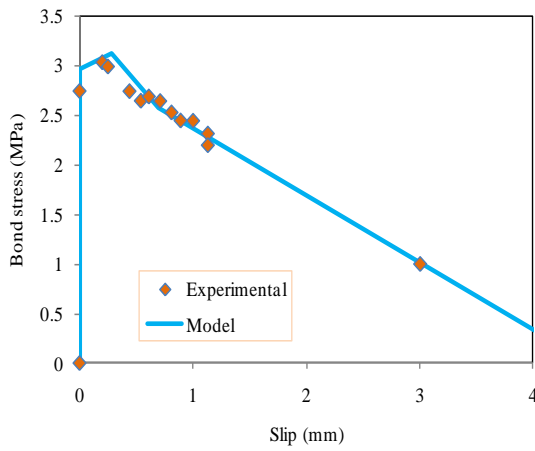
Figure D.3 Experimental and model results for unwrapped five percent corrosion level



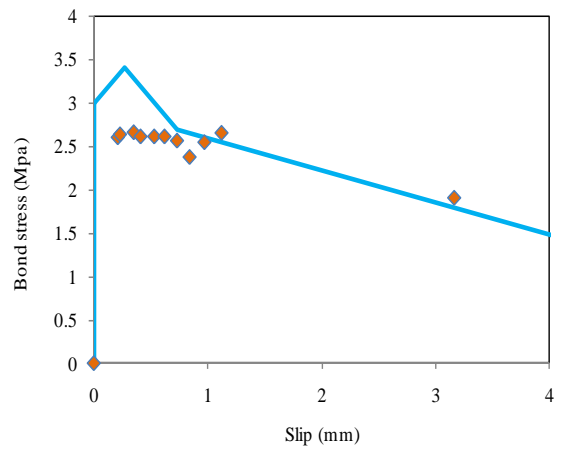
a) F40-N-T9a



b) F35-N-T9b



c) F40-N-T9b

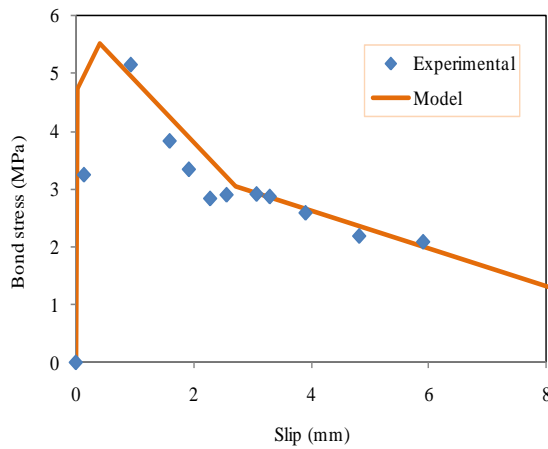


d) F45-N-T9b

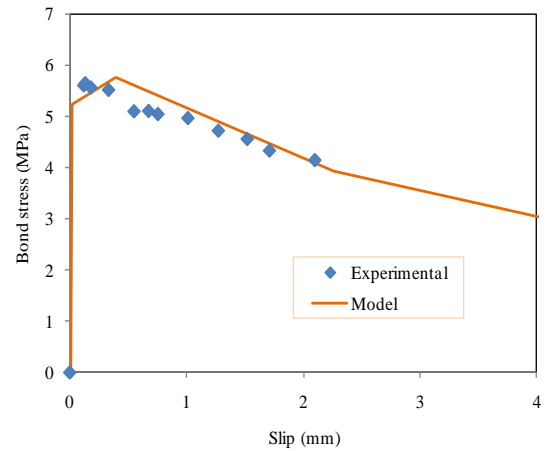
Figure D.4 Experimental and model results for unwrapped nine percent corrosion level

Appendix E

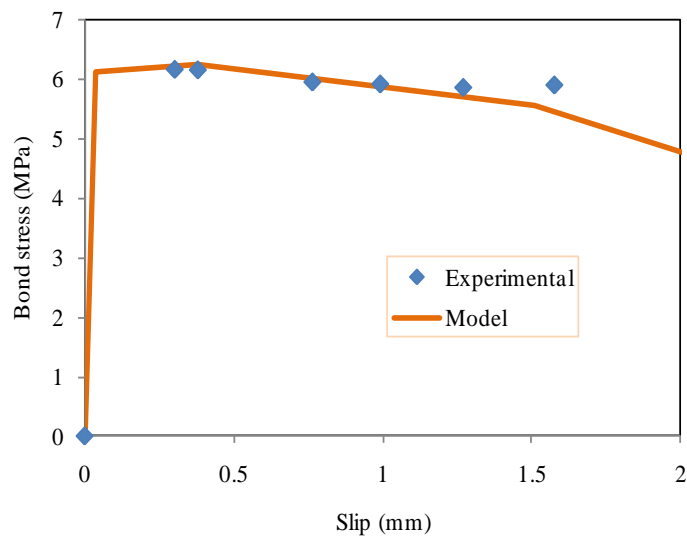
Cyclic Bond Stress-Slip for FRP wrapped Specimens



a) F62-W0-T0

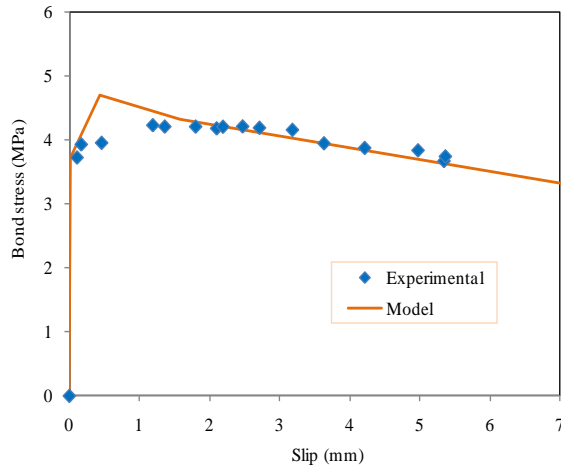


b) F65-W0-T0

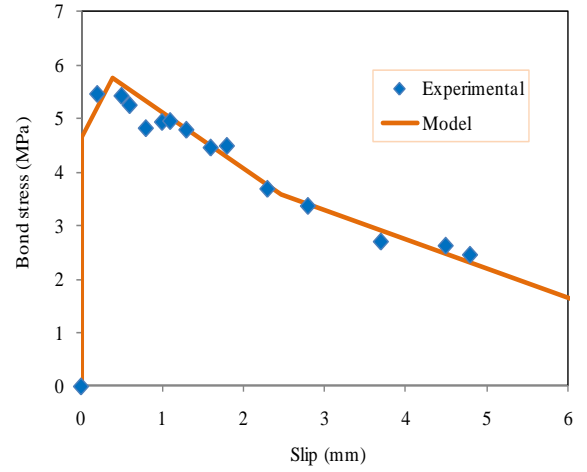


c) F70-W0-T0

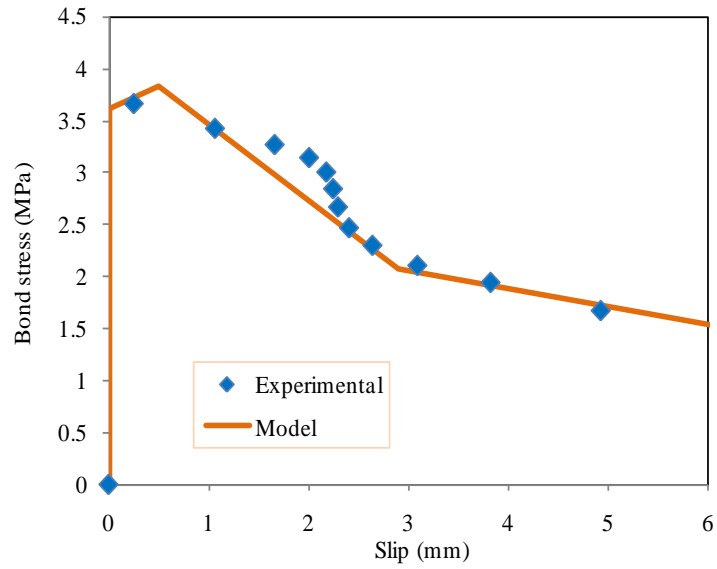
Figure E.1 Experimental and model results for FRP wrapped zero percent corrosion level



a) F50-W5-T5

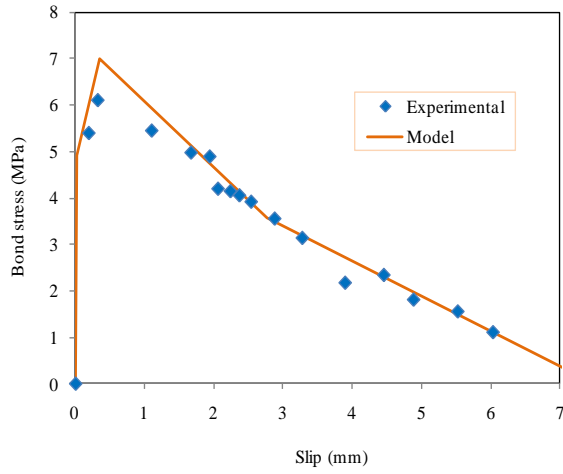


b) F52-W5-T5

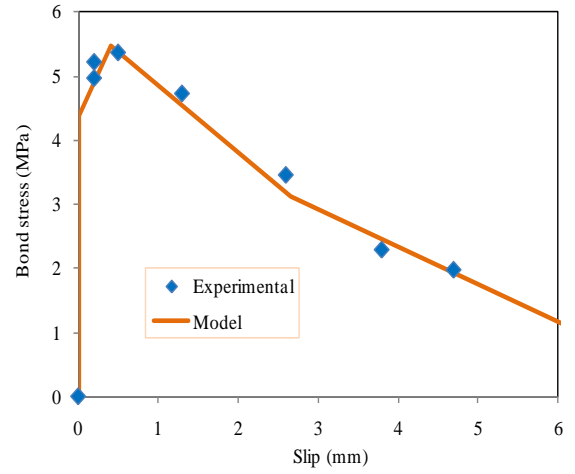


c) F65-W5-T5

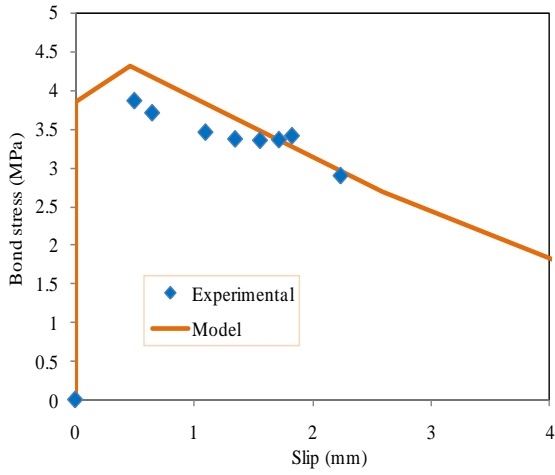
Figure E.2 Experimental and model results for FRP wrapped five percent corrosion level



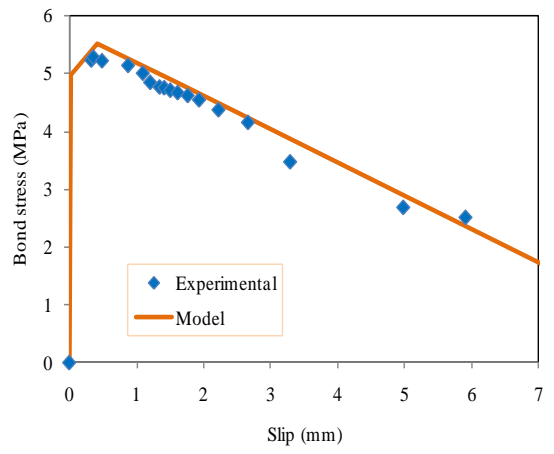
a) F48-W9-T9a



b) F52-W9-T9a

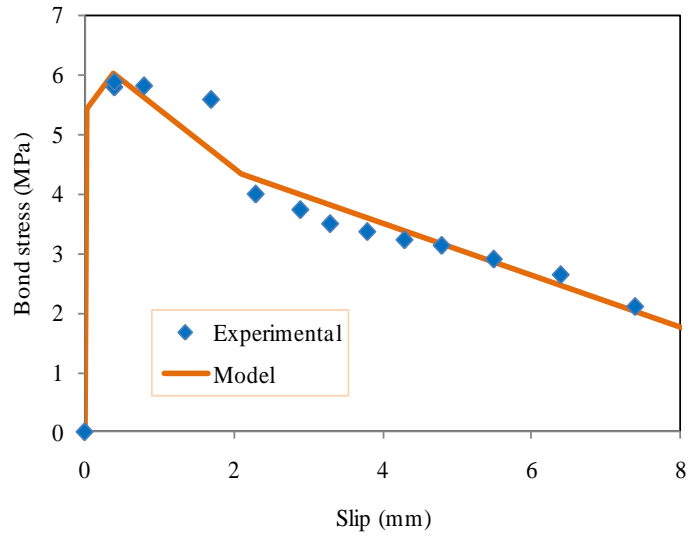


c) F55-W9-T9a



d) F50-W9-T9b

Figure E.3 Experimental and model results for FRP wrapped nine percent corrosion level



e) F52-W9-T9b

Figure E.4 Experimental and model results for FRP wrapped nine percent corrosion level (cont.)

Bibliography

- ACI Committee 408, 1992. State of the Art Report on Bond under Cyclic Loads (ACI 408.2-92, Reapproved 2005). American Concrete Institute, Farmington Hills, MI, 32 p.
- ACI Committee 408, 2003. Bond and Development of Straight Reinforcing Bars in Tension (ACI 408-03). American Concrete Institute, Farmington Hills, MI, 49 p.
- ACI Committee 440, 1996. State of the Art Report on Fiber Reinforced Plastic (FRP) Reinforcement for Concrete Structures (ACI 440-96, Reapproved 2002). American Concrete Institute, Farmington Hills, MI, 68 p.
- ACI Committee 222, 2001. Protection of Metals in Concrete against Corrosion (ACI 222-01). American Concrete Institute, Farmington Hills, MI, 41 p.
- ACI Committee 215, 1974. Considerations for Design of Concrete Structures Subjected to Fatigue Loading (ACI 215-74, Reapproved 1999). American Concrete Institute, Farmington Hills, MI, 24p.
- ACI Committee 440, 2002. Bond and Development of Straight Reinforcing Bars in Tension (ACI 440.2-02). American Concrete Institute, Farmington Hills, MI, 49 p.
- ACI Committee 440, 2007. Report on fiber reinforced polymer (FRP) reinforcement for concrete structures. American Concrete Institute.
- Al-Hammoud, R.; Soudki, K. and Topper, T., 2007. "Fatigue Flexural Behaviour of Corroded Reinforced Concrete Beams Repaired with CFRP Sheets," ACI Structural Journal, submitted for review and possible publication, 20 p.
- Al-Sulaimani, G.J; Kaleemullah, M.; Basunbul, I.A. and Rasheeduzzafar, 1990. "Influence of Corrosion and Cracking on Bond Behaviour and Strength of Reinforced Concrete Members," ACI Structural Journal, V. 87, # 2, March, pp. 220-231.
- Almusallam, A. A.; Al-Gahtani, A. S.; Aziz, A. R. and Rasheeduzzafart, 1996. "Effect of reinforcement corrosion on bond strength", Construction and Building Materials, Vol. 10, No. 2, pp. 123-129.
- Amleh, L. and Mirza, S., 1999. "Corrosion Influence on Bond between Steel and Concrete", ACI Structural Journal, V. 96, No. 3.

- Amleh, L., 2000. "Bond deterioration of reinforcing steel in concrete due to corrosion", PhD thesis, McGill University, Montreal, Canada.
- Amleh, L. and Ghosh, A., 2006. "Modeling the effect of corrosion on bond strength at the steel concrete interface with finite element analysis", *Can. J. Civ. Eng.* 33: 673-682.
- Atkinson, A. and Nickerson, A.K., 1984. The diffusion of ions through water saturated cement. *Journal of materials and science*, 19(9), 3068-3078.
- Abrishami, H.H. and Mitchell, D., 1996. "Analysis of Bond Stress Distributions in Pullout Specimens" *J. Struct. Engrg.* Volume 122, Issue 3, pp. 255-261.
- Abaqus Manual; "Getting started with Abaqus", Interactive edition, version 6.9.
- Building code requirements for reinforced concrete, ACI-2005.
- Badawi, M. and Soudki, K., 2005. "Control of Corrosion-Induced Damage in Reinforced Concrete Beams using Carbon Fiber-Reinforced Polymer Laminates," *ASCE Journal of Composites for Construction*, V. 9, #2, March, pp.195-201.
- Balazs, G. and Koch, R., 1992. "Influence of Load History on Bond Behaviour," *Proceedings: Bond in Concrete- From Research to Practice*, Riga, Latvia, October pp.7.1-7.10.
- Balazs, G., 1991. "Fatigue of Bond," *ACI Materials Journal*, V. 88, #6, November, pp.620-629.
- Balazs, G., 1998. "Bond Under Repeated Loading" *Proceedings: Bond and Development of Reinforcement-A Tribute to Peter Gergely*, Leon, R. Ed., ACI SP-180, pp. 125-143.
- Bresler, B. and Bertero, V., 1968. "Behavior of Reinforced Concrete under Repeated Loading," *ASCE Journal of Structural Division*, V. 94, St 6, June, pp. 1567-1589.
- Broomfield, J.P., 1997. "Corrosion of Steel in Concrete: Understanding, Investigation and Repair," E&FN Spon, London.
- Berto, L; Simioni, P; Saetta, A., 2008. "Numerical modelling of bond behaviour in RC structures affected by reinforcement corrosion," *Engineering Structures* 30, 1375–1385.
- Berra, M.; Castellani, A.; Coronelli, D.; Zanni, S. and Zhang, G., 2003. "Steel concrete bond deterioration due to corrosion: finite element analysis for different confinement levels," *Magazine of concrete research*, 55, No. 3, June, 237-247.

- Bilal S. Hamad, Khaled A. Soudki, Mohamad H. Harajli, and Ahmad A. Rteil., 2004. "Experimental and Analytical Evaluation of Bond Strength of Reinforcement in Fiber-Reinforced Polymer-Wrapped High-Strength Concrete Beams." *ACI Structural Journal*, V. 101, No. 6.
- Balaazs, G.L., 1986. "Bond behaviour under repeated loads," *Studi e ricerche-corso filii. Pesenti, Politecnico di Milano*, V. 8, pp. 395-430.
- Borgand, B., Warren, C., Somayagi, S., and Heidersbach, R., 1990. "Mechanisms of corrosion of steel in concrete." *Corrosion rate of steel in concrete, ASTM STP 1065*, N. S. Berke, V. Chaker, and D. Whiting, Eds., American society for testing and materials, Philadelphia, pp. 174-188.
- Choo, B.S. and Newman, J., 2003. *Advance Concrete Technology*, Elsevier Ltd, pp. 9/1-9/27.
- Craig, B.C. and Soudki, K.A., 2005. "Post-Repair Performance of Corroded Bond Critical RC Beams Repaired with CFRP," *Proceedings: FRP Reinforcement for Concrete Structures (FRPRCS-7), 7th International Symposium*, Sheild, C. et al. Eds., ACI SP-230, pp. 563-578.
- Carino, N.J., and Lew, H.S., 1982. "Re-examination of the relation between splitting tensile and compressive strength of normal weight concrete," *ACI journal*, V.79, #3, pp. 214-219.
- Collins, M.P., and Mitchell, D., 1997. *Pre stressed concrete structure*, Response publication, Toronto, Canada.
- El Maaddawy, T. and Soudki, K., 2005a. "Carbon-Fiber-Reinforced Polymer Repair to Extend the Service Life of Corroded Reinforced Concrete Beams," *ASCE Journal of Composites in Construction*, V. 9, #2, pp. 187-194.
- El Maaddawy, T.; Soudki, K. and Topper, T., 2005b. "Computer-Based Mathematical Model for Performance Prediction of Corroded Beams Repaired with Fiber Reinforced Polymers," *ASCE Journal of Composites for Construction*, V. 9, #3, June, pp.227-235.
- El-Sayed, A.K.; El-Salakawy, E.F. and Benmokrane, B. "Shear strength of concrete beams reinforced with FRP bars: Design methods," *FRPRCS-7*, pp. 955-974.
- Eligehausen, R. 1979. "Bond in tensile lapped splices of ribbed bars with straight anchorages," *German institute for reinforced concrete*, Berlin, 118pp.

- Fang, C.; Lundgren, K.; Chen, L and Zhu, C., 2004. "Corrosion Influence on Bond in Reinforced Concrete," *Cement and Concrete Research*, V. 34, pp.2159-2167.
- Fang, C.; Lundgren, K.; Plos, M. and Gylltoft, k., 2006. "Bond behavior of corroded reinforcing steel bars in concrete," *Cement and concrete research* 36, 1931-1938.
- Glass G.K. and Buenfeld, N.R., 2000a. "Chloride induced corrosion of steel in concrete," *Progress in structural engineering and materials*, 2(4), 448-458.
- Glass G.K. and Buenfeld, N.R., 2000b. "The influence of chloride binding on the chloride induced corrosion risk in reinforced concrete," *Corrosion science*, 42(4), 329-344.
- Glass, G.K. and Buenfeld, N.R., 1996. "Reinforced concrete-The principles of its deterioration and repair," In Macdonald, S. (ed.), *Modern matters-Principles and practice in conserving recent architecture*. Donhead publishing, Shaftesbury, pp. 101-112.
- Glass, G.K., Page, C.L. and Short, N.R., 1991. "Factors affecting steel corrosion in carbonated mortars," *Corrosion science*, 32(12), 1283-1294.
- Glass, G.K. and Buenfeld, N.R., 1998. "Theoretical assessment of the steady state diffusion cell test," *Journal of Materials Science* 33(21), 5111-5118.
- Glass, G.K., Reddy, B. and Buenfeld, N.R., 2000a. "Corrosion inhibition in concrete arising from its acid neutralization capacity," *Corrosion Science*. 42(9), 1587-1598.
- Glass, G.K., Page, C.L. and short, N.R., 1991. "Factors affecting steel corrosion in carbonated mortars," *Corrosion Science*, 32(12), 1283-1294.
- Glass, G.K. and Buenfeld, N.R., 1996. "Reinforced Concrete-The principles of its deterioration and repair," In Macdonald, S. (ed.), *Modern Matters-Principles and Practice in Conserving Recent Architecture*. Donhead Publishing, Shaftesbury,. Pp. 101-112.
- Hamad, B.S.; Rteil, A.A. and Soudki, K.A., 2004a. "Bond Strength of Tension Lap Splices in High-Strength Concrete Beams Strengthened with Glass Fiber Reinforced Polymer Wraps," *ASCE Journal of Composites for Construction*, V. 8, No. 1, February, pp. 14-21.
- Hamad, B.S.; Rteil, A.A.; Selwan, B. and Soudki, K.A., 2004b. "Behavior of Bond-Critical Regions Wrapped with Fiber-Reinforced Polymer Sheets in Normal and High-Strength Concrete," *ASCE Journal of Composites for Construction*, V. 8, # 3, May, pp. 248-257.

- Hamad, B.S.; Soudki, K.A.; Rteil, A.A. and Harajli, M.H., 2004c. "Experimental and Analytical Evaluation of the Bond Strength of Reinforcement in Fiber Reinforced Polymer-Wrapped High-Strength Concrete Beams," *ACI Structural Journal*, V. 101, #6, November, pp 747-754.
- Harajli, M.H. and Rteil, A.A., 2004. "Effect of Confinement Using Fiber-Reinforced Polymer or Fiber-Reinforced Concrete on Seismic Performance of Gravity Load-Designed Columns," *ACI Structural Journal*, V. 101, #1, January, pp 47-56.
- Harajli, M.H., 2006. "Effect of Confinement Using Steel, FRC, or FRP on the Bond Stress-Slip Response of Steel Bars under Cyclic Loading," *Materials and Structures*, V. 39, pp. 621-634.
- Harajli, M.H.; Hamad, B.S. and Rteil, A.A., 2004. "Effect of Confinement on Bond Strength between Steel Bars and Concrete," *ACI Structural Journal*, V 101, #5, September, pp. 595-603.
- Harajli, M. H., 2009. "Bond stress slip model for steel bars in unconfined or steel, FRC or FRP confined concrete under cyclic loading," *Journal of structural engineering*, Vol. 135, No. 5.
- Holmen, J.O., 1982. "Fatigue of concrete by constant and variable amplitude loading," SP-75, *Fatigue of concrete structures*, ACI, pp. 71-110.
- Huebner, K.H., Dewhirst, D.L., Smith, D.E., and Byrom, T.G., 2001. *Finite element methods for engineers*, 4th edition. New York: Wiley interscience.
- Isecke, B., 1982. "Failure analysis of the collapse of the Berlin Congress Hall." *Journal of material performance.*" 1982 (12): 36.
- Kono, S.; Inazumi, M. and Kaku, T., 1997. "Bond splitting behavior of reinforced concrete members confined with CFRP sheets", *Proceedings of the third international symposium*, Vol. 2.
- Kono, S.; Inazumi, M. and Kaku, T., 1998. "Evaluation of Confining Effects of CFRP sheets on Reinforced Concrete Members," *Proceedings: Composites in Infrastructure, 2nd International Conference*, Saadatmanesh, H. and Ehsani, M. R., Eds, Tucson, AZ, USA, Vol. I, pp. 343-355.
- Kono, S.; Matsuno, K. and Kaku, T., 1999. "Experimental Study on Bond-Slip Behavior of Longitudinal Bars in Reinforced Concrete Beams Confined with Fiber Reinforced Polymer

- Sheets,” Proceedings: FRP Reinforcement for Reinforced Concrete Structures (FRPRCS-4), 4th International Symposium, Dolan, C.; et al. Eds, ACI SP-188, pp. 333-346.
- Lutz, L.A. and Gergely, P., 1967. “Mechanics of Bond and Slip of Deformed Bars in Concrete,” ACI Journal, V. 64, # 11, November, pp. 711-721.
- Li, J.; Gao, X.; Zhang, P., 2007. “Experimental investigation on the bond of reinforcing bars in high performance concrete under cyclic loading”, Materials and structures, pp. 1027-1044.
- Lowes, L. N.; Moehle, J. P. and Govindjee, S., 2004. “Concrete steel bond model for use in finite element modeling of reinforced concrete structures”, ACI structural journal, Vol. 101, No. 4.
- Lindorf, A. et al., 2009. “Experimental investigations on bond behaviour of reinforced concrete under transverse tension and repeated loading”, Engineering Structures, V. 31, pp. 1469-1476.
- Mangat, P.S. and Elgarf, M.S., 1999a. “Bond Characteristics of Corroded Reinforcement in Concrete Beams,” Materials and Structures, V. 32, March, pp. 89-97.
- Masoud, S.; Soudki, K. and Topper, T., 2001. “CFRP Strengthened and Corroded RC Beams under Monotonic and Fatigue Loads,” ASCE Journal of Composites for Construction, V. 5, # 4, November, pp. 228-236.
- Masoud, S.; Soudki, K. and Topper, T., 2005. “Post-Repair Fatigue Performance of FRP-Repaired Corroded RC Beams: Experimental and Analytical Investigation,” ASCE Journal of Composites in Construction, V. 9, # 5, September, pp. 441-449.
- Mor, A.; Gerwick, B.C. and Hester, W.T., 1992. “Fatigue of High-Strength Reinforced Concrete,” ACI Materials Journal, V. 89, # 2, March, pp. 197-207.
- Ngo, D., and Scordelis, A.C. 1967. “Finite-element analysis of reinforced concrete beams.” ACI J., 64(3), 152–163.
- Montgomery DC. Design and Analysis of Experiments, 7th Edition: John Wiley & Sons Inc, 2009.
- Oh, B.H. and Kim, S.H., 2007. “Realistic Models for Local Bond Stress-Slip of Reinforced Concrete under Repeated Loading,” ASCE Journal of Structural Engineering, V. 133, #2, pp. 216-224.

- Okada, K.; Kobayashi, K. and Miyagawa, T., 1988. "Influence of Longitudinal Cracking due to Reinforcement Corrosion on Characteristics of Reinforced Concrete Members," *ACI Structural Journal*, V. 85, # 2, March, pp. 134-140.
- Orangun, C. O., Jirsa, J.O., and Breen, J.E., "A re-evaluation of test data on development length and splices," *ACI journal*, V. 74, #3, pp. 114-122.
- Plizzari, G.; Lundgren, K. and Balazs, G., 2002. "Bond and Splitting in Fibre Reinforced Concrete under Repeated Loading," *Proceedings: Bond in Concrete-From Research to Standards*, Budapest, Hungary, pp. 221-229.
- Pisani, M.A., 2005. "Evaluation of bending strength of RC beams strengthened with FRP sheets," *Journal of composite for construction*, V. 10, #4, pp. 313-320.
- Rehm, G. and Eligehausen, R., 1979. "Bond of Ribbed Bars under High Cycle Repeated Loads," *ACI Journal*, V. 76, # 2, February, pp. 297-309.
- Rteil, A., 2007, "Fatigue bond behaviour of corroded reinforcement and CFRP confined concrete", PhD thesis, University of Waterloo, Waterloo, Ontario, Canada.
- Rteil, A.; soudki, K. and Topper, T.; "Effect of CFRP sheets on concrete steel bond strength", 1st CSCE specialty conference on infrastructure technologies, management and policy, June 2-4, 2005.
- Rehm, G., and Eligehausen, R., 1979. "Bond of ribbed bars under high cyclic repeated loads," *ACI journal*, V. 76, # 2.
- Rehm, G., and Eligehausen, R., 1977. "Bond of ribbed bars under repeated loads," Report 291, German institute for reinforced concrete, Berlin.
- Soudki, K.A. and Sherwood, T., 2003. "Bond Behavior of Corroded Steel Reinforcement in Concrete Wrapped with Carbon Fiber Reinforced Polymer Sheets," *ASCE Journal of Materials in Civil Engineering*, V. 15, # 4, August, pp. 358-370.
- Soudki, K.A. and Sherwood, T.G., 2000. "Behaviour of Reinforced Concrete Beams Strengthened with Carbon Fibre Reinforced Polymer Laminates Subjected to Corrosion Damage," *Canadian Journal of Civil Engineering*, V. 27, # 5, October, pp. 1005-1010.

- Soudki, K. A., 2006. "FRP repair of corrosion damaged concrete beams waterloo experience"; *Advances in engineering structures, mechanics and construction*, 165-173.
- Serge, G. and Glass, G.K., 2000. "A method of ranking the aggressive nature of chloride contaminated concrete," *Corrosion science*, 42(12); 2043-2049.
- Schiesst, P. and Raupach, M., 1997. "Laboratory studies and calculations on the influence of crack width on chloride induced corrosion of steel in concrete," *ACI materials journal*, 94(1), 56-62.
- Saadatmanesh, H. and Malek, A.M., 1998. "Design guidelines for flexural strengthening of RC beams with FRP plates," *Journal of composites for construction*, 2(4), 158-164.
- Soretz, S., and Holzenbeim, H., 1979. "Influence of rib dimensions of reinforcing bars on bond and bendability," *ACI journal*, V. 76, # 1, pp. 111-127.
- Telford JK., 2007. "A brief introduction to design of experiment," *Johns Hopkins apl technical digest*; 27(3).
- Tepfers, R. 1973. "A theory of bond applied to overlapped tensile reinforcement splices for deformed bars," *Publ. 73.2, Div. of concrete structures, Chalmers University, Goteborg*.
- Tilly, G.P., 1979. "Fatigue of Steel Reinforcement Bars in Concrete: A Review," *Fatigue of Materials and Structures*, V. 2, # 3, pp. 251-268.
- Verna, J.R. and Stelson, T.E., 1962. "Failure of Small Reinforced Concrete Beams under Repeated Loading," *ACI Journal*, V. 59, #10, October, pp. 1489-1503.
- Whitmore, D.W. and Ball, J.C., 2004. "Corrosion Management," *ACI Concrete International*, V. 26, #12, December, pp. 82-85.
- Wallbank, E.J., 1989. "The Performance of Concrete in Bridges: A survey of 200 Highway Bridges", HMSO London.
- Zuo, J., and Darwin, D. 2000. "Splice strength of conventional strength and high relative rib area bars in normal and high strength concrete," *ACI Structural Journal*, 97(4): 630-631.
- Zheng, H., and Abel, A., 1998. "Stress concentration and fatigue of profiled reinforcing steels" *International Journal of Fatigue*, V. 20, Issue 10, pp. 767-773.